Title:

De novo assembly, annotation, and comparative analysis of 26 diverse maize genomes

Authors:

Matthew B. Hufford[1], Arun S. Seetharam[1,2], Margaret R. Woodhouse[3], Kapeel M. Chougule[4], Shujun Ou[1], Jianing Liu[5], William A. Ricci[6], Tingting Guo[8], Andrew Olson[4] , Yinjie Qiu[9], Rafael Della Coletta[9], Silas Tittes[10,11], Asher I. Hudson[10,11], Alexandre P. Marand[5], Sharon Wei[4], Zhenyuan Lu[4], Bo Wang[4], Marcela K. Tello-Ruiz[4], Rebecca D. Piri[7], Na Wang[6], Dong won Kim[6], Yibing Zeng[5], Christine H. O'Connor[9,12], Xianran Li[8], Amanda M. Gilbert[9], Erin Baggs[13], Ksenia V. Krasileva[13], John L. Portwood II[3], Ethalinda K.S. Cannon[3], Carson M. Andorf[3], Nancy Manchanda[1], Samantha J. Snodgrass[1], David E. Hufnagel[1,14], Qiuhan Jiang[1], Sarah Pedersen[1], Michael L. Syring[1], David A. Kudrna[15], Victor Llaca[16], Kevin Fengler[16], Robert J. Schmitz[5], Jeffrey Ross-Ibarra[9,11,17], Jianming Yu[8], Jonathan I. Gent[6], Candice N. Hirsch[9], Doreen Ware[4,18], R. Kelly Dawe[5,6,7]*

Affiliations:

[1]Department of Ecology, Evolution, and Organismal Biology, Iowa State University, Ames, IA 50011
[2]Genome Informatics Facility, Iowa State University, Ames, IA 50011
[3]USDA-ARS Corn Insects and Crop Genetics Research Unit, Iowa State University, Ames, IA 50011
[4]Cold Spring Harbor Laboratory, Cold Spring Harbor, NY 11724
[5]Department of Genetics, University of Georgia, Athens, GA 30602
[6]Department of Plant Biology, University of Georgia, Athens, GA 30602
[7]Institute of Bioinformatics, University of Georgia, Athens, GA 30602
[8]Department of Agronomy, Iowa State University, Ames, IA 50011
[9]Department of Agronomy and Plant Genetics, University of Minnesota, St. Paul, MN 55108
[10]Center for Population Biology, University of California, Davis, CA 95616
[11]Department of Evolution and Ecology, University of California, Davis, CA 95616
[12]Department of Ecology, Evolution, and Behavior, University of Minnesota, St. Paul, MN 55108
[13]Department of Plant and Microbial Biology, University of California, Berkeley, CA 94720
[14]Virus and Prion Research Unit, National Animal Disease Center, USDA-ARS, Ames, IA, 50010
[15]Arizona Genomics Institute, School of Plant Sciences, University of Arizona, Tucson, AZ 85721
[16]Corteva Agriscience, Johnston, IA 50131
[17]Genome Center, University of California, Davis, CA 95616
[18]USDA ARS NAA Robert W. Holley Center for Agriculture and Health, Agricultural Research Service, Ithaca, NY 14853

*correspondence to: kdawe@uga.edu

One sentence summary:

A multi-genome analysis of maize reveals previously unknown variation in gene content, genome structure, and methylation.

Abstract:

We report *de novo* genome assemblies, transcriptomes, annotations, and methylomes for the 26 inbreds that serve as the founders for the maize nested association mapping population. The data indicate that the number of pan-genes exceeds 103,000 and that the ancient tetraploid character of maize continues to degrade by fractionation to the present day. Excellent contiguity over repeat arrays and complete annotation of centromeres further reveal the locations and internal structures of major cytological landmarks. We show that combining structural variation with SNPs can improve the power of quantitative mapping studies. Finally, we document variation at the level of DNA methylation, and demonstrate that unmethylated regions are enriched for cis-regulatory elements that overlap QTL and contribute to changes in gene expression.

Main text:

Maize is the most widely planted crop in the world and an important model system for the study of gene function. The species is known for its extreme genetic diversity, which has allowed for broad adaptation throughout the tropics and intensive use in temperate regions. Much of its success can be attributed to a remarkable degree of heterosis when divergent inbred lines are crossed to make F1 hybrids. Nevertheless, most current genomic resources are referenced to a single inbred, B73. Yet prior data suggest the B73 genome contains only 63-74% of the genes and/or low-copy sequences in the full maize pan-genome (*1*–*4*). Moreover, there is extensive structural polymorphism in non-coding and regulatory genomic regions that has been shown to contribute to variation in numerous traits (*5*). In recent years, additional maize genomes have been assembled, allowing limited characterization of the species pan-genome and the extent of structural variation (*2*, *6*–*10*). However, comparisons across genome projects are often confounded by differences in assembly and annotation methods.

The maize Nested Association Mapping (NAM) population was developed as a means to study the genetic architecture of quantitative traits (*11*). Twenty-five founder inbred lines were strategically selected to represent the breadth of maize diversity including lines from temperate,

tropical, sweet corn, and popcorn germplasm (*12*). Each NAM parental inbred was crossed to B73 and selfed to generate 25 distinct populations of 200 recombinant inbred lines that combine the advantages of linkage and association mapping for important agronomic traits (*13*). Important biological infrastructure continues to be developed around these lines (e.g. (*14–16*)) but comprehensive genomic resources are needed to fully realize the power of the NAM population.

Here we describe the 25 assembled and annotated genomes for the NAM founder inbreds and an improved reference assembly of B73 (**Table S1**). In our comprehensive characterization of maize genomic diversity, we evaluate the maize pan-genome and its fractionation from a tetraploid ancestor, visualize the diversity of transposons and tandem repeat arrays, deploy enzymatic methyl-seq and ATAC-seq to characterize the pan-epigenome, and identify structural and epigenetic variation that impact phenotype.

Consistency and quality of genome assemblies

The 26 genomes were sequenced to high depth (63-85X) using PacBio long-read technology, assembled into contigs using a hybrid approach (see Methods), corrected with long-read and Illumina short-read data, scaffolded using Bionano optical maps, and ordered into pseudomolecules using linkage data from the NAM recombinant inbred lines and maize pan-genome anchor markers (*4*). Assembly and annotation statistics far exceed nearly all available maize assemblies, with the total length of placed scaffolds (2.102-2.162Gb) at the estimated genome size of maize, a mean scaffold N50 of 119.2Mb (contig N50 of 25.7Mb), complete gene space (mean of 96% complete BUSCOs; (*17*)), and, based on the LTR Assembly Index (LAI, mean of 28; (*18*)), full assembly of the transposable-element-laden portions of the genome (**Table 1; Table S2**).

Gene identification and diversity in gene content

We sequenced mRNA from ten tissues in replicate for each inbred. These data were used as the basis for evidence-based gene annotation of each line, which was then improved using public B73 full-length cDNA and expressed sequence tags (ESTs). The evidence set was augmented with *ab initio* gene models and the gene structures uniformly refined for all accessions using phylogeny-based methods. This pipeline revealed an average of 40,621 (SE = 117) protein-coding and 4,998 (SE = 100) non-coding gene models per genome, with well over

a million independent gene models generated across the 26 lines. Phylostrata analysis revealed that the great majority of genes share orthologs with species in the *Andropogoneae* tribe and grass family (**Fig. 1A**). The accuracy of the annotations, measured by the congruence between annotations and supporting evidence (Annotation Edit Distance, AED) (*19*), is substantially higher than previous reference maize and sorghum annotations (**Fig. S1**) (*2*, *6*, *10*, *20*–*22*).

Based on the canonical transcripts from this complete set of annotations, we assessed the gene catalog of the pan-genome. Genes with high sequence similarity, located within blocks of homologous sequence in pairwise comparisons, were grouped together as one pan-gene. In many cases, a gene was not annotated by our computational pipeline in a particular inbred line, yet at least 90% of the gene was present in the correct homologous location; when this occurred, the pan-gene was considered present (**Fig. S2 A-B;** see Methods), even though in some cases the absence of annotation may be associated with fractionation and/or pseudogenization.

Across the 26 genomes, a total of 103,538 pan-genes were identified. Previous analysis of the maize pan-genome reported ~63,000 pan-genes based on transcriptome assemblies of seedling RNA-seq reads from 500 individuals (*1*). The superior contiguity of our assemblies, as well as the application of both *ab initio* and evidence-based annotation using RNA-seq from a diverse set of ten tissues, likely accounts for the increased sensitivity here. Over 80% of pan-genes were identified within just ten inbred lines based on a bootstrap resampling of genomes; the rate of pan-gene increase as new genomes were added diminished beyond this point (**Fig. 1B**).

Pan-genes, excluding tandem duplicates, were classified as core (present in all 26 lines), near-core (present in 24-25 lines), dispensable (present in 2-23 lines), and private (present in only one line) (**Fig. 1C**). For each genotype, the portion of genes classified into each of these groups was consistent, with an average of 58.39% (SE = 0.07%) belonging to the core genome, 8.22% (SE = 0.05%) to the near-core genome, 31.75% (SE = 0.09%) to the dispensable genome, and 1.64% (SE = 0.08%) private genes (**Fig. 1C**; **Fig. S2 C-D; Table S3**). In total, there are 32,052 genes in the core/near-core portion of the pan-genome and 71,486 genes in the dispensable/private portion. The majority of core/near-core genes are syntenic to sorghum (57.8%) whereas this is rarely the case for dispensable/private genes (1.8% syntenic). Similarly, the core genes are generally from higher phylostrata levels (i.e. *Viridiplanteae* and *Poaceae*), while those in the near-core and dispensable sets either share orthologs only with closely related species or are maize-specific (**Fig. S2 F)**. A total of 16,267 pan-genes had a putative tandem duplicate in at least one genome, of which 6,556 were found in a single

genome. On a per gene basis in genomes with at least one tandem duplicate the average copy number is 2.20 (SE = 0.01) (**Fig. S2 E**).

Partial tetraploidy and tempo of fractionation

The maize ancestor underwent a whole-genome duplication (WGD) allopolyploidy event 5-20 MYA ((*23*, *24*), **Fig. 2A**). Evidence for WGD is found in the existence of two separate genomes that are broken and rearranged, yet still show clear synteny to sorghum (*23*, *25*). Many duplicated genes have since undergone loss, or fractionation, reducing maize to its current diploid state (*25*, *26*). Further, fractionation is biased towards one homoeologous genome (M2, more fractionated) over the other (M1, less fractionated) (*25*). The M1 and M2 subgenomes are composed almost exclusively of core (87.23%) and near-core (6.19%) pan-genes (**Figs. 1C, 2A**).

Given the ancient timeframe of the WGD in maize and the rapid tempo of fractionation observed in other species (*27*, *28*), little variation in homoeolog retention is expected at the species level. In fact, prior work in temperate maize has suggested that most fractionation occurred long before maize was domesticated (*6*, *29*). However, this diverse set of genomes allows for a more complete characterization of fractionation within the coalescence of the species. Since fractionation can occur at the level of small deletions (*26*, *30*), we evaluated both partial and complete homoeolog loss beginning with a conservative set of 16,195 maize pan-orthologs. We determined that 7,043 were single-copy orthologs, where the homoeologous gene was likely deleted prior to maize speciation (**Fig. 2A**). Fractionation bias was substantial in this set, with 70% of single-copy orthologs retained in M1 and 30% retained in M2. In addition, we identified 4,576 homoeologous pairs (**Fig. 2A**) of which 2,155 had the same exon structure of the sorghum ortholog in both homoeologs. In 1,281 pairs, at least one copy of the gene differed from its sorghum ortholog, but did not vary among NAM lines, likely representing fractionation that pre-dated *Zea mays*. These ancient deletions were also biased toward M2, but much less substantially (9.4% deletion excess in M2), potentially reflecting different exon structure in the paleopolyploid progenitors. Another 1,140 pairs varied across the genomes in their pattern of exon retention, segregating for deletions or structural differences in at least one copy of the gene. This segregating set was manually curated (**Dataset S1**) to remove loci where exons or flanking sequence could not be confidently identified (**Fig. 2A**), resulting in a curated set of 494 homoeolog pairs segregating for fractionation, which represents more than 10% of the homoeologous pairs present in the pan-genome. Of these, 281 M2 homoeologs had exon

loss compared to 236 M1 homoeologs, a 19% difference ($p < 0.05$, χ^2 test), suggesting ongoing biased fractionation.

Coalescent theory predicts that segregating mutations, like the fractionation deletions identified, should have arisen within the last $4N_e$ generations. If the effective population size in the maize progenitor teosinte is a reasonable upward bound for maize ($N_e = 150{,}000$; (*31*)), we can infer that the majority of segregating neutral variation arose within the last 600,000 generations. Barring pervasive balancing selection for homoeologs, these data indicate that the majority of segregating fractionation substantially post-dates the last whole-genome duplication. Coalescent theory also predicts that rare deletions should be much younger than those segregating at intermediate frequency. We constructed the unfolded site frequency spectrum (SFS) of fractionation deletions in our curated set of homoeolog pairs and compared this to the unfolded SFS of non-coding SNPs using sorghum to define the ancestral state (**Fig. 2B**). The data reveal a similar frequency distribution in deletions and SNPs with a preponderance of rare variants in both, suggesting that a subset of fractionation may be quite young, potentially continuing in modern-day populations of maize. We also evaluated patterns of co-exon-retention in non-stiff-stalk temperate maize, tropical maize, and flint-derived maize, and observed clear evidence of population-specific fractionation (**Fig. 2C).** This surprising variation in homoeolog retention at the population level may reflect relaxed constraint following domestication and migration of maize to temperate climates.

Analysis of gene ontology terms revealed that fully retained homoeologous loci were enriched ($p < 1\times10^{-05}$) for DNA-binding, nucleic acid binding, phosphatase regulation, and transcription factor activity (consistent with prior results; (*32*), whereas segregating fractionated loci were enriched ($p < 1\times10^{-05}$) for transporter and catalytic activity (**Fig. S3, Dataset S1**). These results support the hypothesis that fractionated loci have distinct functions from those that are retained, presumably due to differential selection on multi-protein pathways or metabolic networks (*32*, *33*).

The repetitive fraction of the pan-genome

Transposable elements (TEs) were annotated in each assembly using both structural features and sequence homology (*34*). Individual TE libraries from each inbred were then combined to form a pan-genome library, which was used to identify TE sequences missed by individual libraries. The annotations reveal that DNA transposons and LTR retrotransposons comprise 8.5% and 74.4% of the genome, respectively (**Table S4, Fig. S4**). A total of 27,228 TE

families were included in the pan-genome TE library, of which 59.7% were present in all 26 NAM founders and 2.5% were unique to one genome (**Fig. S5**). The average percentage of intact and fragmented TEs were 30.5% and 69.5% (SE = 0.06%), respectively. As reported previously, *Gypsy* LTR retrotransposon families are more abundant in pericentromeric regions, while *Copia* LTR retrotransposons are more abundant in the gene-dense chromosome arms (**Fig. S6**) (*35*). Tropical lines have significantly more *Gypsy* elements than temperate lines (p = 0.002, *t*-test), with mean *Gypsy* content of 1,018 Mbp and 988 Mbp, respectively (**Table S4, Fig. S4**). This may reflect increasing constraint on *Gypsy* proliferation in temperate lines that have, on average, smaller genomes (**Table 1**).

In some maize lines, over 15% of the genome is composed of tandem repeat arrays that include the centromere repeat CentC, the two knob repeats knob180 and TR-1, subtelomere, and telomere repeats (*36*, *37*). Repeats of this type remain a major impediment to assembly. A mean of 60% of CentC, 70% of the 4-12-1 subtelomeric sequence (*38*)), 28.9% of TR-1, 1% of knob180, and 0.09% of rDNA repeat units were incorporated in the final assemblies (**Table 1**).

A total of 110 (of 260) functional centromeres identified by CENH3 ChIP-seq (*39*, *40*) were fully assembled, and of these 88 are gapless ((**Fig. S7A** and (*40*)). Chromosomes with very long CentC arrays (such as chromosomes 1, 6, and 7) often have assembly gaps and the precise location of the centromere could not be determined. However many centromeres either have fully assembled small CentC arrays or the functional centromeres are located to one side of the CentC tracts in regions dominated by retrotransposons (**Fig. 3A**). By projecting all centromere locations onto B73, we were able to identify twelve centromere movement events (three on chr5 and chr9, and two on chr3, chr8 and chr10), clarifying and extending prior evidence for centromere shifting (*39*) (**Fig. 3B, Fig. S7B**). The variation in CentC abundance and positional polymorphism made it possible to gaplessly assemble at least two variants of all ten centromeres (**Fig. S7A**).

Both knob180 and TR-1 arrays are subject to meiotic drive and accumulate when a chromosome variant known as Abnormal chromosome 10 (Ab10) is present (*37*, *41*). Although Ab10 is absent from modern inbreds, its legacy remains in the form of many large knobs. The majority of knob180 and TR-1 repeat arrays were identified in mid-arm positions (81.9%) where meiotic drive is most effective. Long knob180 and TR-1 repeat arrays can occur separately, but are more frequently intermingled in fragmented arrays along with transposons (**Fig. 3A, Fig. S8**) (*42*). Analysis of classical (cytologically visible) knobs on chromosome 1S, 2S, 2L, 3L, 4L, 5L, 6L, 7L, 8L, and 9S revealed that their locations are syntenic and that several are composed of a series of disjointed smaller knobs (**Fig. 3A, Fig. S9)**. In some lines, knobs are not visible

cytologically but can still be detected as smaller arrays at the sequence level; however, this is not always the case, as many show strict presence-absence variation among the NAM founder inbreds.

Tandem repeat arrays are also commonly found at the ends of chromosome arms (**Table S5**). Among the 520 chromosome ends, 57.9% contained knob180 repeats and 30.5% contained subtelomere repeats. At least 65.6% of the ends were fully assembled as indicated by the presence of telomere sequences.

Structural variation and impact on phenotype

Comparative analyses among the NAM genotypes through mapping of long-reads to B73 revealed a cumulative total of 791,101 structural variants (SVs) greater than 100bp in size. Tropical lines, which are the most divergent NAM genomes from B73, include a substantially higher number of SVs than temperate lines (mean = 32,976 versus 29,742; p = 0.00013) **(Tables S6, S7).** Structural variants are more common on chromosome arms where recombination is highest (**Fig. S10**), similar to SNPs and other forms of genetic variation (*43*)**.** Almost half (49.6%) of SVs were <5 kbp in size, with 25.7% being less than 500bp. Across all size classes SVs are skewed toward rare variants (**Fig. S11**). Several large SVs were found segregating within the 26 NAM genomes (**Fig. 3B**), including 35 distinct inversion polymorphisms and 5 insertion-deletion polymorphisms >1 Mbp. For example, a 14.6 Mbp inversion on chromosome 5 in the CML52 and CML322 lines, which was previously hypothesized based on suppressed recombination in the NAM RILs (*11*), is confirmed here based on assembly. Additionally, there is a 1.9 Mbp deletion with seven genes on chromosome 2 in the MS71 inbred, and a 1.8 Mbp deletion with two genes on chromosome 8 found in eight lines. Our data also capture a very large reciprocal translocation (involving >47 Mbp of DNA) between the short arms of chromosomes 9 and 10 in Oh7B that had been previously detected in cytological studies (*38*) (**Fig. 3B**).

The high proportion of rare SVs in maize suggests these may be a particularly deleterious class of variants, as observed in other species (*44*, *45*). Indels and inversions occur in regions that have 49.8% fewer genic base pairs than the genomic background. Furthermore, SVs are 17% less likely to be found in conserved regions than SNPs (odds ratios of 0.27 and 0.58 for SVs and SNPs, respectively, Fisher's Exact Test, $p < 0.001$). Approximate Bayesian computation modeling revealed that selection against SVs is at least as strong as that against

nonsynonymous substitutions (**Fig. S12**; See Supplemental Methods). These results suggest that, when they occur, SVs are particularly consequential and are likely relevant to fitness.

To estimate the phenotypic impact of SVs, we assessed the genetic basis of 36 complex traits (*13*) using 71,196 filtered SVs in 4,027 recombinant inbred lines derived from the NAM founder inbreds (*11*) (**Fig. S13A)**. The analysis revealed that SVs explain a high percentage of phenotypic variance for disease traits (60.10% ~ 61.75%) and less for agronomic/morphological traits (20.04% ~ 61.04%) and metabolic traits (4.79% ~ 26.78%). Disease traits are often conferred by one or a few genes, whereas metabolic traits may be more sensitive to the environment and involve epistatic interactions that would not have been detected by our approach (*46*). Much of the phenotypic variation was also explained by SNPs, which were much more numerous (288-fold more) relative to our conservative set of SVs (**Fig. S13A**). When the SNP and SV data were integrated into one linear mixed model, the combined markers only slightly surpassed values from SNPs, consistent with the fact that most SVs are in high linkage disequilibrium with SNPs (**Fig. S13A**). We also carried out genome-wide association analyses (GWAS) to identify specific SVs contributing to phenotypic variation for the same suite of traits (**Fig. S13B-G**). Among the detected GWAS signals, 93.05% overlapped with those identified with SNPs and 6.95% were unique to SVs (no significant SNPs detected within 5 Mbp of significant SVs). The most significant association between a SV and a trait not identified using SNP markers was a QTL for northern leaf blight (NLB) on chromosome 10 (**Fig. S13F**). This SV is within a gene encoding a thylakoid lumenal protein; such proteins could be linked to plant immunity through the regulation of cell death during viral infection (*47*).

Disease resistance in plants is frequently associated with SV in the form of tandem arrays of resistance genes. Complex arrays of resistance genes are retained, potentially through birth-death dynamics in an evolutionary arms race with pathogens, or through balancing selection for the maintenance of diverse plant defenses (*48*). Nucleotide-binding, leucine-rich-repeat (NLR) proteins provide a common type of resistance. Our data reveal that there are fewer NLR genes in maize than other Poaceae (**Fig. S14**) and that most NAM lines have lost the same clades of NLRs as sorghum (**Fig. S15**). Only one line (CML277) retains the MIC1 NLR clade, which is particularly fast-evolving in Poaceae (*49*). Nevertheless, there is clear NLR variation among the NAM lines (**Fig. S16**), and tropical genomes contain a significantly higher number of NLR genes than temperate genomes (p=0.006), suggesting ongoing co-evolution with pathogens, particularly where disease pressure is high.

The annotated NLR genes were significantly enriched relative to random samples of genes for overlap with SVs (boot-strap permutation test, p<0.001). An extreme example is found

at the *rp1* (resistance to *Puccinia sorghi1*) locus on the short arm of chromosome 10, which is known to be highly variable (*50*). We observed exceptional diversity in the NAM lines with as few as 4 *rp1* copies in P39, and as many as 30 in M37W (**Table S8**). However, due to its repetitive nature, only 18 NAM lines have gapless assemblies of the *rp1* locus.

SVs linked to transposons have been shown, through the modulation of gene expression, to underlie flowering-time adaptation in maize during tropical-to-temperate migration (*51*, *52*). Our SV and TE-annotation pipelines identified the adaptive *CACTA*-like insertion previously reported upstream of the flowering-time locus *ZmCCT10 (52)*. We also surveyed an additional 173 genes linked to flowering-time (*53*, *54*) and discovered three genes (*GL15*, *ZCN10*, and *Dof21*) with TE-derived SVs <5 kbp upstream of their transcription start sites. These SVs distinguish temperate from tropical lines ($t < -2.346$, $p < 0.0358$) (**Fig. S17**) and show significant correlation ($F > 8.658$, $p < 0.001$) with expression levels.

Discovery of candidate cis-regulatory elements through DNA methylation

Based on sequence alone, it can be difficult to distinguish functional regulatory sequences from the multitude of non-functional and potentially deleterious genetic elements in the intergenic spaces. The problem is complicated by the fact that regulatory regions can be separated from their promoters by tens or hundreds of kilobases (*5*, *55*). One way to identify functional regions is to score for unmethylated DNA, which provides both a tissue-independent indicator of gene regulatory elements and evidence that annotated genes are active (*5*, *55*, *56*). To incorporate DNA methylation to the NAM genomes resource, we sequenced enzymatic methyl-seq (EM-seq) libraries from each line and identified methylated bases in three sequence contexts, CG, CHG, and CHH (where H = A, T, or C). The results are consistent across genes and transposons, demonstrating the quality of the libraries (**Figs. S18, S19**). There is minor variation in total methylation across inbreds, with CML247 being noteworthy for uniformly lower CG methylation in several tissues (**Fig. S20)** pointing to the existence of a genetic variant that compromises mCG methylation in this line.

Each of the three methylation contexts reveal information on the locations of repeats, genes and regulatory elements. mCHH levels are generally low in maize except in heterochromatin borders, whereas mCHG is abundant in repetitive regions and depleted from regulatory elements and exons (**Fig. 4**) (*57*). mCG is also depleted from regulatory elements but can be abundant in exons, especially of broadly expressed genes (*58*). Thus, to identify unmethylated regions (UMRs) corresponding to both regulatory elements and gene bodies, we

defined UMRs using a method that takes into account mCHG and mCG but does not exclude high mCG-only regions. Comparison of the 26 methylomes revealed uniformity in number and length of UMRs, averaging about 180 Mbp in total length in each genome (**Figs. S21, S22**). To confirm the accuracy of the UMR data, we also identified accessible chromatin regions (ACRs) using ATAC-seq for each inbred. We expect chromatin to be accessible mainly in the subset of genes expressed in the tissue sampled (primarily leaves) and to show a high level of concordance with UMRs. The data reveal that at least 98% of genic ACRs overlap with UMRs in each genome (**Fig. S23, S24)**. For non-genic ACRs, the percent overlap was lower, but typically greater than 90%.

To assess methylation diversity, we mapped UMRs from all inbreds to the B73 genome. The data reveal that ~95% of genic UMRs identified in one methylome overlap with a UMR in at least one other genome in pairwise comparisons (**Fig. S25**). UMR polymorphism is higher in the intergenic space, particularly among UMRs greater than 5 kbp from genes, where typically ~75% of UMRs identified in one methylome overlap with a UMR identified in any other (**Fig, S25**). Even when the UMR sequence is conserved, its position relative to the closest gene may vary dramatically among inbreds. This is exemplified by the *Miniature Seed1* gene where a UMR proximal to the promoter in Mo18W is displaced nearly 14 kbp upstream in B73 by a single *Huck* element (*Gypsy* LTR superfamily) (**Fig. 4**). The *Huck* insertion is present in 23 of the 26 genomes, and in two of these (Oh43 and CML322), additional nested TE insertions increased the distance between the gene and the UMR to 27 kbp. Although the overlap of UMRs in pairs of lines is generally consistent with genetic distance across NAM lines (**Fig. S26**), UMRs from the inbred Tzi8 were not substantially shared with other tropical genomes. Tzi8 also has longer ACRs (**Fig. S24)** despite grouping well with other tropical lines in terms of gene expression patterns.

Variation in DNA methylation has been associated with adaptive traits in maize (*59*), most likely through effects on gene expression. To estimate how well UMRs predict transcriptional competency in these genomes, we identified a conservative subset of UMRs overlapping genes that were unmethylated in B73 but methylated in at least one other methylome. These differentially methylated regions were strongly correlated with gene expression in B73 and gene silencing in the other genomes (**Fig. 4, Fig. S27**). We further evaluated the enrichment of significant GWAS SNPs across 36 traits in UMRs. Based on genome-wide estimates, UMRs show 2.50- to 3.26-fold enrichment across traits for significant associations. Roughly 18% of SNPs identified by GWAS lie outside of genic regions but within

UMRs (**Table S9**), consistent with the view that UMRs can be used to identify regulatory regions with important roles in determining phenotype (*5*, *55*, *56*).

Summary

Our analysis of 26 genomes has uncovered previously unknown variation in both the genic and repetitive fractions of the pan-genome and provided new evidence of genome reorganization both before and after domestication. The available data will have broad utility for genetic and genomic studies and facilitate rapid associations to phenotyping information from the NAM lines. More generally, these new resources should motivate a shift away from the single reference mindset to a multi-reference view where any one of 26 inbreds, each with different experimental and agronomic advantages, can be deployed for the purposes of basic discovery and crop improvement. All data including annotations for genes, transposons, repeats, centromeres, UMRs, and ACRs are available with browser support at the maize community database, www.MaizeGDB.org.

Acknowledgments:

We appreciate the sequencing services provided by the University of Arizona, Oregon State University, Brigham Young University and the University of Georgia, as well as coordination among sequencing centers provided by Pacific Biosciences. The authors further acknowledge the High Performance Computing facility at Iowa State University (partially funded by NSF 1726447), Minnesota Supercomputing Institute, the Georgia Advanced Computing Resource Center, BlacknBlue high performance computing center at Cold Spring Harbor Laboratory and the participants of the Virtual Maize Annotation Jamboree who evaluated the initial gene predictions for benchmarking and improvements in the final gene annotations.

Funding: Primary support for this work came from a generous grant from the National Science Foundation (IOS-1744001). Additional support came from NSF IOS-1546727 to CNH, USDA 2018-67013-27571 to CNH, USDA-ARS 8062-21000-041-00D and NSF IOS-1127112 to DW, NSF IOS-1546719 to MBH, NSF IOS-1822330 to JRI and MBH, USDA Hatch project CA-D-PLS-2066-H to JRI, NSF IOS-1856627 to RJS, an NSF Postdoctoral Fellowship in Biology DBI-1905869 to APM, NSF Graduate Research Fellowships 1650042 to AIH and 1744592 to SJS, NSF Research Traineeship (DGE-1545463) to Iowa State University (Trainee SJS), USDA-ARS 58-5030-8-064 to MBH and CMA, USDA-ARS project 5030-21000-068-00D to CMA and MW

and NSF IOS-1546657 to JY; **Author contributions:** Conceptualization – RKD, DW, MBH, CNH, JIG; Data curation – MW, AS, KMC, SO, JL, SW, ZL, BW, MKT-R, JLP, EKSC, CMA; Formal analysis – AS, MW, KMC, SO, JL, WAR, TG, AO, YQ, RDC, ST, AIH, SW, ZL, BW, MKT-R, RDP, YZ, CHO, XL, AMG, EB, JLP, NM, SJS, QJ, SP, MLS, KF, JIG; Funding acquisition - RKD, DW, MBH, CNH, JIG; Investigation – DK, DAK, APM, NW, DEH, VL, KF, JIG; Methodology – MBH, DW, CNH, AS, MW, KF, WAR, JL, JIG, JR-I, JY, RKD; Project administration – RKD, MBH, DW, CNH, JIG; Software – AS, DEH, NM, SO; Supervision – MBH, DW, RKD, CNH, JIG, KVK, JIG, RJS, JR-I, JY; Visualization – MW, AS, JL, WAR, YQ, KMC, SO, WAR, RDP, SJS, CNH; Writing – MBH, RKD, CNH, JIG. **Competing interests:** RJS is a co-founder of REquest Genomics, LLC, a company that provides epigenomic services. All other authors declare no competing interests. **Data and materials availability:** Links to all data are provided in supplementary materials.

List of Supplementary Materials:

MAIN PAPER FIGURES

Table 1: Quality metrics for genome assemblies and gene model annotations. Darker shading indicates higher quality.

	B73_v4	B73_v5	B97	Ky21	M162W	Ms71	OH43	OH7B	M37W	Mo18W	Tx303	HP301	P39	Il14H	CML52	CML69	CML103	CML228	CML247	CML277	CML322	CML333	Ki3	Ki11	NC350	NC358	Tzi8
Assembly Size (Mb)	2134	2182	2193	2172	2184	2214	2177	2165	2192	2223	2216	2141	2139	2125	2308	2225	2162	2301	2215	2191	2219	2231	2216	2274	2291	2227	2271
Contig N50 (Mb)	1.2	52.36	49.77	19.07	27.81	34.1	28.63	13.62	39.62	24.98	27.97	35.6	35.78	19.64	11.2	21.34	11.34	9.553	11.43	6.255	30.49	28.82	16.18	31.4	49	25.94	11.61
Scaffold N50 (Mb)	10.69	160.85	137.68	115.38	111.38	98.45	105.60	140.13	105.37	111.10	99.16	135.87	147.88	135.80	92.05	107.57	129.92	108.07	101.10	98.85	102.20	99.84	107.93	110.07	100.66	98.95	100.58
Pseudomolecule % N	1.43	0.175	0.156	0.306	0.175	0.23	0.121	0.407	0.087	0.338	0.314	0.198	0.117	0.158	0.936	0.296	0.241	1.207	0.459	0.426	0.144	0.146	0.392	0.121	0.072	0.175	0.567
BUSCO (% complete)	95.70	95.76	95.69	96.04	96.04	95.97	95.76	95.76	95.97	96.60	95.83	95.63	95.76	95.63	95.76	95.90	95.56	96.25	96.32	96.18	95.42	96.32	96.67	95.83	96.18	96.18	96.11
LTR Assembly Index (LAI)	26.68	27.84	28.06	28.08	28.09	27.91	27.89	28.04	28.09	27.81	27.71	28.05	27.61	27.83	27.92	28.34	28.3	27.93	28.44	27.95	28.44	28.33	28.27	27.64	27.96	28.22	27.9
CentC (% assembled)	17.52	87.94	38.89	56.78	44.54	75.47	66.73	47.55	79.84	75.75	76.42	65.64	69.96	55.31	45.25	56.92	54.95	55.32	47.43	29.33	69.96	69.24	43.82	74.21	64.18	52.69	62.81
Knob180 (% assembled)	5.651	18.63	8.24	8.96	7.89	7.79	4.34	8.35	6.91	10.73	7.49	22	22.24	55.54	4.89	2.21	10.57	3.97	3.65	3.2	4.73	3.83	3.44	12.71	13.9	5.61	2.7
TR-1 (% assembled)	23.01	89.43	66.41	15.67	36.98	25.13	8.26	36.76	79.14	13.93	34.96	110.8	42.22	86.81	6.93	3.17	8.45	3.3	5.54	9.55	4.08	11.42	10.76	20.3	12.6	5.29	2.48
rDNA arrays (% assembled)	0.352	9.41	7.16	10.71	8.76	6.05	6.5	9.74	7.5	16.34	6.38	13.54	6.53	6.89	13.5	9.77	8.33	5.64	8.48	8.02	11.56	11.64	7.33	3.97	10.9	9.44	7.88
Subtelomere (% assembled)	1.963	90.31	69	52.2	73.43	60.75	60.06	48.66	70.63	70.47	68.71	65.19	116.5	97.04	19.65	85.34	34.06	85.15	52.76	32.95	94.6	70.27	86.82	91.63	88.51	64.07	83.64
Gene Length (average)	4163	4477	4403	4371	4403	4349	4408	4332	4377	4327	4278	4405	4232	4337	4477	4446	4436	4318	4564	4348	4280	4432	4439	4442	4445	4406	4382
Genic Space Annotated (%)	8.03	8.17	8.12	8.23	8.38	8.12	8.25	7.97	8.17	8.05	7.97	8.2	8.22	8.24	7.93	8.07	8.23	7.9	8.36	8.04	7.94	8.04	8.26	7.8	7.86	7.88	8.07

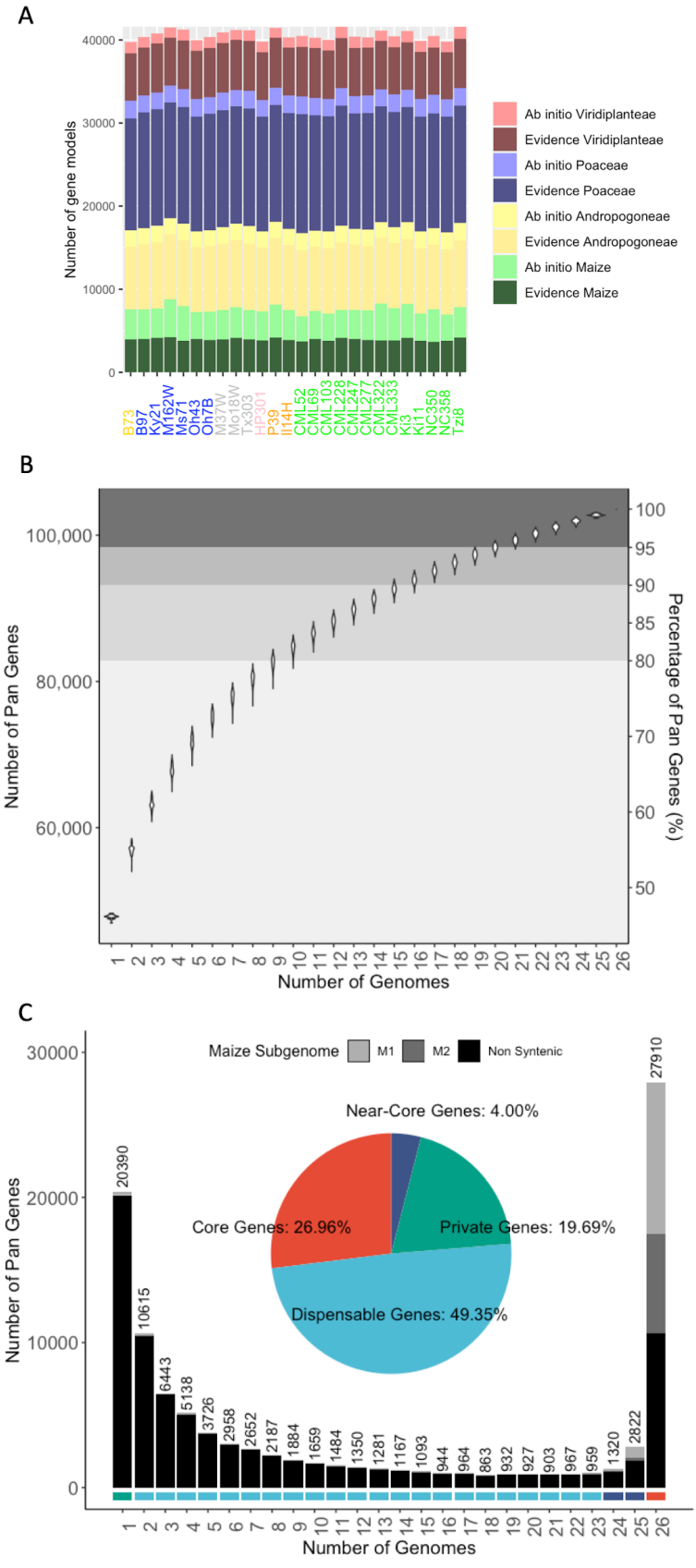

Figure 1. The gene space in the NAM genomes. **A**) Pan-genes categorized by annotation method and phylostrata. Genes annotated with evidence have mRNA support whereas *ab initio* genes are predicted based on DNA sequence alone. Genes within progressing phylostrata - species *Zea mays* (maize), tribe *Andropogoneae*, family *Poaceae*, kingdom *Viridiplantae* - are more conserved. **B**) The number of pan-genes added with each additional genome assembly. The error bars reflect different outcomes when the order of genomes was changed (the data were bootstrapped 1000 times). **C**) Frequency of pan-genes in the NAM genomes. The lower graph shows the number of genes present in only one genome (private), present in 2-23 genomes (dispensable), present in 24 or 25 genomes (near-core), and present in all 26 genomes (core). Grey shades indicate the proportion present in syntenic (M1 and M2 genomes) and non-syntenic positions. For B and C, tandem duplicates were considered as a single gene.

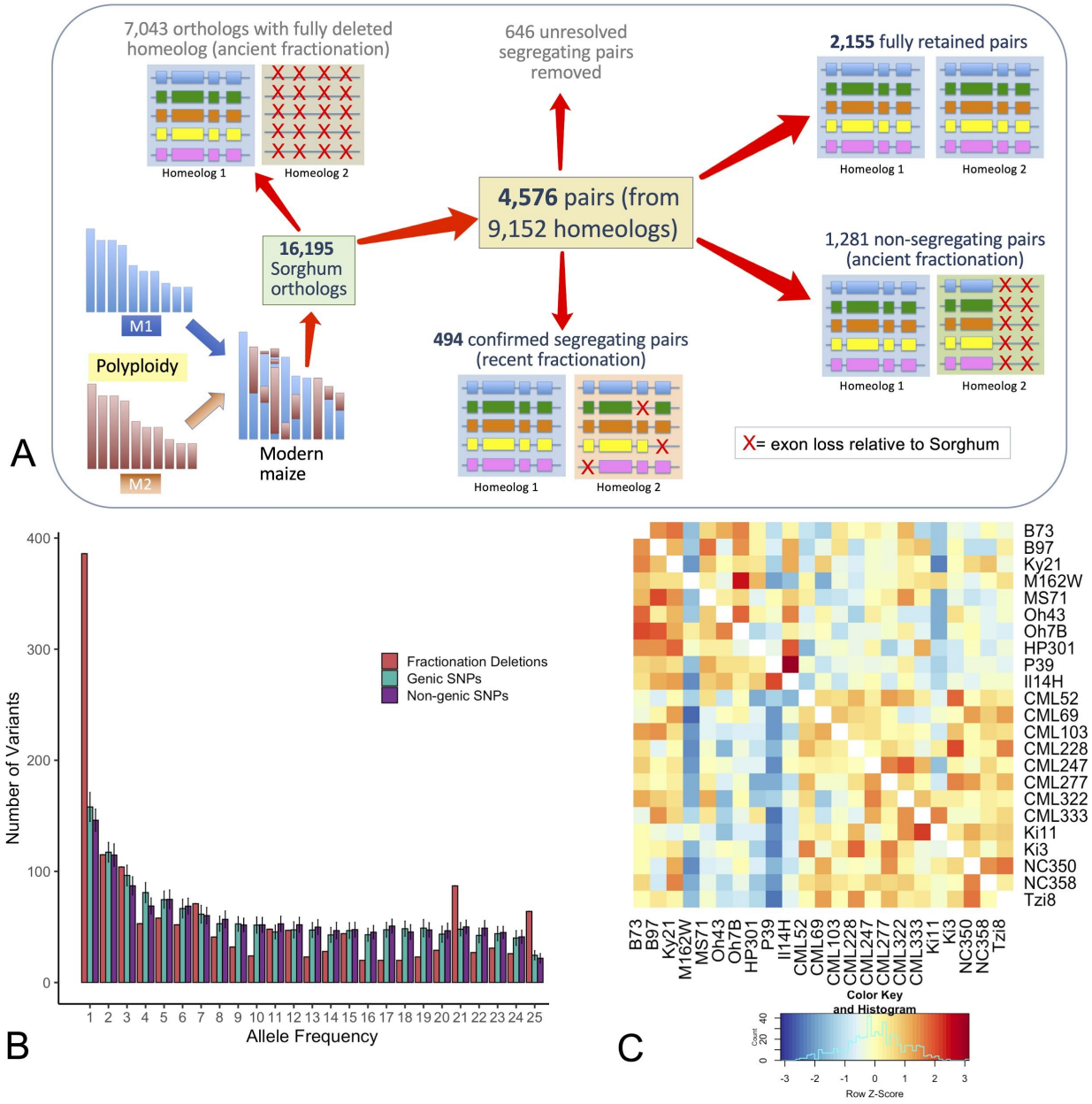

Figure 2. The tempo of fractionation in maize. **A**) Schematic showing how genes were categorized. 16,195 conservatively chosen orthologs were subdivided into classes representing retained pairs, ancient fractionation, and recent fractionation. **B**) Unfolded site frequency spectrum (SFS) of segregating exon loss and non-coding SNPs (genic and non-genic) using sorghum to define the ancestral state. **C**) Heatmap of the number of co-retained exons between any two NAM lines. Lines with mixed ancestry (M37W, Mo18W, Tx303) are excluded. Colors indicate the Z-score (the difference measured in standard deviations between a single pairwise comparison and all others in the row).

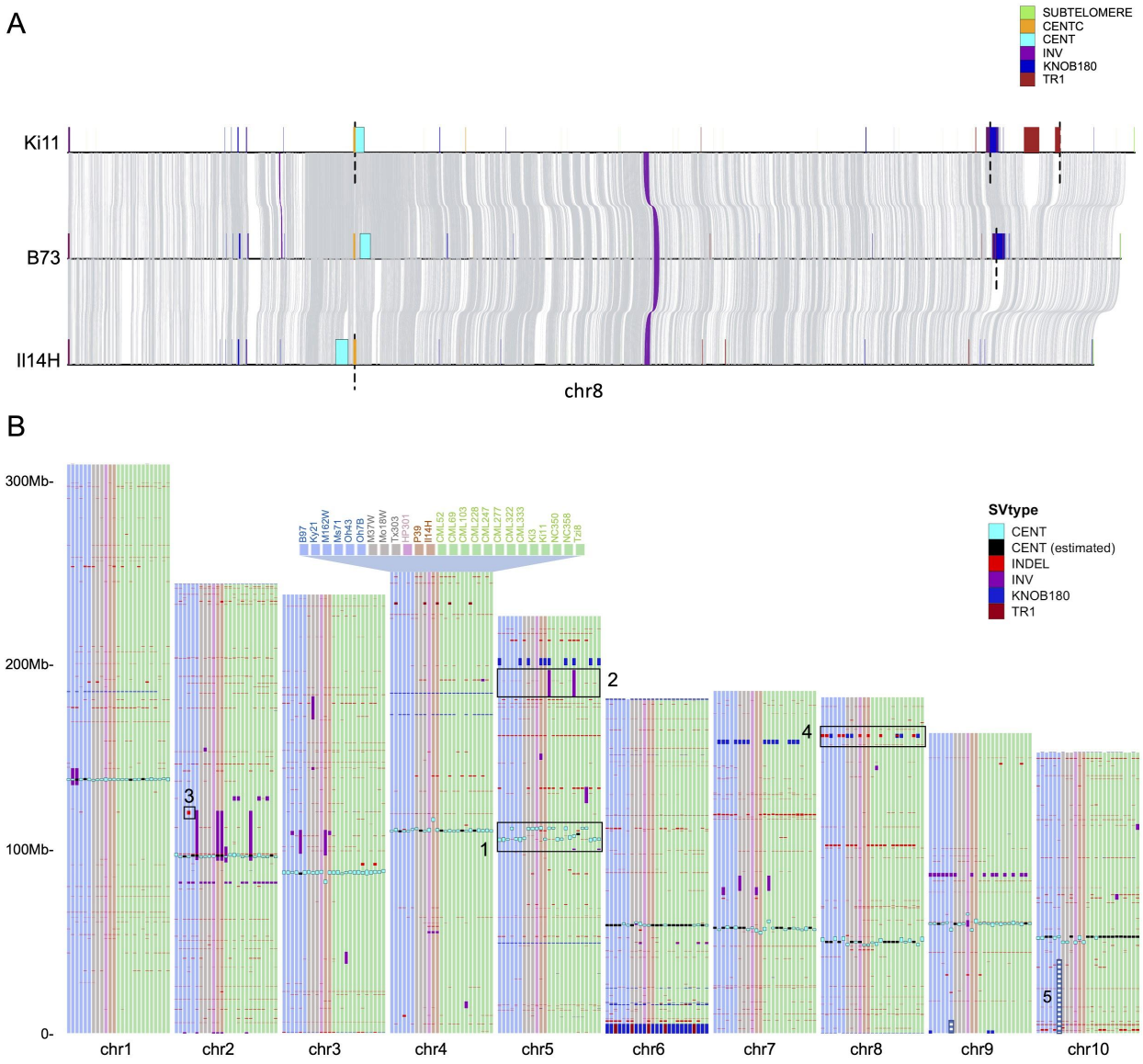

Figure 3. Structural variation in the NAM founders. **A**) Pairwise alignments between Ki11, B73, Il14H on chromosome 8. Grey links represent syntenic aligned regions; gaps of unknown size (scaffold gaps) are marked by dashed lines. **B**) Large (>100 kbp) structural variants, centromeres, and knobs across the NAM lines versus the B73 reference. The subset of SVs larger than 1 Mbp were manually curated, and only those containing genes are represented. Features 1-5 highlight major SVs: 1) Multiple centromere movement events; 2) A major inversion hypothesized to suppress recombination; 3) A large deletion in the Ms71 inbred; 4) Knob polymorphism; 5) Reciprocal translocation between chromosome 9 and 10 in the Oh7B inbred (both segments placed in their standard positions for display).

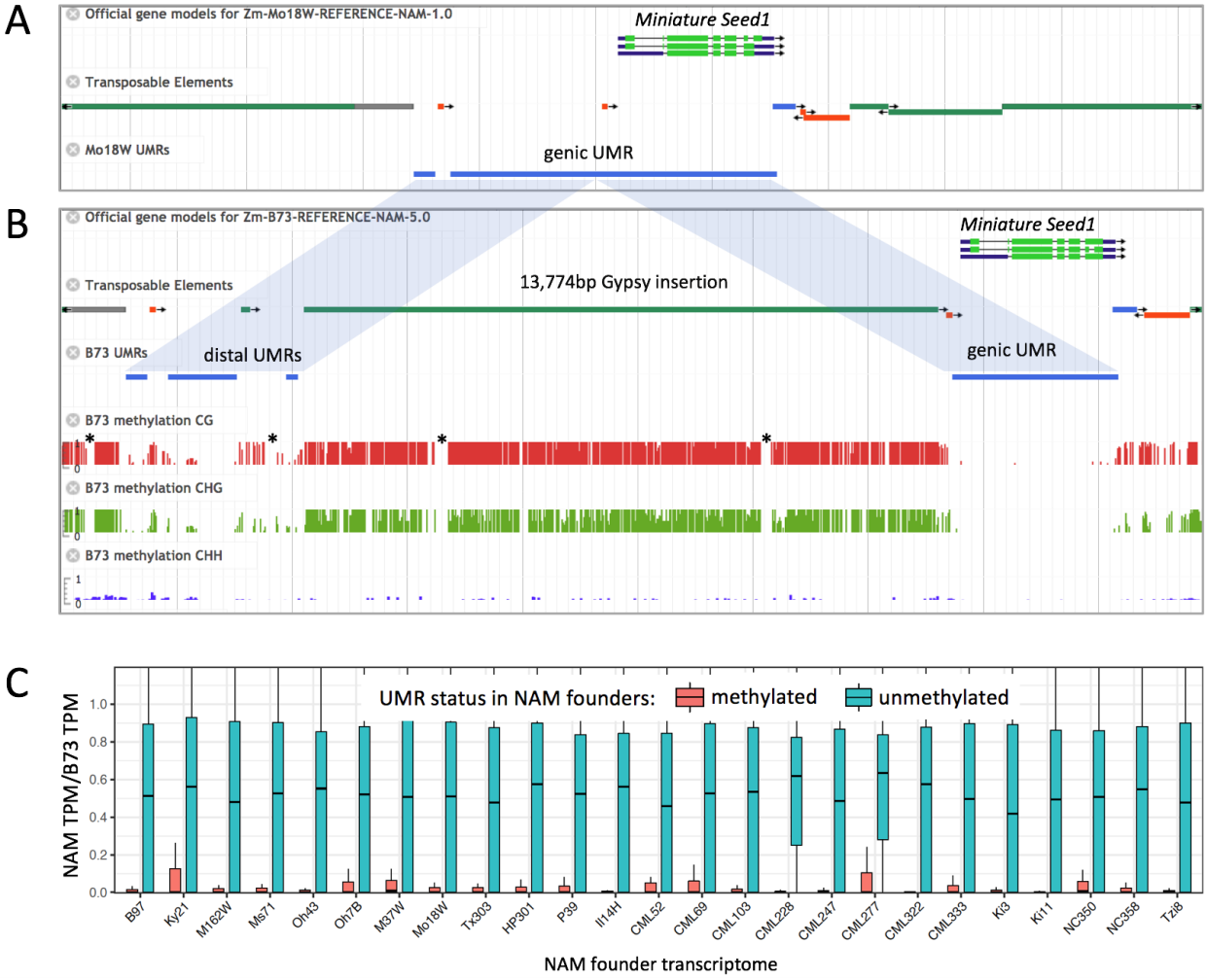

Figure 4. UMR variation across the NAM founders. **A**) Annotation of the *Miniature seed1* gene in the Mo17W inbred. An image from MaizeGDB browser shows gene, TE, and UMR tracks. TE tracks are color-coded by superfamily: green/grey = LTR, red = TIR, blue = LINE. The grey vertical lines show 2.5 kbp intervals. **B**) Annotation and underlying methylation data for *Miniature seed1* in the B73 inbred. The insertion of a *Gypsy* element moved part of the proximal UMR to a position 14 kbp upstream from the transcription start site (TSS). Methylation tracks indicate base-pair level methylation values from 0 to 100%. Asterisks indicate gaps in coverage, which are visible in separate tracks not shown here. **C**) Relationship between methylation and gene expression. UMRs were mapped to B73 to identify UMRs that overlap with TSS. The Y axis indicates the ratio of transcripts per million (TPM, compared to B73) when the region is methylated (red) or unmethylated (teal).

References Cited

1. C. N. Hirsch, J. M. Foerster, J. M. Johnson, R. S. Sekhon, G. Muttoni, B. Vaillancourt, F. Peñagaricano, E. Lindquist, M. A. Pedraza, K. Barry, N. de Leon, S. M. Kaeppler, C. R. Buell, Insights into the maize pan-genome and pan-transcriptome. *Plant Cell*. **26**, 121–135 (2014).

2. C. N. Hirsch, C. D. Hirsch, A. B. Brohammer, M. J. Bowman, I. Soifer, O. Barad, D. Shem-Tov, K. Baruch, F. Lu, A. G. Hernandez, C. J. Fields, C. L. Wright, K. Koehler, N. M. Springer, E. Buckler, C. R. Buell, N. de Leon, S. M. Kaeppler, K. L. Childs, M. A. Mikel, Draft Assembly of Elite Inbred Line PH207 Provides Insights into Genomic and Transcriptome Diversity in Maize. *Plant Cell*. **28**, 2700–2714 (2016).

3. M. Jin, H. Liu, C. He, J. Fu, Y. Xiao, Y. Wang, W. Xie, G. Wang, J. Yan, Maize pan-transcriptome provides novel insights into genome complexity and quantitative trait variation. *Sci. Rep.* **6**, 18936 (2016).

4. F. Lu, M. C. Romay, J. C. Glaubitz, P. J. Bradbury, R. J. Elshire, T. Wang, Y. Li, Y. Li, K. Semagn, X. Zhang, A. G. Hernandez, M. A. Mikel, I. Soifer, O. Barad, E. S. Buckler, High-resolution genetic mapping of maize pan-genome sequence anchors. *Nat. Commun.* **6**, 6914 (2015).

5. W. A. Ricci, Z. Lu, L. Ji, A. P. Marand, C. L. Ethridge, N. G. Murphy, J. M. Noshay, M. Galli, M. K. Mejía-Guerra, M. Colomé-Tatché, F. Johannes, M. J. Rowley, V. G. Corces, J. Zhai, M. J. Scanlon, E. S. Buckler, A. Gallavotti, N. M. Springer, R. J. Schmitz, X. Zhang, Widespread long-range cis-regulatory elements in the maize genome. *Nature Plants* (2019), doi:10.1038/s41477-019-0547-0.

6. S. Sun, Y. Zhou, J. Chen, J. Shi, H. Zhao, H. Zhao, W. Song, M. Zhang, Y. Cui, X. Dong, H. Liu, X. Ma, Y. Jiao, B. Wang, X. Wei, J. C. Stein, J. C. Glaubitz, F. Lu, G. Yu, C. Liang, K. Fengler, B. Li, A. Rafalski, P. S. Schnable, D. H. Ware, E. S. Buckler, J. Lai, Extensive intraspecific gene order and gene structural variations between Mo17 and other maize genomes. *Nat. Genet.* **50**, 1289–1295 (2018).

7. G. Haberer, N. Kamal, E. Bauer, H. Gundlach, I. Fischer, M. A. Seidel, M. Spannagl, C. Marcon, A. Ruban, C. Urbany, A. Nemri, F. Hochholdinger, M. Ouzunova, A. Houben, C.-C. Schön, K. F. X. Mayer, European maize genomes highlight intraspecies variation in repeat and gene content. *Nat. Genet.* **52**, 950–957 (2020).

8. N. Yang, J. Liu, Q. Gao, S. Gui, L. Chen, L. Yang, J. Huang, T. Deng, J. Luo, L. He, Y. Wang, P. Xu, Y. Peng, Z. Shi, L. Lan, Z. Ma, X. Yang, Q. Zhang, M. Bai, S. Li, W. Li, L. Liu, D. Jackson, J. Yan, Genome assembly of a tropical maize inbred line provides insights into structural variation and crop improvement. *Nat. Genet.* **51**, 1052–1059 (2019).

9. G. Lin, C. He, J. Zheng, D.-H. Koo, H. Le, H. Zheng, T. M. Tamang, J. Lin, Y. Liu, M. Zhao, Y. Hao, F. McFraland, B. Wang, Y. Qin, H. Tang, D. R. McCarty, H. Wei, M.-J. Cho, S. Park, H. Kaeppler, S. M. Kaeppler, Y. Liu, N. Springer, P. S. Schnable, G. Wang, F. F. White, S. Liu, Chromosome-level Genome Assembly of a Regenerable Maize Inbred Line A188 (2020), p. 2020.09.09.289611.

10. N. M. Springer, S. N. Anderson, C. M. Andorf, K. R. Ahern, F. Bai, O. Barad, W. B.

Barbazuk, H. W. Bass, K. Baruch, G. Ben-Zvi, E. S. Buckler, R. Bukowski, M. S. Campbell, E. K. S. Cannon, P. Chomet, R. K. Dawe, R. Davenport, H. K. Dooner, L. H. Du, C. Du, K. A. Easterling, C. Gault, J.-C. Guan, C. T. Hunter, G. Jander, Y. Jiao, K. E. Koch, G. Kol, T. G. Köllner, T. Kudo, Q. Li, F. Lu, D. Mayfield-Jones, W. Mei, D. R. McCarty, J. M. Noshay, J. L. Portwood 2nd, G. Ronen, A. M. Settles, D. Shem-Tov, J. Shi, I. Soifer, J. C. Stein, M. C. Stitzer, M. Suzuki, D. L. Vera, E. Vollbrecht, J. T. Vrebalov, D. Ware, S. Wei, K. Wimalanathan, M. R. Woodhouse, W. Xiong, T. P. Brutnell, The maize W22 genome provides a foundation for functional genomics and transposon biology. *Nat. Genet.* **50**, 1282–1288 (2018).

11. M. D. McMullen, S. Kresovich, H. S. Villeda, P. Bradbury, H. Li, Q. Sun, S. Flint-Garcia, J. Thornsberry, C. Acharya, C. Bottoms, P. Brown, C. Browne, M. Eller, K. Guill, C. Harjes, D. Kroon, N. Lepak, S. E. Mitchell, B. Peterson, G. Pressoir, S. Romero, M. Oropeza Rosas, S. Salvo, H. Yates, M. Hanson, E. Jones, S. Smith, J. C. Glaubitz, M. Goodman, D. Ware, J. B. Holland, E. S. Buckler, Genetic properties of the maize nested association mapping population. *Science*. **325**, 737–740 (2009).

12. J. Yu, J. B. Holland, M. D. McMullen, E. S. Buckler, Genetic design and statistical power of nested association mapping in maize. *Genetics*. **178**, 539–551 (2008).

13. J. G. Wallace, P. J. Bradbury, N. Zhang, Y. Gibon, M. Stitt, E. S. Buckler, Association mapping across numerous traits reveals patterns of functional variation in maize. *PLoS Genet.* **10**, e1004845 (2014).

14. S. R. Eichten, R. Briskine, J. Song, Q. Li, R. Swanson-Wagner, P. J. Hermanson, A. J. Waters, E. Starr, P. T. West, P. Tiffin, C. L. Myers, M. W. Vaughn, N. M. Springer, Epigenetic and genetic influences on DNA methylation variation in maize populations. *Plant Cell*. **25**, 2783–2797 (2013).

15. E. Rodgers-Melnick, P. J. Bradbury, R. J. Elshire, J. C. Glaubitz, C. B. Acharya, S. E. Mitchell, C. Li, Y. Li, E. S. Buckler, Recombination in diverse maize is stable, predictable, and associated with genetic load. *Proc. Natl. Acad. Sci. U. S. A.* **112**, 3823–3828 (2015).

16. R. J. Schaefer, J.-M. Michno, J. Jeffers, O. Hoekenga, B. Dilkes, I. Baxter, C. L. Myers, Integrating Coexpression Networks with GWAS to Prioritize Causal Genes in Maize. *The Plant Cell*. **30** (2018), pp. 2922–2942.

17. F. A. Simão, R. M. Waterhouse, P. Ioannidis, E. V. Kriventseva, E. M. Zdobnov, BUSCO: assessing genome assembly and annotation completeness with single-copy orthologs. *Bioinformatics*. **31**, 3210–3212 (2015).

18. S. Ou, J. Chen, N. Jiang, Assessing genome assembly quality using the LTR Assembly Index (LAI). *Nucleic Acids Research* (2018), , doi:10.1093/nar/gky730.

19. K. Eilbeck, B. Moore, C. Holt, M. Yandell, Quantitative measures for the management and comparison of annotated genomes. *BMC Bioinformatics*. **10**, 67 (2009).

20. M. Law, K. L. Childs, M. S. Campbell, J. C. Stein, A. J. Olson, C. Holt, N. Panchy, J. Lei, D. Jiao, C. M. Andorf, C. J. Lawrence, D. Ware, S.-H. Shiu, Y. Sun, N. Jiang, M. Yandell, Automated update, revision, and quality control of the maize genome annotations using MAKER-P improves the B73 RefGen_v3 gene models and identifies new genes. *Plant Physiol.* **167**, 25–39 (2015).

21. Y. Jiao, P. Peluso, J. Shi, T. Liang, M. C. Stitzer, B. Wang, M. S. Campbell, J. C. Stein, X. Wei, C.-S. Chin, K. Guill, M. Regulski, S. Kumari, A. Olson, J. Gent, K. L. Schneider, T. K. Wolfgruber, M. R. May, N. M. Springer, E. Antoniou, W. R. McCombie, G. G. Presting, M. McMullen, J. Ross-Ibarra, R. K. Dawe, A. Hastie, D. R. Rank, D. Ware, Improved maize reference genome with single-molecule technologies. *Nature*. **546**, 524–527 (2017).

22. R. F. McCormick, S. K. Truong, A. Sreedasyam, J. Jenkins, S. Shu, D. Sims, M. Kennedy, M. Amirebrahimi, B. D. Weers, B. McKinley, A. Mattison, D. T. Morishige, J. Grimwood, J. Schmutz, J. E. Mullet, The Sorghum bicolor reference genome: improved assembly, gene annotations, a transcriptome atlas, and signatures of genome organization. *Plant J.* **93**, 338–354 (2018).

23. Z. Swigonová, J. Lai, J. Ma, W. Ramakrishna, V. Llaca, J. L. Bennetzen, J. Messing, Close split of sorghum and maize genome progenitors. *Genome Res.* **14**, 1916–1923 (2004).

24. X. Wang, J. Wang, D. Jin, H. Guo, T.-H. Lee, T. Liu, A. H. Paterson, Genome Alignment Spanning Major Poaceae Lineages Reveals Heterogeneous Evolutionary Rates and Alters Inferred Dates for Key Evolutionary Events. *Mol. Plant*. **8**, 885–898 (2015).

25. J. C. Schnable, N. M. Springer, M. Freeling, Differentiation of the maize subgenomes by genome dominance and both ancient and ongoing gene loss. *Proc. Natl. Acad. Sci. U. S. A.* **108**, 4069–4074 (2011).

26. M. R. Woodhouse, J. C. Schnable, B. S. Pedersen, E. Lyons, D. Lisch, S. Subramaniam, M. Freeling, Following tetraploidy in maize, a short deletion mechanism removed genes preferentially from one of the two homologs. *PLoS Biol.* **8**, e1000409 (2010).

27. J. C. Schnable, M. Freeling, E. Lyons, Genome-wide analysis of syntenic gene deletion in the grasses. *Genome Biol. Evol.* **4**, 265–277 (2012).

28. T. Mandáková, S. Joly, M. Krzywinski, K. Mummenhoff, M. A. Lysak, Fast diploidization in close mesopolyploid relatives of Arabidopsis. *Plant Cell*. **22**, 2277–2290 (2010).

29. A. B. Brohammer, T. J. Y. Kono, N. M. Springer, S. E. McGaugh, C. N. Hirsch, The limited role of differential fractionation in genome content variation and function in maize (Zea mays L.) inbred lines. *Plant J.* **93**, 131–141 (2018).

30. H. Tang, M. R. Woodhouse, F. Cheng, J. C. Schnable, B. S. Pedersen, G. Conant, X. Wang, M. Freeling, J. C. Pires, Altered patterns of fractionation and exon deletions in Brassica rapa support a two-step model of paleohexaploidy. *Genetics*. **190**, 1563–1574 (2012).

31. T. M. Beissinger, L. Wang, K. Crosby, A. Durvasula, Recent demography drives changes in linked selection across the maize genome. *Nature plants* (2016) (available at https://idp.nature.com/authorize/casa?redirect_uri=https://www.nature.com/articles/nplants201684&casa_token=7sFGx3N5XbMAAAAA:x3XPZleo_ibdXWVrF14tBCL2cGPlEWvm6pwWeEBkNSfjy9c02HFP70RmYWV8zfVG6gpYK22vcFqFZXpm2g).

32. M. Freeling, Bias in plant gene content following different sorts of duplication: tandem, whole-genome, segmental, or by transposition. *Annu. Rev. Plant Biol.* **60**, 433–453 (2009).

33. F. Cheng, J. Wu, X. Cai, J. Liang, M. Freeling, X. Wang, Gene retention, fractionation and

subgenome differences in polyploid plants. *Nat Plants*. **4**, 258–268 (2018).

34. S. Ou, W. Su, Y. Liao, K. Chougule, D. Ware, T. Peterson, N. Jiang, C. N. Hirsch, M. B. Hufford, Benchmarking Transposable Element Annotation Methods for Creation of a Streamlined, Comprehensive Pipeline. *bioRxiv* (2019), p. 657890.

35. R. S. Baucom, J. C. Estill, C. Chaparro, N. Upshaw, A. Jogi, J.-M. Deragon, R. P. Westerman, P. J. Sanmiguel, J. L. Bennetzen, Exceptional diversity, non-random distribution, and rapid evolution of retroelements in the B73 maize genome. *PLoS Genet.* **5**, e1000732 (2009).

36. P. Bilinski, P. S. Albert, J. J. Berg, J. A. Birchler, M. N. Grote, A. Lorant, J. Quezada, K. Swarts, J. Yang, J. Ross-Ibarra, Parallel altitudinal clines reveal trends in adaptive evolution of genome size in Zea mays. *PLoS Genet.* **14**, e1007162 (2018).

37. R. K. Dawe, E. G. Lowry, J. I. Gent, M. C. Stitzer, K. W. Swentowsky, D. M. Higgins, J. Ross-Ibarra, J. G. Wallace, L. B. Kanizay, M. Alabady, W. Qiu, K.-F. Tseng, N. Wang, Z. Gao, J. A. Birchler, A. E. Harkess, A. L. Hodges, E. N. Hiatt, A Kinesin-14 Motor Activates Neocentromeres to Promote Meiotic Drive in Maize. *Cell*. **173**, 839–850.e18 (2018).

38. P. S. Albert, Z. Gao, T. V. Danilova, J. A. Birchler, Diversity of chromosomal karyotypes in maize and its relatives. *Cytogenet. Genome Res.* **129**, 6–16 (2010).

39. K. L. Schneider, Z. Xie, T. K. Wolfgruber, G. G. Presting, Inbreeding drives maize centromere evolution. *Proc. Natl. Acad. Sci. U. S. A.* **113**, E987–96 (2016).

40. N. Wang, J. Liu, W. A. Ricci, J. Gent, R. Kelly Dawe, Maize centromeric chromatin scales with changes in genome size. *Cold Spring Harbor Laboratory* (2020), p. 2020.11.05.370262.

41. K. W. Swentowsky, J. I. Gent, E. G. Lowry, V. Schubert, X. Ran, K.-F. Tseng, A. E. Harkess, W. Qiu, R. K. Dawe, Distinct kinesin motors drive two types of maize neocentromeres. *Genes Dev.* **34**, 1239–1251 (2020).

42. J. Liu, A. S. Seetharam, K. Chougule, S. Ou, K. W. Swentowsky, J. I. Gent, V. Llaca, M. R. Woodhouse, N. Manchanda, G. G. Presting, D. A. Kudrna, M. Alabady, C. N. Hirsch, K. A. Fengler, D. Ware, T. P. Michael, M. B. Hufford, R. K. Dawe, Gapless assembly of maize chromosomes using long-read technologies. *Genome Biol.* **21**, 121 (2020).

43. J.-M. Chia, C. Song, P. J. Bradbury, D. Costich, N. de Leon, J. Doebley, R. J. Elshire, B. Gaut, L. Geller, J. C. Glaubitz, M. Gore, K. E. Guill, J. Holland, M. B. Hufford, J. Lai, M. Li, X. Liu, Y. Lu, R. McCombie, R. Nelson, J. Poland, B. M. Prasanna, T. Pyhäjärvi, T. Rong, R. S. Sekhon, Q. Sun, M. I. Tenaillon, F. Tian, J. Wang, X. Xu, Z. Zhang, S. M. Kaeppler, J. Ross-Ibarra, M. D. McMullen, E. S. Buckler, G. Zhang, Y. Xu, D. Ware, Maize HapMap2 identifies extant variation from a genome in flux. *Nat. Genet.* **44**, 803–807 (2012).

44. H. J. Abel, D. E. Larson, A. A. Regier, C. Chiang, I. Das, K. L. Kanchi, R. M. Layer, B. M. Neale, W. J. Salerno, C. Reeves, S. Buyske, NHGRI Centers for Common Disease Genomics, T. C. Matise, D. M. Muzny, M. C. Zody, E. S. Lander, S. K. Dutcher, N. O. Stitziel, I. M. Hall, Mapping and characterization of structural variation in 17,795 human genomes. *Nature*. **583**, 83–89 (2020).

45. E. V. Leushkin, G. A. Bazykin, A. S. Kondrashov, Strong mutational bias toward deletions in the Drosophila melanogaster genome is compensated by selection. *Genome Biol. Evol.* **5**, 514–524 (2013).

46. E. K. F. Chan, H. C. Rowe, B. G. Hansen, D. J. Kliebenstein, The complex genetic architecture of the metabolome. *PLoS Genet.* **6**, e1001198 (2010).

47. S. Seo, M. Okamoto, T. Iwai, M. Iwano, K. Fukui, A. Isogai, N. Nakajima, Y. Ohashi, Reduced Levels of Chloroplast FtsH Protein in Tobacco Mosaic Virus-Infected Tobacco Leaves Accelerate the Hypersensitive Reaction. *The Plant Cell*. **12** (2000), p. 917.

48. H. Mizuno, S. Katagiri, H. Kanamori, Y. Mukai, T. Sasaki, T. Matsumoto, J. Wu, Evolutionary dynamics and impacts of chromosome regions carrying R-gene clusters in rice. *Sci. Rep.* **10**, 872 (2020).

49. P. C. Bailey, C. Schudoma, W. Jackson, E. Baggs, G. Dagdas, W. Haerty, M. Moscou, K. V. Krasileva, Dominant integration locus drives continuous diversification of plant immune receptors with exogenous domain fusions. *Genome Biol.* **19**, 23 (2018).

50. S. H. Hulbert, J. L. Bennetzen, Recombination at the Rp1 locus of maize. *Mol. Gen. Genet.* **226**, 377–382 (1991).

51. C. Huang, H. Sun, D. Xu, Q. Chen, Y. Liang, X. Wang, G. Xu, J. Tian, C. Wang, D. Li, L. Wu, X. Yang, W. Jin, J. F. Doebley, F. Tian, ZmCCT9 enhances maize adaptation to higher latitudes. *Proc. Natl. Acad. Sci. U. S. A.* **115**, E334–E341 (2018).

52. Q. Yang, Z. Li, W. Li, L. Ku, C. Wang, J. Ye, K. Li, N. Yang, Y. Li, T. Zhong, J. Li, Y. Chen, J. Yan, X. Yang, M. Xu, CACTA-like transposable element in ZmCCT attenuated photoperiod sensitivity and accelerated the postdomestication spread of maize. *Proc. Natl. Acad. Sci. U. S. A.* **110**, 16969–16974 (2013).

53. Z. Dong, O. Danilevskaya, T. Abadie, C. Messina, N. Coles, M. Cooper, A gene regulatory network model for floral transition of the shoot apex in maize and its dynamic modeling. *PLoS One*. **7**, e43450 (2012).

54. Y.-X. Li, C. Li, P. J. Bradbury, X. Liu, F. Lu, C. M. Romay, J. C. Glaubitz, X. Wu, B. Peng, Y. Shi, Y. Song, D. Zhang, E. S. Buckler, Z. Zhang, Y. Li, T. Wang, Identification of genetic variants associated with maize flowering time using an extremely large multi-genetic background population. *Plant J.* **86**, 391–402 (2016).

55. R. Oka, J. Zicola, B. Weber, S. N. Anderson, C. Hodgman, J. I. Gent, J.-J. Wesselink, N. M. Springer, H. C. J. Hoefsloot, F. Turck, M. Stam, Genome-wide mapping of transcriptional enhancer candidates using DNA and chromatin features in maize. *Genome Biol.* **18**, 137 (2017).

56. P. A. Crisp, A. P. Marand, J. M. Noshay, P. Zhou, Z. Lu, R. J. Schmitz, N. M. Springer, Stable unmethylated DNA demarcates expressed genes and their cis-regulatory space in plant genomes. *Proc. Natl. Acad. Sci. U. S. A.* **117**, 23991–24000 (2020).

57. J. I. Gent, N. A. Ellis, L. Guo, A. E. Harkess, Y. Yao, X. Zhang, R. K. Dawe, CHH islands: de novo DNA methylation in near-gene chromatin regulation in maize. *Genome Res.* **23**, 628–637 (2013).

58. A. J. Bewick, R. J. Schmitz, Gene body DNA methylation in plants. *Curr. Opin. Plant Biol.* **36**, 103–110 (2017).

59. G. Xu, J. Lyu, Q. Li, H. Liu, D. Wang, M. Zhang, N. M. Springer, J. Ross-Ibarra, J. Yang, Evolutionary and functional genomics of DNA methylation in maize domestication and improvement. *Nat. Commun.* **11**, 5539 (2020).

60. S. Ou, J. Liu, K. M. Chougule, A. Fungtammasan, A. Seetharam, J. Stein, V. Llaca, N. Manchanda, A. M. Gilbert, X. Wei, C.-S. Chin, D. E. Hufnagel, S. Pedersen, S. Snodgrass, K. Fengler, M. Woodhouse, B. P. Walenz, S. Koren, A. M. Phillippy, B. Hannigan, R. Kelly Dawe, C. N. Hirsch, M. B. Hufford, D. Ware, Effect of Sequence Depth and Length in Long-read Assembly of the Maize Inbred NC358. *bioRxiv* (2019), p. 858365.

61. J. J. Doyle, J. L. Doyle, A rapid DNA isolation procedure for small quantities of fresh leaf tissue. *Phytochemical Bulletin*. **19**, 11–15 (1987).

62. M. Luo, R. A. Wing, An improved method for plant BAC library construction. *Methods Mol. Biol.* **236**, 3–20 (2003).

63. M. Vasimuddin, S. Misra, H. Li, S. Aluru, in *2019 IEEE International Parallel and Distributed Processing Symposium (IPDPS)* (2019), pp. 314–324.

64. R. Poplin, V. Ruano-Rubio, M. A. DePristo, T. J. Fennell, M. O. Carneiro, G. A. Van der Auwera, D. E. Kling, L. D. Gauthier, A. Levy-Moonshine, D. Roazen, K. Shakir, J. Thibault, S. Chandran, C. Whelan, M. Lek, S. Gabriel, M. J. Daly, B. Neale, D. G. MacArthur, E. Banks, Scaling accurate genetic variant discovery to tens of thousands of samples. *Cold Spring Harbor Laboratory* (2018), p. 201178.

65. T.-H. Lee, H. Guo, X. Wang, C. Kim, A. H. Paterson, SNPhylo: a pipeline to construct a phylogenetic tree from huge SNP data. *BMC Genomics*. **15**, 162 (2014).

66. C.-S. Chin, P. Peluso, F. J. Sedlazeck, M. Nattestad, G. T. Concepcion, A. Clum, C. Dunn, R. O'Malley, R. Figueroa-Balderas, A. Morales-Cruz, G. R. Cramer, M. Delledonne, C. Luo, J. R. Ecker, D. Cantu, D. R. Rank, M. C. Schatz, Phased diploid genome assembly with single-molecule real-time sequencing. *Nat. Methods*. **13**, 1050–1054 (2016).

67. S. Koren, B. P. Walenz, K. Berlin, J. R. Miller, N. H. Bergman, A. M. Phillippy, Canu: scalable and accurate long-read assembly via adaptive k-mer weighting and repeat separation. *Genome Res.* **27**, 722–736 (2017).

68. H. Li, Minimap2: pairwise alignment for nucleotide sequences. *Bioinformatics*. **34**, 3094–3100 (2018).

69. H. Tang, X. Zhang, C. Miao, J. Zhang, R. Ming, J. C. Schnable, P. S. Schnable, E. Lyons, J. Lu, ALLMAPS: robust scaffold ordering based on multiple maps. *Genome Biol.* **16**, 3 (2015).

70. M. Lee, N. Sharopova, W. D. Beavis, D. Grant, M. Katt, D. Blair, A. Hallauer, Expanding the genetic map of maize with the intermated B73 x Mo17 (IBM) population. *Plant Mol. Biol.* **48**, 453–461 (2002).

71. CyVerse Data Commons, (available at

http://datacommons.cyverse.org/browse/iplant/home/shared/commons_repo/curated/Daniel_Laspisa_B73_RefGen_v4CEN_Feb_2019).

72. S. Deschamps, Y. Zhang, V. Llaca, L. Ye, A. Sanyal, M. King, G. May, H. Lin, A chromosome-scale assembly of the sorghum genome using nanopore sequencing and optical mapping. *Nat. Commun.* **9**, 4844 (2018).

73. R. Vaser, I. Sović, N. Nagarajan, M. Šikić, Fast and accurate de novo genome assembly from long uncorrected reads. *Genome Res.* **27**, 737–746 (2017).

74. J. M. Hancock, REPEATMASKER. *Dictionary of Bioinformatics and Computational Biology* (2004), , doi:10.1002/9780471650126.dob0616.pub2.

75. P. S. Schnable, D. Ware, R. S. Fulton, J. C. Stein, F. Wei, S. Pasternak, C. Liang, J. Zhang, L. Fulton, T. A. Graves, P. Minx, A. D. Reily, L. Courtney, S. S. Kruchowski, C. Tomlinson, C. Strong, K. Delehaunty, C. Fronick, B. Courtney, S. M. Rock, E. Belter, F. Du, K. Kim, R. M. Abbott, M. Cotton, A. Levy, P. Marchetto, K. Ochoa, S. M. Jackson, B. Gillam, W. Chen, L. Yan, J. Higginbotham, M. Cardenas, J. Waligorski, E. Applebaum, L. Phelps, J. Falcone, K. Kanchi, T. Thane, A. Scimone, N. Thane, J. Henke, T. Wang, J. Ruppert, N. Shah, K. Rotter, J. Hodges, E. Ingenthron, M. Cordes, S. Kohlberg, J. Sgro, B. Delgado, K. Mead, A. Chinwalla, S. Leonard, K. Crouse, K. Collura, D. Kudrna, J. Currie, R. He, A. Angelova, S. Rajasekar, T. Mueller, R. Lomeli, G. Scara, A. Ko, K. Delaney, M. Wissotski, G. Lopez, D. Campos, M. Braidotti, E. Ashley, W. Golser, H. Kim, S. Lee, J. Lin, Z. Dujmic, W. Kim, J. Talag, A. Zuccolo, C. Fan, A. Sebastian, M. Kramer, L. Spiegel, L. Nascimento, T. Zutavern, B. Miller, C. Ambroise, S. Muller, W. Spooner, A. Narechania, L. Ren, S. Wei, S. Kumari, B. Faga, M. J. Levy, L. McMahan, P. Van Buren, M. W. Vaughn, K. Ying, C.-T. Yeh, S. J. Emrich, Y. Jia, A. Kalyanaraman, A.-P. Hsia, W. B. Barbazuk, R. S. Baucom, T. P. Brutnell, N. C. Carpita, C. Chaparro, J.-M. Chia, J.-M. Deragon, J. C. Estill, Y. Fu, J. A. Jeddeloh, Y. Han, H. Lee, P. Li, D. R. Lisch, S. Liu, Z. Liu, D. H. Nagel, M. C. McCann, P. SanMiguel, A. M. Myers, D. Nettleton, J. Nguyen, B. W. Penning, L. Ponnala, K. L. Schneider, D. C. Schwartz, A. Sharma, C. Soderlund, N. M. Springer, Q. Sun, H. Wang, M. Waterman, R. Westerman, T. K. Wolfgruber, L. Yang, Y. Yu, L. Zhang, S. Zhou, Q. Zhu, J. L. Bennetzen, R. K. Dawe, J. Jiang, N. Jiang, G. G. Presting, S. R. Wessler, S. Aluru, R. A. Martienssen, S. W. Clifton, W. R. McCombie, R. A. Wing, R. K. Wilson, The B73 maize genome: complexity, diversity, and dynamics. *Science*. **326**, 1112–1115 (2009).

76. S. F. Altschul, W. Gish, W. Miller, E. W. Myers, D. J. Lipman, Basic local alignment search tool. *J. Mol. Biol.* **215**, 403–410 (1990).

77. N. Manchanda, J. L. Portwood 2nd, M. R. Woodhouse, A. S. Seetharam, C. J. Lawrence-Dill, C. M. Andorf, M. B. Hufford, GenomeQC: a quality assessment tool for genome assemblies and gene structure annotations. *BMC Genomics.* **21**, 193 (2020).

78. D. Ellinghaus, S. Kurtz, U. Willhoeft, LTRharvest, an efficient and flexible software for de novo detection of LTR retrotransposons. *BMC Bioinformatics*. **9**, 18 (2008).

79. S. Ou, N. Jiang, LTR_FINDER_parallel: parallelization of LTR_FINDER enabling rapid identification of long terminal repeat retrotransposons. *bioRxiv* (2019), p. 722736.

80. S. Ou, N. Jiang, LTR_retriever: A Highly Accurate and Sensitive Program for Identification of Long Terminal Repeat Retrotransposons. *Plant Physiol.* **176**, 1410–1422 (2018).

81. A. Seetharam, U. Singh, J. Li, P. Bhandary, Z. Arendsee, E. S. Wurtele, Maximizing prediction of orphan genes in assembled genomes. *Cold Spring Harbor Laboratory* (2019), p. 2019.12.17.880294.

82. M. G. Grabherr, B. J. Haas, M. Yassour, J. Z. Levin, D. A. Thompson, I. Amit, X. Adiconis, L. Fan, R. Raychowdhury, Q. Zeng, Z. Chen, E. Mauceli, N. Hacohen, A. Gnirke, N. Rhind, F. di Palma, B. W. Birren, C. Nusbaum, K. Lindblad-Toh, N. Friedman, A. Regev, Full-length transcriptome assembly from RNA-Seq data without a reference genome. *Nature Biotechnology*. **29** (2011), pp. 644–652.

83. M. Pertea, G. M. Pertea, C. M. Antonescu, T.-C. Chang, J. T. Mendell, S. L. Salzberg, StringTie enables improved reconstruction of a transcriptome from RNA-seq reads. *Nat. Biotechnol.* **33**, 290–295 (2015).

84. R. Liu, J. Dickerson, Strawberry: Fast and accurate genome-guided transcript reconstruction and quantification from RNA-Seq. *PLoS Comput. Biol.* **13**, e1005851 (2017).

85. C. Trapnell, A. Roberts, L. Goff, G. Pertea, D. Kim, D. R. Kelley, H. Pimentel, S. L. Salzberg, J. L. Rinn, L. Pachter, Differential gene and transcript expression analysis of RNA-seq experiments with TopHat and Cufflinks. *Nature Protocols*. **7** (2012), pp. 562–578.

86. L. Song, S. Sabunciyan, L. Florea, CLASS2: accurate and efficient splice variant annotation from RNA-seq reads. *Nucleic Acids Res.* **44**, e98 (2016).

87. L. Venturini, S. Caim, G. G. Kaithakottil, D. L. Mapleson, D. Swarbreck, Leveraging multiple transcriptome assembly methods for improved gene structure annotation. *Gigascience*. **7** (2018), doi:10.1093/gigascience/giy093.

88. A. Dobin, C. A. Davis, F. Schlesinger, J. Drenkow, C. Zaleski, S. Jha, P. Batut, M. Chaisson, T. R. Gingeras, STAR: ultrafast universal RNA-seq aligner. *Bioinformatics*. **29**, 15–21 (2013).

89. H. Li, B. Handsaker, A. Wysoker, T. Fennell, J. Ruan, N. Homer, G. Marth, G. Abecasis, R. Durbin, 1000 Genome Project Data Processing Subgroup, The Sequence Alignment/Map format and SAMtools. *Bioinformatics*. **25** (2009), pp. 2078–2079.

90. D. Mapleson, L. Venturini, G. Kaithakottil, D. Swarbreck, Efficient and accurate detection of splice junctions from RNA-seq with Portcullis. *Gigascience*. **7** (2018), doi:10.1093/gigascience/giy131.

91. B. J. Haas, A. Papanicolaou, M. Yassour, M. Grabherr, P. D. Blood, J. Bowden, M. B. Couger, D. Eccles, B. Li, M. Lieber, M. D. MacManes, M. Ott, J. Orvis, N. Pochet, F. Strozzi, N. Weeks, R. Westerman, T. William, C. N. Dewey, R. Henschel, R. D. LeDuc, N. Friedman, A. Regev, De novo transcript sequence reconstruction from RNA-Seq: reference generation and analysis with Trinity. *Nat. Protoc.* **8** (2013), doi:10.1038/nprot.2013.084.

92. K. J. Hoff, A. Lomsadze, M. Borodovsky, M. Stanke, in *Gene Prediction: Methods and Protocols*, M. Kollmar, Ed. (Springer New York, New York, NY, 2019), pp. 65–95.

93. B. J. Haas, A. L. Delcher, S. M. Mount, J. R. Wortman, R. K. Smith Jr, L. I. Hannick, R. Maiti, C. M. Ronning, D. B. Rusch, C. D. Town, S. L. Salzberg, O. White, Improving the Arabidopsis genome annotation using maximal transcript alignment assemblies. *Nucleic Acids Res.* **31**, 5654–5666 (2003).

94. C. Soderlund, A. Descour, D. Kudrna, M. Bomhoff, L. Boyd, J. Currie, A. Angelova, K. Collura, M. Wissotski, E. Ashley, D. Morrow, J. Fernandes, V. Walbot, Y. Yu, Sequencing, mapping, and analysis of 27,455 maize full-length cDNAs. *PLoS Genet.* **5**, e1000740 (2009).

95. B. Wang, M. Regulski, E. Tseng, A. Olson, S. Goodwin, W. R. McCombie, D. Ware, A comparative transcriptional landscape of maize and sorghum obtained by single-molecule sequencing. *Genome Res.* **28**, 921–932 (2018).

96. T. D. Wu, C. K. Watanabe, GMAP: a genomic mapping and alignment program for mRNA and EST sequences. *Bioinformatics*. **21**, 1859–1875 (2005).

97. W. J. Kent, BLAT—The BLAST-Like Alignment Tool. *Genome Res.* **12**, 656–664 (2002).

98. B. Wang, E. Tseng, M. Regulski, T. A. Clark, T. Hon, Y. Jiao, Z. Lu, A. Olson, J. C. Stein, D. Ware, Unveiling the complexity of the maize transcriptome by single-molecule long-read sequencing. *Nat. Commun.* **7**, 11708 (2016).

99. R.-G. Zhang, Z.-X. Wang, S. Ou, G.-Y. Li, TEsorter: lineage-level classification of transposable elements using conserved protein domains, , doi:10.1101/800177.

100. M. K. Tello-Ruiz, S. Naithani, P. Gupta, A. Olson, S. Wei, J. Preece, Y. Jiao, B. Wang, K. Chougule, P. Garg, J. Elser, S. Kumari, V. Kumar, B. Contreras-Moreira, G. Naamati, N. George, J. Cook, D. Bolser, P. D'Eustachio, L. D. Stein, A. Gupta, W. Xu, J. Regala, I. Papatheodorou, P. J. Kersey, P. Flicek, C. Taylor, P. Jaiswal, D. Ware, Gramene 2021: harnessing the power of comparative genomics and pathways for plant research. *Nucleic Acids Res.* (2020), doi:10.1093/nar/gkaa979.

101. R. C. Edgar, Search and clustering orders of magnitude faster than BLAST. *Bioinformatics*. **26**, 2460–2461 (2010).

102. M.-J. M. Chen, H. Lin, L.-M. Chiang, C. P. Childers, M. F. Poelchau, The GFF3toolkit: QC and Merge Pipeline for Genome Annotation. *Methods Mol. Biol.* **1858**, 75–87 (2019).

103. P. Jones, D. Binns, H.-Y. Chang, M. Fraser, W. Li, C. McAnulla, H. McWilliam, J. Maslen, A. Mitchell, G. Nuka, S. Pesseat, A. F. Quinn, A. Sangrador-Vegas, M. Scheremetjew, S.-Y. Yong, R. Lopez, S. Hunter, InterProScan 5: genome-scale protein function classification. *Bioinformatics*. **30**, 1236–1240 (2014).

104. A. J. Olson, D. Ware, Ranked Choice Voting for Representative Transcripts with TRaCE. *Cold Spring Harbor Laboratory* (2020), p. 2020.12.15.422742.

105. A. Stabenau, G. McVicker, C. Melsopp, G. Proctor, M. Clamp, E. Birney, The Ensembl core software libraries. *Genome Res.* **14**, 929–933 (2004).

106. F. Ramírez, F. Dündar, S. Diehl, B. A. Grüning, T. Manke, deepTools: a flexible platform for exploring deep-sequencing data. *Nucleic Acids Res.* **42**, W187–91 (2014).

107. A. R. Quinlan, I. M. Hall, BEDTools: a flexible suite of utilities for comparing genomic features. *Bioinformatics*. **26**, 841–842 (2010).

108. H. Thorvaldsdóttir, J. T. Robinson, J. P. Mesirov, Integrative Genomics Viewer (IGV): high-performance genomics data visualization and exploration. *Brief. Bioinform.* **14**, 178–192 (2013).

109. M. Martin, Cutadapt removes adapter sequences from high-throughput sequencing reads. *EMBnet.journal*. **17**, 10–12 (2011).

110. W. Guo, P. Fiziev, W. Yan, S. Cokus, X. Sun, M. Q. Zhang, P.-Y. Chen, M. Pellegrini, BS-Seeker2: a versatile aligning pipeline for bisulfite sequencing data. *BMC Genomics*. **14**, 774 (2013).

111. W. Guo, P. Zhu, M. Pellegrini, M. Q. Zhang, X. Wang, Z. Ni, CGmapTools improves the precision of heterozygous SNV calls and supports allele-specific methylation detection and visualization in bisulfite-sequencing data. *Bioinformatics*. **34**, 381–387 (2018).

112. W. A. Ricci, Unmethylated Regions Encompass the Functional Space Within the Maize Genome. *BiorXiv*.

113. M. D. Schultz, R. J. Schmitz, J. R. Ecker, "Leveling" the playing field for analyses of single-base resolution DNA methylomes. *Trends Genet.* **28**, 583–585 (2012).

114. gnu.org (available at https://www.gnu.org/software/datamash/).

115. M. Lawrence, W. Huber, H. Pagès, P. Aboyoun, M. Carlson, R. Gentleman, M. T. Morgan, V. J. Carey, Software for computing and annotating genomic ranges. *PLoS Comput. Biol.* **9**, e1003118 (2013).

116. R. Bukowski, X. Guo, Y. Lu, C. Zou, B. He, Z. Rong, B. Wang, D. Xu, B. Yang, C. Xie, L. Fan, S. Gao, X. Xu, G. Zhang, Y. Li, Y. Jiao, J. F. Doebley, J. Ross-Ibarra, A. Lorant, V. Buffalo, M. C. Romay, E. S. Buckler, D. Ware, J. Lai, Q. Sun, Y. Xu, Construction of the third-generation Zea mays haplotype map. *Gigascience*. **7**, 1–12 (2018).

117. H. M. Kang, M. Subramaniam, S. Targ, M. Nguyen, L. Maliskova, E. McCarthy, E. Wan, S. Wong, L. Byrnes, C. M. Lanata, R. E. Gate, S. Mostafavi, A. Marson, N. Zaitlen, L. A. Criswell, C. J. Ye, Multiplexed droplet single-cell RNA-sequencing using natural genetic variation. *Nat. Biotechnol.* **36**, 89–94 (2018).

118. S. Chen, Y. Zhou, Y. Chen, J. Gu, fastp: an ultra-fast all-in-one FASTQ preprocessor. *Bioinformatics*. **34**, i884–i890 (2018).

119. B. Langmead, S. L. Salzberg, Fast gapped-read alignment with Bowtie 2. *Nat. Methods*. **9**, 357–359 (2012).

120. A. Tarasov, A. J. Vilella, E. Cuppen, I. J. Nijman, P. Prins, Sambamba: fast processing of NGS alignment formats. *Bioinformatics*. **31**, 2032–2034 (2015).

121. J. M. Gaspar, Improved peak-calling with MACS2. *Cold Spring Harbor Laboratory* (2018), p. 496521.

122. P. J. Monnahan, J.-M. Michno, C. O'Connor, A. B. Brohammer, N. M. Springer, S. E.

McGaugh, C. N. Hirsch, Using multiple reference genomes to identify and resolve annotation inconsistencies. *BMC Genomics*. **21** (2020), , doi:10.1186/s12864-020-6696-8.

123. G. Marçais, A. L. Delcher, A. M. Phillippy, R. Coston, S. L. Salzberg, A. Zimin, MUMmer4: A fast and versatile genome alignment system. *PLoS Comput. Biol.* **14**, e1005944 (2018).

124. R. C. Team, Others, R: A language and environment for statistical computing (2013), (available at http://finzi.psych.upenn.edu/R/library/dplR/doc/intro-dplR.pdf).

125. W. Su, X. Gu, T. Peterson, TIR-Learner, a New Ensemble Method for TIR Transposable Element Annotation, Provides Evidence for Abundant New Transposable Elements in the Maize Genome. *Mol. Plant*. **12**, 447–460 (2019).

126. A. F. A. Smit, R. Hubley, P. Green, RepeatMasker Open-4.0. 2013--2015 (2015).

127. A. Kato, J. C. Lamb, J. A. Birchler, Chromosome painting using repetitive DNA sequences as probes for somatic chromosome identification in maize. *Proc. Natl. Acad. Sci. U. S. A.* **101**, 13554–13559 (2004).

128. G. Benson, Tandem repeats finder: a program to analyze DNA sequences. *Nucleic Acids Res.* **27**, 573–580 (1999).

129. B. J. Haas, A. L. Delcher, J. R. Wortman, S. L. Salzberg, DAGchainer: a tool for mining segmental genome duplications and synteny. *Bioinformatics*. **20**, 3643–3646 (2004).

130. E. Lyons, M. Freeling, How to usefully compare homologous plant genes and chromosomes as DNA sequences: How to usefully compare plant genomes. *Plant J.* **53**, 661–673 (2008).

131. T. Tian, Y. Liu, H. Yan, Q. You, X. Yi, Z. Du, W. Xu, Z. Su, agriGO v2.0: a GO analysis toolkit for the agricultural community, 2017 update. *Nucleic Acids Res.* **45**, W122–W129 (2017).

132. F. J. Sedlazeck, P. Rescheneder, M. Smolka, H. Fang, M. Nattestad, A. von Haeseler, M. C. Schatz, Accurate detection of complex structural variations using single-molecule sequencing. *Nat. Methods*. **15**, 461–468 (2018).

133. D. C. Jeffares, C. Jolly, M. Hoti, D. Speed, L. Shaw, C. Rallis, F. Balloux, C. Dessimoz, J. Bähler, F. J. Sedlazeck, Transient structural variations have strong effects on quantitative traits and reproductive isolation in fission yeast. *Nat. Commun.* **8**, 14061 (2017).

134. J. T. Robinson, H. Thorvaldsdóttir, W. Winckler, M. Guttman, E. S. Lander, G. Getz, J. P. Mesirov, Integrative genomics viewer. *Nat. Biotechnol.* **29**, 24–26 (2011).

135. Y. Benjamini, Y. Hochberg, Controlling the false discovery rate: a practical and powerful approach to multiple testing. *J. R. Stat. Soc.* (1995) (available at https://rss.onlinelibrary.wiley.com/doi/abs/10.1111/j.2517-6161.1995.tb02031.x).

136. B. Steuernagel, K. Witek, S. G. Krattinger, Physical and transcriptional organisation of the bread wheat intracellular immune receptor repertoire (2018) (available at https://repository.kaust.edu.sa/handle/10754/628448).

137. S. P. Gordon, B. Contreras-Moreira, D. P. Woods, D. L. Des Marais, D. Burgess, S. Shu,

C. Stritt, A. C. Roulin, W. Schackwitz, L. Tyler, J. Martin, A. Lipzen, N. Dochy, J. Phillips, K. Barry, K. Geuten, H. Budak, T. E. Juenger, R. Amasino, A. L. Caicedo, D. Goodstein, P. Davidson, L. A. J. Mur, M. Figueroa, M. Freeling, P. Catalan, J. P. Vogel, Extensive gene content variation in the Brachypodium distachyon pan-genome correlates with population structure. *Nat. Commun.* **8**, 2184 (2017).

138. P. F. Sarris, V. Cevik, G. Dagdas, J. D. G. Jones, K. V. Krasileva, Comparative analysis of plant immune receptor architectures uncovers host proteins likely targeted by pathogens. *BMC Biol.* **14**, 8 (2016).

139. de W. Van, F. Monteiro, O. J. Furzer, M. T. Nishimura, V. Cevik, K. Witek, J. D. G. Jones, J. L. Dangl, D. Weigel, F. Bemm, A Species-Wide Inventory of NLR Genes and Alleles in Arabidopsis thaliana. *Cell*. **178**, 126–1272.e14 (2019).

140. H. Wickham, *ggplot2: Elegant Graphics for Data Analysis* (Springer, 2016).

141. A. Stamatakis, RAxML version 8: a tool for phylogenetic analysis and post-analysis of large phylogenies. *Bioinformatics*. **30**, 1312–1313 (2014).

142. I. Letunic, P. Bork, Interactive tree of life (iTOL) v3: an online tool for the display and annotation of phylogenetic and other trees. *Nucleic Acids Res.* **44**, W242–5 (2016).

143. M. C. Frith, Gentle masking of low-complexity sequences improves homology search. *PLoS One*. **6**, e28819 (2011).

144. M. C. Frith, R. Kawaguchi, Split-alignment of genomes finds orthologies more accurately. *Genome Biol.* **16**, 106 (2015).

145. M. C. Frith, L. Noé, Improved search heuristics find 20,000 new alignments between human and mouse genomes. *Nucleic Acids Res.* **42**, e59 (2014).

146. M. Hamada, Y. Ono, K. Asai, M. C. Frith, Training alignment parameters for arbitrary sequencers with LAST-TRAIN. *Bioinformatics* (2016), p. btw742.

147. S. M. Kielbasa, R. Wan, K. Sato, P. Horton, M. C. Frith, Adaptive seeds tame genomic sequence comparison. *Genome Research*. **21** (2011), pp. 487–493.

148. B. Song, H. Wang, Y. Wu, E. Rees, D. J. Gates, M. Burch, Constrained non-coding sequence provides insights into regulatory elements and loss of gene expression in maize. *bioRxiv* (2020) (available at https://www.biorxiv.org/content/10.1101/2020.07.11.192575v2.abstract).

149. M. Hubisz, K. Pollard, A. Siepel, Package “rphast” (available at https://mran.microsoft.com/snapshot/2017-04-22/web/packages/rphast/rphast.pdf).

150. E. V. Davydov, D. L. Goode, M. Sirota, G. M. Cooper, A. Sidow, S. Batzoglou, Identifying a high fraction of the human genome to be under selective constraint using GERP++. *PLoS Comput. Biol.* **6**, e1001025 (2010).

151. F. Ogut, Y. Bian, P. J. Bradbury, J. B. Holland, Joint-multiple family linkage analysis predicts within-family variation better than single-family analysis of the maize nested association mapping population. *Heredity* . **114**, 552–563 (2015).

152. B. C. Haller, P. W. Messer, SLiM 3: Forward Genetic Simulations Beyond the Wright–Fisher Model. *Molecular Biology and Evolution*. **36** (2019), pp. 632–637.

153. M. B. Hufford, X. Xu, J. van Heerwaarden, T. Pyhäjärvi, J.-M. Chia, R. A. Cartwright, R. J. Elshire, J. C. Glaubitz, K. E. Guill, S. M. Kaeppler, J. Lai, P. L. Morrell, L. M. Shannon, C. Song, N. M. Springer, R. A. Swanson-Wagner, P. Tiffin, J. Wang, G. Zhang, J. Doebley, M. D. McMullen, D. Ware, E. S. Buckler, S. Yang, J. Ross-Ibarra, Comparative population genomics of maize domestication and improvement. *Nat. Genet.* **44**, 808–811 (2012).

154. R. M. Clark, S. Tavaré, J. Doebley, Estimating a Nucleotide Substitution Rate for Maize from Polymorphism at a Major Domestication Locus. *Mol. Biol. Evol.* **22**, 2304–2312 (2005).

155. B. C. Haller, SLiM: An Evolutionary Simulation Framework. Note: If you wish to cite SLiM 2 in a publication, please DO NOT cite this manual (unless you are, in fact, specifically referring to this manual--such as citing one of the recipes given here). We expect to have a publication on SLiM 2 out soon; in the meantime, you can cite the paper on the original version of SLiM: Messer, PW (2013). SLiM: Simulating Evolution with Selection and Linkage. *Genetics*. **194**, 1037–1039 (2016).

156. J. Ross-Ibarra, M. Tenaillon, B. S. Gaut, Historical divergence and gene flow in the genus Zea. *Genetics*. **181**, 1399–1413 (2009).

157. A. Eyre-Walker, R. L. Gaut, H. Hilton, D. L. Feldman, B. S. Gaut, Investigation of the bottleneck leading to the domestication of maize. *Proceedings of the National Academy of Sciences*. **95** (1998), pp. 4441–4446.

158. A. J. Ranere, D. R. Piperno, I. Holst, R. Dickau, J. Iriarte, The cultural and chronological context of early Holocene maize and squash domestication in the Central Balsas River Valley, Mexico. *Proceedings of the National Academy of Sciences*. **106** (2009), pp. 5014–5018.

159. K. Csilléry, O. François, M. G. B. Blum, abc: an R package for approximate Bayesian computation (ABC). *Methods Ecol. Evol.* **3**, 475–479 (2012).

160. J. Koster, S. Rahmann, Snakemake--a scalable bioinformatics workflow engine. *Bioinformatics*. **28** (2012), pp. 2520–2522.

161. E. S. Buckler, J. B. Holland, P. J. Bradbury, C. B. Acharya, P. J. Brown, C. Browne, E. Ersoz, S. Flint-Garcia, A. Garcia, J. C. Glaubitz, M. M. Goodman, C. Harjes, K. Guill, D. E. Kroon, S. Larsson, N. K. Lepak, H. Li, S. E. Mitchell, G. Pressoir, J. A. Peiffer, M. O. Rosas, T. R. Rocheford, M. C. Romay, S. Romero, S. Salvo, H. Sanchez Villeda, H. S. da Silva, Q. Sun, F. Tian, N. Upadyayula, D. Ware, H. Yates, J. Yu, Z. Zhang, S. Kresovich, M. D. McMullen, The genetic architecture of maize flowering time. *Science*. **325**, 714–718 (2009).

162. F. Tian, P. J. Bradbury, P. J. Brown, H. Hung, Q. Sun, S. Flint-Garcia, T. R. Rocheford, M. D. McMullen, J. B. Holland, E. S. Buckler, Genome-wide association study of leaf architecture in the maize nested association mapping population. *Nat. Genet.* **43**, 159–162 (2011).

163. J. A. Poland, P. J. Bradbury, E. S. Buckler, R. J. Nelson, Genome-wide nested association

mapping of quantitative resistance to northern leaf blight in maize. *Proc. Natl. Acad. Sci. U. S. A.* **108**, 6893–6898 (2011).

164. H.-Y. Hung, C. Browne, K. Guill, N. Coles, M. Eller, A. Garcia, N. Lepak, S. Melia-Hancock, M. Oropeza-Rosas, S. Salvo, N. Upadyayula, E. S. Buckler, S. Flint-Garcia, M. D. McMullen, T. R. Rocheford, J. B. Holland, The relationship between parental genetic or phenotypic divergence and progeny variation in the maize nested association mapping population. *Heredity* . **108**, 490–499 (2012).

165. P. J. Brown, N. Upadyayula, G. S. Mahone, F. Tian, P. J. Bradbury, S. Myles, J. B. Holland, S. Flint-Garcia, M. D. McMullen, E. S. Buckler, T. R. Rocheford, Distinct genetic architectures for male and female inflorescence traits of maize. *PLoS Genet.* **7**, e1002383 (2011).

166. H.-Y. Hung, L. M. Shannon, F. Tian, P. J. Bradbury, C. Chen, S. A. Flint-Garcia, M. D. McMullen, D. Ware, E. S. Buckler, J. F. Doebley, J. B. Holland, ZmCCT and the genetic basis of day-length adaptation underlying the postdomestication spread of maize. *Proc. Natl. Acad. Sci. U. S. A.* **109**, E1913–21 (2012).

167. K. L. Kump, P. J. Bradbury, R. J. Wisser, E. S. Buckler, A. R. Belcher, M. A. Oropeza-Rosas, J. C. Zwonitzer, S. Kresovich, M. D. McMullen, D. Ware, P. J. Balint-Kurti, J. B. Holland, Genome-wide association study of quantitative resistance to southern leaf blight in the maize nested association mapping population. *Nat. Genet.* **43**, 163–168 (2011).

168. P. Danecek, A. Auton, G. Abecasis, C. A. Albers, E. Banks, M. A. DePristo, R. E. Handsaker, G. Lunter, G. T. Marth, S. T. Sherry, G. McVean, R. Durbin, 1000 Genomes Project Analysis Group, The variant call format and VCFtools. *Bioinformatics*. **27** (2011), pp. 2156–2158.

169. A. McKenna, M. Hanna, E. Banks, A. Sivachenko, K. Cibulskis, A. Kernytsky, K. Garimella, D. Altshuler, S. Gabriel, M. Daly, M. A. DePristo, The Genome Analysis Toolkit: a MapReduce framework for analyzing next-generation DNA sequencing data. *Genome Res.* **20**, 1297–1303 (2010).

170. G. A. Auwera, M. O. Carneiro, C. Hartl, R. Poplin, G. del Angel, A. Levy-Moonshine, T. Jordan, K. Shakir, D. Roazen, J. Thibault, E. Banks, K. V. Garimella, D. Altshuler, S. Gabriel, M. A. DePristo, From FastQ Data to High-Confidence Variant Calls: The Genome Analysis Toolkit Best Practices Pipeline. *Curr. Protoc. Bioinformatics*. **43** (2013), doi:10.1002/0471250953.bi1110s43.

171. H. Li, R. Durbin, Fast and accurate short read alignment with Burrows-Wheeler transform. *Bioinformatics*. **25**, 1754–1760 (2009).

172. J. Catchen, P. A. Hohenlohe, S. Bassham, A. Amores, W. A. Cresko, Stacks: an analysis tool set for population genomics. *Mol. Ecol.* **22**, 3124–3140 (2013).

173. X. Huang, Q. Feng, Q. Qian, Q. Zhao, L. Wang, A. Wang, J. Guan, D. Fan, Q. Weng, T. Huang, G. Dong, T. Sang, B. Han, High-throughput genotyping by whole-genome resequencing. *Genome Res.* **19**, 1068–1076 (2009).

174. P. J. Bradbury, Z. Zhang, D. E. Kroon, T. M. Casstevens, Y. Ramdoss, E. S. Buckler, TASSEL: software for association mapping of complex traits in diverse samples.

Bioinformatics. **23**, 2633–2635 (2007).

175. J. Yang, S. Hong Lee, M. E. Goddard, P. M. Visscher, GCTA: A Tool for Genome-wide Complex Trait Analysis. *The American Journal of Human Genetics*. **88** (2011), pp. 76–82.

SUPPLEMENTARY DATA

Materials and Methods

Data Availability

Browsers: The NAM assemblies and gene models can be accessed through their genome assembly pages https://maizegdb.org/NAM_project, which provide the genome browser metadata and links to downloads for each assembly.

Downloads: Downloads can be accessed directly from the MaizeGDB download site (https://maizegdb.org/download). NAM gene models can be downloaded, viewed on the genome browsers, and searched via the gene center (https://maizegdb.org/gene_center/gene). BLAST targets for the NAM assemblies and their gene models are available for the MaizeGDB BLAST tool (https://blast.maizegdb.org).

Raw sequence data: Raw data used for all the assemblies including the PacBio Sequel reads, Illumina short reads, BioNano optical maps are available through ENA BioProject IDs PRJEB31061 and PRJEB32225. RNA-Seq reads for various tissues can be found through ENA ArrayExpress IDs E-MTAB-8633 and E-MTAB-8628 and EM-Seq reads are available through ENA ArrayExpress under ID E-MTAB-10028.

Other data: Other files, tables and supplemental data can be found in CyVerse /iplant/home/shared/NAM/NAM_genome_and_annotation_Jan2021_release. Links to the NLR trees can be found at https://itol.embl.de/shared/xCJbI9ndshEK.

Scripts: Scripts used to generate and analyze data are at https://github.com/HuffordLab/NAM-genomes.

USDA funding statement

This research was supported in part by the US. Department of Agriculture, Agricultural Research Service. Mention of trade names or commercial products in this publication is solely for the purpose of providing specific information and does not imply recommendation or endorsement by the U.S. Department of Agriculture. USDA is an equal opportunity provider and Employer.

Plant Material

Inbred NAM lines were obtained from GRIN Global (**Table S1**) and tissue collected as previously reported (*60*). Briefly, original accessions were selfed for one generation at Curtiss Farm at Iowa State University. Using single-seed-descent ears derived from this propagation, 144 seedlings were greenhouse grown to V2 vegetative growth stage at Iowa State University. After 48hr etiolation, 30 grams young leaf tissue was harvested, flash frozen, and submitted for CTAB, or nuclei-based high molecular weight DNA isolation for downstream analysis. Remaining seed from our single-seed-descent ears has been deposited and is publicly available through GRIN Global (**Table S1**).

DNA preparation for sequencing

High molecular weight DNA was isolated using either a standard CTAB protocol or a modified version in which nuclei were first isolated, thereby removing the plastid and mitochondrial genomes (**Table S1**). The CTAB procedure was a slightly modified version of the original method (*61*). Nuclei isolations were based on the method of Luo and Wing (*62*), with collected and washed nuclei then being resuspended in CTAB buffer and isolations completed following (*61*).

PacBio Sequencing

Sequencing libraries were constructed following PacBio's template prep protocols for the Express Template Prep Kit 2.0. For all lines except Ki11, NC350, and B73, samples were sequenced using Sequel binding and sequencing chemistry v2.1. Ki11, NC350, and B73 were sequenced using Sequel binding and sequencing chemistry v3.0.

Illumina Sequencing

The same DNA used for PacBio sequencing was used for Illumina sequencing. PCR-free DNA sequencing libraries were prepared using the Kapa HyperPrep PCR-free kit (#KK8505). The sequencing libraries were checked for quality on an Agilent Fragment Analyzer and the final concentrations estimated using qPCR. PE150 libraries were sequenced on the Illumina NextSeq 500 using the 300 cycles high output kit.

Optical Map Generation

DNA was extracted for optical map construction using the Bionano Prep™ Plant Tissue DNA Isolation Kit and a slightly modified protocol. For each inbred, approximately 0.5 g of etiolated leaf tissue was harvested from young seedlings germinated under soil-free conditions and grown in the dark for approximately 2 weeks. Leaves were treated with a 2% formaldehyde fixing solution, washed, cut into small pieces, and homogenized with a Qiagen Tissueruptor probe. Free nuclei were then concentrated through centrifugation at 2000 x g, washed, isolated by gradient centrifugation, and embedded in a low-melting-point agarose plug. The plug was treated with proteinase K and RNase A and washed four times in Bionano Wash Buffer and five times in TE buffer. Finally, purified, ultra-high-molecular-weight nuclear DNA (uHMW nDNA) was recovered by melting the plug, digesting with agarase and subjecting the sample to drop dialysis against TE.

Labeling was performed using the DLS Kit (Bionano Genomics Cat.80005) following manufacturer's recommendations with slight modification. In total, 1 ug uHMW nDNA was incubated along with DLE-1 Enzyme, DL-Green and DLE-1 Buffer for 2:20 h at 37 °C, followed by 20 min at 70 °C. Subsequently, a second proteinase K digestion and cleanup of unincorporated DL-Green label was performed, and labeled DNA was combined with Flow Buffer, DTT, and incubated overnight at 4 °C. DNA was stained and quantified by adding Bionano DNA Stain to a final concentration of 1 microliter per 0.1 microgram of DNA. The labeled sample was then loaded onto a Bionano chip flow cell where molecules were separated, imaged, and digitized in the Saphyr System according to the manufacturer's recommendations (https://bionanogenomics.com/support-page/saphyr-system/). Data visualization, processing, and DLS map assembly were conducted using the Bionano Genomics software Access, Solve and Tools.

Genome Assembly and Hybrid Scaffolding

Raw illumina reads were first used to verify homozygosity of inbreds by comparing percent heterozygosity of SNPs using BWA-MEM (*63*) and GATK (*64*) to publicly available HapMap2 maize SNP data (*43*). Loci that were monomorphic across lines were removed for this analysis. The data were also subsampled to 10,000 to 50,000 SNPs in order to generate a phylogenetic tree using SNPhylo (*65*) for the purpose of verifying line identity.

PacBio subreads were error-corrected with Falcon (*66*) using the longest 50x coverage and an average read correction rate set to 75% (-e 0.75) with local alignments at a minimum of 3000 bp (-l 3000). The usage of -l 3000 instead of the default -l 2500 performs better for highly repetitive genome species such as maize. We required a minimum of two reads and a maximum of 200 reads for error corrections (--min_cov 2 --max_n_read 200). For sequence assembly, the exact matching k-mers between two reads was set to 24 bp (-k 24) with a read correction rate of 95% (-e 0.95) and local alignments of at least 1000 bp (-l 1000). Corrected reads ranged from 32x-56x coverage and were characterized by N50s ranging from 16.2 – 23.2 kbp. These reads were trimmed and assembled with Canu (v1.8) (*67*) with the following modification of default parameters: correctedErrorRate=0.065 corMhapSensitivity=normal ovlMerThreshold=500 utgOvlMerThreshold=150. This version of Canu fixes a bug in previous versions that generated truncations in large contigs during the consensus stage. The resulting contigs were filtered to a minimum contig length of 30 kbp.

Sequence polishing of contigs was conducted using both PacBio and Illumina data sets. First, raw PacBio reads were aligned to contigs using the software pbmm2 (a PacBio wrapper for minimap2 (*68*)). The PacBio consensus algorithm tool Arrow was then run under default parameters (https://github.com/PacificBiosciences/pbbioconda). PacBio polished contigs were then polished with either PE 150 bp Illumina reads (the majority of samples) or 10X Chromium linked reads (CML52 and Il14H). The PE Illumina reads ranged from 26x-73x depth and were aligned to contigs using minimap2. Subsequently, the assembly tool Pilon v1.22 (https://github.com/broadinstitute/pilon) was used to correct individual base errors and small indels under the following modifications to default parameters: --fix bases --minmq 30 --mindepth 10. Chromium linked reads were aligned to contigs using Longranger v2.2.2 (https://support.10xgenomics.com/genome-exome/software/downloads/latest?) with Pilon run as described above.

The PacBio sequence assembly was merged with the optical map using the hybrid scaffolding module of BionanoSolve (v3.4.0) and Bionano Access (v1.3.0). Default parameters from optArguments_nonhaplotype_noES_DLE1_saphyr.xml were used. At this stage three forms of gaps were generated: 1) N gaps of various sizes (not 100Ns or 13Ns). These are rough estimates of missing sequence where the Bionano map was contiguous but there were no PacBio contigs that matched. Sizes are calibrated by the Bionano software and are generally accurate within 500 bp. 2) 100N gaps. These represent gaps of unknown size between scaffolds. They generally occur in centromeres and knobs. 3) 13N gaps. These are assembly artifacts associated with repetitive regions. They occur when two contigs are aligned to the

same optical map and they overlap on the ends, indicating that they are independently assembled parts of a single contiguous region (however due to the repetitiveness or residual heterozygosity, were not assembled together at the sequence level). Bionano software does not remove this overlap and instead joins the contigs end-to-end and marks the join by 13Ns. This creates a software-induced sequence duplication of several hundred bp to several kb. For the B73 assembly **only** (version 5.0) the contig overlaps marked by 13Ns were hand curated and removed.

We emphasize that any segment of a genome containing a 13N gap, when aligned to any other genome, will show apparent structural variation that does not reflect a biological difference, but instead reflects an assembly artifact associated with contig overlap. These can be identified by scanning the sequence for 13N gaps.

Pseudomolecule Construction

Pseudomolecules were constructed from the hybrid scaffolds using ALLMAPS (v0.8.12; (*69*) as described in our previous assembly of the B73-Ab10 line (*42*). Briefly, we used pan-genome anchor (*4*) and Golden Gate (*11*) markers for all NAM lines and the IBM (Intermated B73 x Mo17) genetic map (*70*) in the case of B73 for pseudomolecule construction. Pan-genome anchor markers were downloaded from the CyVerse Data Commons (*71*) and processed to obtain coordinates 50 bp upstream and downstream of the marker position, and sequences from the B73 V3 assembly were then extracted. These sequences were mapped to an indexed NAM assembly using HiSat2 (v2.1.0) (*72*, *73*) with fine-tuning to map short sequences reliably. By disabling splicing (--no-spliced-alignment), forcing global alignment (--end-to-end), and including high read, reference gap open, and extension penalties (--rdg 10000,10000 and --rfg 10000,10000), full-length mapping of marker sequence was achieved. Only reads with mapping quality higher than 30 and tag XM:0 (unique mapping) were retained as the final set of mapped marker sequences. These markers were then combined with the metadata to generate a pan-genome marker input file for ALLMAPS (predicted distance information with their mapped position) in CSV format. For preparing the IBM and the Golden Gate genetic maps, the marker information was downloaded from MaizeGDB (IBM: https://www.maizegdb.org/complete_map?id=887740; GoldenGate: https://www.maizegdb.org/data_center/map?id=1160762) and processed to yield markers in fasta format and metadata in a tsv file. Methods for mapping and processing these markers were identical to pan-genome anchor markers.

ALLMAPS was run using CSV files as inputs (pangenome.csv and goldengate.csv) and configured to use scaffolds with more than 20 uniquely mapped markers (--mincount=20). Gap inserts between the scaffolds was set to 100 (--gapsize-100). Pseudomolecules were finalized after inspecting the marker placement plot and the scaffold directions. Any small scaffolds nested within the large scaffolds were identified as heterozygous and were excluded from the final pseudomolecule. These scaffolds were named with the prefix "alt-scaf" and were saved as unplaced scaffolds. Synteny dotplots were generated using the scaffolds as well as pseudomolecule assemblies against the B73 genome by following the ISUgenomics Bioinformatics Workbook (https://bioinformaticsworkbook.org/dataWrangling/genome-dotplots.html). Dot plots helped confirm the placement and orientation of scaffolds. Briefly, the repeats were masked using RepeatMasker (v4.0.9) (*74*) and the Maize TE Consortium (MTEC) curated library (https://github.com/oushujun/MTEC) (*75*). RepeatMasker was configured to use the NCBI engine (rmblastn) (*76*) with a quick search option (-q) and GFF as a preferred output. The repeat-masked genomes were then aligned using minimap2 (*68*) (v2.2) and set to break at 5% divergence (-x asm5). The paf files were filtered to eliminate alignments less than 1 kbp and dotplots were generated using the R package dotPlotly (https://github.com/tpoorten/dotPlotly). The AGP construction method along with the scripts are detailed in the "agp-generation" section of the companion GitHub site.

Genome Quality Assessment

To assess the contiguity and gene space completeness of the NAM genome assemblies, different quality metrics (**Table S2**) were calculated using the GenomeQC tool (*77*). Embryophyta odb9 dataset (n = 1,440) and Augustus species 'maize' were provided as the input parameters to calculate the BUSCO metrics.

The LTR Assembly Index (LAI) (*18*) was used to assess the contiguity of TE assembly. First, intact LTR retrotransposon (LTR-RT) candidates of each genome (pseudomolecules only) were identified using LTRharvest (v1.6.1) (*78*) and LTR_FINDER_parallel (v1.1) (*79*), then filtered by LTR_retriever (v2.9.0) (*80*) with default parameters. The LAI program (beta3.2) was used to calculate LAI values of each genome based on a total LTR content of 76.34%, an LTR identity of 94.854% (-totLTR 76.34 -iden 94.854), and the intact LTR-RTs identified from the genome. The LAI was comparable among NAM lines with an average of 28 (SD = 0.23), which is considered "gold" quality (*18*). The percentage of structurally annotated TEs was lower than

previously reported (*21*) due to more effective filtering of false positives (*80*) and the fact that only intact TEs were structurally annotated in this study.

RNA-seq

Total RNA was extracted using the Qiagen RNeasy plant mini kit from ten tissues. These were (1) primary root and (2) coleoptile at six days after planting, (3) base of the 10th leaf, (4) middle of the 10th leaf, (5) tip of the 10th leaf at the Vegetative 11 (V11) growth stage, (6) meiotic tassel and (7) immature ear at the V18 growth stage, (8) anthers at the Reproductive 1 (R1) growth stage, (9) endosperm and (10) embryo at 16 days after pollination. With a few exceptions, for each tissue in each NAM founder, mRNA was sequenced from two biological replicates that were composed of mRNA from three individual plants. In the case of endosperm and embryo, 50 kernels per plant were used (for a total of 150 per biological replicate). For tissues 1-5, plants were grown in University of Minnesota greenhouses in Metro-Mix300 (Sun Gro Horticulture) at 27°C/24°C day/night and 16h/8h light/dark. For tissues 6-10, plants were grown outdoors at the Minnesota Agricultural Experiment Station in Saint Paul, MN with 30-inch row spacing at ~52,000 plants per hectare.

For each sample, total RNA was assayed by Bioanalyzer to determine the quantity and integrity of the sample. Concentrations were normalized in 25uL of nuclease-free water and sequencing libraries prepared using KAPA's Stranded mRNA-seq kit (#KK4821). The mRNA was enriched using oligo-dT beads, fragmented, and converted to double stranded cDNA using random hexamer priming and amplification. Libraries were pooled and sequenced on NextSeq 500 instruments using the PE75 protocol.

Gene Model Annotation

The 26 NAM genomes were annotated using a hybrid evidence and *ab initio* based gene prediction pipeline (*81*). Evidence-based predictions were directly inferred from the assembled transcripts, which were generated using five different genome-guided transcript assembly programs, Trinity (v2.6.6) (*76*, *82*), StringTie (v1.3.4a) (*83*), Strawberry (v1.1.1) (*84*), Cufflinks (v2.2.1) (*83*, *85*) and Class2 (*83*, *85*, *86*)) and processed using Mikado (v1.2.4) (*87*) to pick the optimal set of transcripts for each locus. To generate assembled transcripts, quality inspected RNA-seq reads from each library were mapped to their respective NAM genomes using STAR (v2.5.3a) (*88*) with an iterative 2-pass mapping approach in which splice junctions generated

from the first round were used to refine alignments in the subsequent round. STAR was configured to output SAM format (with options --outSAMattributes All, --outSAMmapqUnique 10, --outFilterMismatchNmax 0) to ensure downstream analysis compatibility. Mapped reads from each library were merged, sorted, and indexed using SAMTools (v1.9)(*89*) to generate input for transcript assembly programs. All programs were run with default options with the exception of the minimum transcript length setting (when allowed), which was set to 100 bp (Trinity using --min_contig_length 100, StringTie using -m 100 and Strawberry using -t 100) and enabling of RNAseq strandedness (Trinity using -SS_lib_type FR, Cufflinks using --library-type fr-firststrand), when available. Maximum intron size was also set to 10000 (--genome_guided_max_intron 10000) in Trinity. While most of the assembly programs generated a GFF3 as the final output, Trinity provided fasta format transcripts. These transcripts were mapped back to the gmap (v2019-05-12) indexed genome to generate a GFF3 file (by setting the output format option -f to gff3_match_cdna).

In order to pick the final transcripts, Mikado uses assembled transcripts combined with high-confidence splice junctions generated by Portcullis (v1.1.2) (*90*) with the mapped reads as input (merged and sorted), predicted ORFs for the assembled transcripts generated by TransDecoder (v5.5.0) (*91*), and homology results of transcripts to SwissProt (viridiplantae) sequences generated by NCBI-BLAST (blastx) (v2.9.0) (*76*). While default options were used for Portcullis and TransDecoder, for blastx, maximum target sequences were set to 5 (-max_target_seqs 5) and output format to xml (-outfmt 5). The following were provided as inputs for Mikado: all transcript assemblies (with strandedness marked as True for all except for Trinity, and with equal weights) in GFF3 format, portcullis generated splice sites in bed format, TransDecoder results in bed format, homology results in XML format, and a scoring matrix in yaml. Final transcripts from Mikado were exported in GFF3 format, and transcripts and proteins were then converted to fasta format using the gffread utility of the Cufflinks package.

Ab initio predictions were performed using BRAKER (v2.1.2) (*92*) with both evidence-based predicted proteins and mapped RNA-seq reads as input. BRAKER was run iteratively, with the first round using the hard-masked genome (primarily to speed-up the protein alignments and to generate a hints file from the BAM file) and the second round using a soft-masked genome with proteins/RNA-seq hints for finalizing the *ab initio* predictions. Default options were used in BRAKER, with the exception that gth was substituted as the protein aligner (--prg=gth), models trained using protein alignments (--gth2traingenes), the soft-masked genome was provided as input (--softmasking), and output predictions were generated in GFF3 format (--gff3).

A working set (WS) of models was generated for each NAM line to capture the complete gene space by combining evidence based and non-overlapping BRAKER gene models using BEDtools (v2.17.0) (Aaron. A et al 2010). Additional structural improvements on the WS models were completed using the software PASA (v2.3.3) (*93*) iteratively with default options. 69,163 B73 full-length cDNA (*94*) and an additional 46,311 transcripts from 11 developmental tissues (*95*) were filtered for intron retention and then used in combination with ~2 million maize ESTs from genbank with the Mikado generated transcripts as evidence to update WS gene models with PASA. PASA was run with default options, with a first step of aligning transcript evidence to the masked NAM genomes using GMAP (v.2018-07-04) (*96*) and Blat (v.36) (*97*). The full-length cDNA and Iso-seq transcript IDs (*98*) were passed in a text file (-f FL.acc.list) during the PASA alignment step. Valid, near-perfect alignments with 95% identity were clustered based on genome mapping location and assembled into gene structures that included the maximal number of compatible transcript alignments. PASA assemblies were then compared with NAM-generated transcript models using default parameters. PASA on average updated 12,927 protein coding models across the NAM lines (Supplementary Table3) with the majority of updates being UTR modifications (73.8%), followed by alternative isoforms (35.1%) and novel genes (5.5%). Transposable element (TE) related genes were filtered from the evidence and non-overlapping BRAKER sets using the TEsorter tool (*99*), which uses the REXdb (viridiplantae_v3.0 + metazoa_v3) database of TEs. The TE filtered WS had 110,498 gene models on average across the NAM lines (lowest of 101,754 in B73 and highest of 118,596 in Tzi8).

The TE filtered WS models were given Annotation Edit Distance (AED) scores using MAKER-P (v.3.0) (Campbell. M et al, 2014). Only models with AED < 0.75 passed to the high-confidence set (HCS). The number of gene models dropped to an average of 45,768 transcripts per NAM accession in the HCS (lowest of 44,424 in B73 and highest of 47,262 in Mo18w) (Supplementary Table4). The HCS gene models were further classified based on homology to related species, and assigned coding and non-coding biotypes. Protein sequences were aligned to the canonical translations of gene models from *Sorghum bicolor*, *Oryza sativa*, *Brachypodium distachyon*, and *Arabidopsis thaliana* obtained from Gramene release 62 (*100*) using USEARCH v11.0.667_i86linux32 (*101*). The HCS gene models were checked for missing start and stop codons. On average 8,078 out of 32,470 conserved genes and 5,003 out of 8,862 lineage-specific genes had incomplete CDS. The CDS boundaries of the transcripts were modified based on conserved start codon positions or extended to a start or stop codon whenever possible. All conserved genes in addition to lineage-specific genes that had a complete CDS

were marked as protein-coding. The remaining lineage-specific genes were marked as non-coding. HCS gene models were checked and potentially split or merged using the GFF3toolkit (2.0.1) (*102*). Gene ID assignment was made as per MaizeGDB nomenclature schema (https://www.maizegdb.org/nomenclature) for each line. Functional domain identification was completed with InterProScan (v5.38-76.0) (*103*). TRaCE (*104*) was used to assign canonical transcripts based on domain coverage, protein length, and similarity to transcripts assembled by Stringtie. Finally, the gene annotations were imported to ensembl core databases, verified, and validated for translation using the ensembl API (*105*). The exported GFF3 annotation files were validated and reformatted again using GFF3toolkit.

Centromere annotation

Functional centromere regions were annotated using ChIP-seq with antisera to maize Centromeric Histone H3 (CENH3) as described (*40*). CENH3 ChIP-seq data from B97, CML228, CML322, CML247, CML52, CML69, Ky21, Mo18W, M37W, M162W, Ms71, NC358, Oh43, and Tx303 are from (*39*) and can be obtained from GenBank (SRP067358); and ChIP-seq reads for B73, CML103, CML277, CML333, HP301, Il14H, Ki11, Ki3, NC350, Oh7B, P39 and Tzi8 are from (*40*) and available under project PRJNA639705.

Centromere positions of each NAM line were projected to B73 by mapping both CENH3 ChIP-seq data and genomic input data to the B73 genome with bwa-mem (v0.7.17) (*63*). ChIP enrichment was calculated by normalizing RPKM values from the ChIP data against the genomic input in 5 kbp windows with deeptools (v3.3) (*106*). Enriched islands with a ratio above 2.5 were identified and merged with a distance interval of 1 Mbp using bedtools (v2.29) (*107*). The final centromere coordinates were determined by visual inspection of the ChIP-seq peaks in IGV (v2.8) (*108*). Centromeres that were not mappable by CENH3 ChIP were defined as the midpoint of the largest CentC array in B73.

DNA methylation and identification of unmethylated regions (UMRs)

DNA methylome sequencing libraries were prepared from the second leaves of 5 to 9 plants (at a stage before the unfurling of the first leaves) using the NEBNext® Enzymatic Methyl-seq Kit (New England Biolabs #E7120S). At least two biological replicates were prepared and analyzed in this way for B73 each NAM founder. The input for each sample consisted of 200 ng of genomic DNA that had been combined with 1 pg of control pUC19 DNA

and 20 pg of control lambda DNA and sonicated to fragments averaging ~700 bp in length using a Diagenode Bioruptor. All libraries were amplified with 4 or 5 PCR cycles. The libraries were Illumina sequenced using paired-end 150 nt reads, with a minimum of 300 million reads per NAM founder, divided between biological replicates. Reads were trimmed of adapter sequence using cutadapt (version 2.6, default parameters except -q 20 -a AGATCGGAAGAGC -A AGATCGGAAGAGC -O) (*109*). Reads were aligned to each genome and methylation values called using BS-Seeker2 (version 2.1.5, default parameters except -m 1 --aligner=bowtie2 -X 1000) (*110*). The previously separate replicates were merged together for subsequent analyses. Methylation averages were calculated for whole genomes and for specific sets of genetic elements using CGmapTools (*111*). UMRs were identified as described in (*112*). Briefly, reference genomes were segmented into 100-bp intervals. Intervals lacking at least four covered CHG-context cytosines (CHGs) were discarded. Coverage was calculated on a per-cytosine basis and summed over each interval, and any interval with less than 20 reads covering CHGs was discarded. Intervals with methylation of greater than 20%, calculated using the weighted methylation formula (*113*), were also discarded. This was repeated on 20bp sliding increments, and all overlapping intervals or intervals separated by only 20 bp were merged to define larger UMRs. UMR edges were then trimmed such that their boundaries were defined by CHGs with less than or equal to 20% methylation. At this stage UMRs that overlapped with blacklisted regions (identified based on abnormally high coverage of the 150nt paired end Illumina reads that were used in each genome's assembly) were discarded. This process was repeated using CG/CHG methylation combined rather than CHG methylation alone and both sets of UMRs were merged. Finally, UMRs that were shorter than 150 bp in length were discarded.

A conservative approach was used to identify UMRs present within B73 that were either methylated or unmethylated in other NAM lines at homologous loci. B73 UMRs were divided into quarters of equal length. Based on EM-seq reads mapped to B73, a minimum CHG coverage of ten and a minimum covered CHG count of four was enforced in each UMR quarter. UMRs that satisfied these criteria were separated into those with >= 50% mCHG in all quarters (methylated) or < 20% mCHG in all quarters (unmethylated). UMRs in which all four quartiles were methylated were classified as high-confidence differentially methylated regions (DMRs), and UMRs in which all four quartiles were unmethylated were classified as high-confidence conserved UMRs. For each B73-NAM pair, the DMRs and conserved UMRs were compared to corresponding pan-gene expression levels averaged across the ten tissues and replicates. TPM was used for normalized pan-gene expression. Pan-genes that were absent from B73 were

excluded from this analysis. A subset of TSS-overlapping pan-genes were selected as those where a region from -10 to +400 bp of the TSS was at least 98% overlapped by a DMR or conserved UMR. The NAM founder TPM/B73 TPM ratio was calculated for each selected pan-gene. This analysis was performed separately on each NAM founder-B73 pan-gene pair.

UMR enrichment analyses

A collapsed set of UMRs identified in all NAM lines using B73 as reference was generated using the bedtools (v2.27.1) (*107*) merge function. These UMRs were then intersected with significant SNPs (p-value $\leqslant$0.05) from GWAS analyses using bedtools intersect. Enrichment of significant associations was calculated by shuffling UMR intervals using the bedtools shuffle function. To estimate genome-wide enrichment of significant associations in UMRs, shuffling was permitted in all regions except for sequencing gaps. To assess enrichment in low-copy, genic regions, shuffling was limited to pan-gene coordinates, plus 15-kb flanking regions (bedtools slop), allowing overlap with known UMRs. Summary statistics of intersecting SNPs were tabulated using bash scripts and GNU datamash (v1.3) (*114*). The interval size distribution, feature overlap and other metrics were computed using the GenomicRanges package (*115*).

UMRs identified in B73 were also examined to assess intersection with coding features using the GFF files. With the bedtools intersect function, the number of significant SNPs (p-value $\leqslant$0.05) from the GWAS that are present in the B73 UMR region and also in the genic feature were computed and tabulated.

ATAC-seq and identification of accessible chromatin regions (ACRs)

Three biological replicates were included in each ATAC-seq sample, from two tissues sources. The first tissue source was V1 stage, above-ground tissue, excluding most of the exposed 1st and 2nd leaf blade but including coleoptile, sheath and ligule portions of 1st and 2nd leaves, developing inner leaves, and shoot apical meristem. The second was the same 2nd leaf tissue used for EM-seq. Oh43 and Mo18w were exceptions in that they only included two biological replicates from the first tissue source and none from the second. Finely-ground, frozen tissue was suspended in 500 uL of LB01 buffer (15mM Tris pH 7.5, 2mM EDTA, 0.5mM Spermine, 80mM KCl, 20mM NaCl, 15mM 2-mercaptoethanol, 0.15% Triton X-100). The lysate was filtered through two layers of miracloth (Millipore #475855), stained with ~1 uM DAPI and

loaded onto a Beckman Coulter Moflo XDP flow cytometer instrument. A total of 20,000 nuclei were sorted from each replicate and NAM founder and combined into a single tube containing ~350 uL of LB01. Sorted nuclei containing all NAM founders within a single tube were spun in a swinging bucket centrifuge (5 minutes, 500 rcf) and resuspended in 10 uL of LB01, visualized and counted on a hemocytometer under a fluorescent microscope, and adjusted to a final concentration of 3,200 nuclei per uL using diluted nuclei buffer (10X Genomics #1000176).

For each replicate, a total of 16,000 nuclei were loaded per well on the Next GEM Chip H (10X Genomics #1000162), targeting a final recovery of ~10,000 single nuclei per library. Single-cell ATAC-seq libraries were prepared according to the manufacturer's instructions (10X Genomics #1000176, Chromium Next GEM v1.1) using the Chromium Controller (10X Genomics #120223). Libraries were sequenced using 100-bp paired-end reads on an Illumina S2 flow cell (NovaSeq 6000) in dual-index mode with 8 and 16 cycles for i7 and i5, respectively. Replicated (3x) libraries were demultiplexed from single-cell ATAC-seq binary base call sequences files (BCL) output from the Illumina S2 NovaSeq 6000 with 10X Genomics *cellranger-atac mkfastq* software (v1.2) and aligned to the B73 RefGen_V4 reference genome (*21*) using *cellranger-atac count* (v1.2), resulting in three distinct sets of FASTQ files containing pooled NAM founders for each replicate. To assign genotypes to individual cells, a VCF file containing NAM founder SNP information mapped to RefGen_V4 (*116*) was used to partition reads by their respective genomes. Specifically, genotype probabilities for individual cells were estimated using *demuxlet* with non-default values (--min-total 100) (*117*). Cells with genotype probabilities less than 0.95 were removed from the analysis. Cell genotype classifications were taken as the genotype with the maximum probability. Finally, raw reads from cells corresponding to the same genotype were concatenated into forward and reverse FASTQ files.

Demultiplexing, genotyping and FASTQ concatenation were repeated for each pool of biological replicates separately. Reads were then processed with fastp (version 0.20.0) (*118*), with the parameters --detect_adapter_for_pe --correction --length_required 35. Reads were aligned to the NAM reference genomes and to the B73v5 genome with Bowtie2 (version 2.3.5.1) (*119*), with parameters --local --very-sensitive-local --seed 1 -q --no-mixed --no-discordant --maxins 1000. Aligned SAM files were converted to BAM files with SAMtools (version 1.10) (*89*), with the parameters view -b -h -S. Duplicate reads were removed with Sambamba (version 0.7.1) (*120*), with the parameters markdup --remove-duplicates and reads were filtered for MAPQ scores of 30 or higher with sort -F "mapping_quality >= 30". ATAC-seq peaks were called with MACS2 (version 2.2.7.1) (*121*), with the parameters callpeak --format BAMPE --gsize 1.8e+9 --keep-dup all --qvalue 0.005.

Pan-genome Analysis

The pipeline described in (*122*) was used to identify homoeologous gene pairs using the canonical transcript for each gene (/iplant/home/shared/NAM/NAM_genome_and_annotation_Jan2021_release). This method requires that genes have high sequence similarity and fall within the same syntenic block. Syntenic blocks were identified by whole-genome alignment using MUMmer4 version 4.0.0.beta2 (*123*) with --mum -c 1000 option. As a result, any genes unanchored to scaffolds would have been excluded.

To compare gene content among genomes, we first created a blast database of all canonical gene model transcripts using the makeblastdb command in ncbi_blast+ version 2.8.1 with default settings. An all-by-all blast was then performed between each pair of genomes. The results were parsed to retain hits between genes within a syntenic block that had a p-value of no more than 1×10^{-10}. Gene pairs from the 26 genomes were added stepwise into a matrix using the custom R script stepwise_add_to_matrix.R and executed in R version 3.6.3 (*124*). Tandem duplicate genes as defined in (*122*) were compressed into semicolon-separated values in the matrix and counted as a single pan-gene for downstream analyses. Lines in the initial pan-genome matrix that had redundant transcripts were compressed such that each transcript was contained in a single line. Additional tandem duplicates identified during this process were also merged and all tandem duplicates are presented as semicolon-separated values in the pan-gene matrix. There remain cases where two biologically separate gene models are annotated as a single combined gene model, as well as genes that are incorrectly split (i.e. one biological transcript annotated as two separate transcripts) within the final annotation that can cause genes to be incorrectly identified as tandem duplicates in the pan-gene matrix.

To recover pan-genes that exist in a genome but were not annotated, representative pan-gene sequences for all pan-genes were mapped to each NAM genome excluding scaffold sequences using GMAP version 2015-09-29 (*96*) with output one path option. Alignments were filtered to have greater than 90% coverage and 90% identity and to be in the same syntenic block to the pan-gene. GMAP canonical transcripts with CDS larger than 200 bp were intersected with annotation gff CDS files containing only the canonical transcript using intersectBed from bedtools v2.29.2 (*107*) with -f 0.90 -r option. GMAP coordinates that intersected with a canonical transcript at these thresholds were replaced by the canonical

transcript name. Pan-genes that overlap with a non-canonical annotated transcript are still represented as GMAP coordinates in the matrix.

Transposable Element Annotation

For each genome, both structurally intact and fragmented transposable elements were annotated using the Extensive *de-novo* TE Annotator (EDTA v1.9.0) (*34*). The curated and updated Maize TE Consortium (MTEC) library (https://github.com/oushujun/MTEC) was used as the base library, so that EDTA could identify novel TE families in each genome (--curatedlib maizeTE02052020). The high-confidence, evidence-based *de-novo* gene annotation of each genome was used to remove genic sequences in the TE annotation (--cds genome.cds.fasta). The species parameter was set to Maize (--species Maize) to use the maize-specific classification model for terminal-inverted repeat (TIR) elements in the TIR-Learner pipeline (*125*) that was included in the EDTA package. To further control false annotations, novel TE families that were single-copy in the source genome were identified using RepeatMasker (v4.0.9) (*126*) and further removed. The remaining novel TE families of all NAM founder genomes were aggregated following the removal of redundant sequences using the "cleanup_nested.pl" script in the EDTA package. The non-redundant, novel TE library was aggregated with the MTEC library to form the pan-NAM founder TE library, which was used to annotate all NAM founder genomes using RepeatMasker (v4.0.9) with parameters "-q -div 40 -cutoff 225". The homology-based annotations (by RepeatMasker) were combined with the structure-based annotation (by EDTA) and formed comprehensive TE annotations for each NAM founder genome. TEs found by structure-based annotations were classified into families using the pan-genome TE library based on the 80-80-80 rule, that is 80% of the TE sequence was covered by a library sequence with more than 80% identity and longer than 80 bp. Annotation statistics were summarized and plotted using custom Perl and R scripts.

Characterization of tandem repeat arrays

The coordinates of CentC, knob180, TR-1 and rDNA repeat arrays were determined by blasting consensus sequences to the assemblies as described previously (*42*). Arrays were defined as ≥100 kbp clusters composed of at least 10% repeat sequences with no more than 100 kbp spacing between repeat units. The completeness of assembled repeat arrays was evaluated by comparing the amount of repeats incorporated in the pseudomolecules with that

estimated with 150bp Illumina reads from the same genomes. Assembled repeats in NAM genomes were identified with BLAST (v2.2.26) and quantified by counting non-overlapping repeat monomers. The absolute repeat abundance for each NAM line was estimated with Illumina reads. Paired-end short reads were subsampled to approximately 3X coverage and aligned as single-end sequences against consensus repeats with BLAST (v2.2.26; -b 5000 -F F). Non-overlapping fragments (≥ 30bp) mapped to repeat sequences in each read were summed as the total repeat abundance. The total repeats were then normalized by read coverage and genome sizes measured by flow cytometry (*40*, *43*).

Knob arrays were categorized as lying in a mid-arm position if they were farther than 2 Mbp from either chromosome end. To identify conserved knob positions, the syntenic positions for each array were defined by the up and downstream sorghum orthologous gene from their respective genome. The knob arrays that correspond to classical knobs were identified by comparing relative coordinates based on karyotypes (*127*) to genomic coordinates of knob arrays in IGV. For the subset of knobs displayed for structural variation (Fig. 3), only arrays that were syntenic to knobs of at least 100 kbp in length in B73 were considered.

Arrays of telomeric 7-mer repeat units (5'-TTTAGGG-3) were identified using the motif search algorithm of the Tandem Repeat Finder tool (version 4.09 with parameters 2 7 7 80 10 50 500 -f -d -m -h) (*128*). To identify the boundaries of subtelomeric repeat arrays, fasta files of the maize subtelomeric sequences were first downloaded from the NCBI database with the following accession numbers: EU253568.1, S46927.1, S46926.1, S46925.1, CL569186.1, AF020266.1, AF020265.1. Subtelomeric sequences were blasted (BLAST v2.7.1+) against each chromosome of the pseudomolecule assembly for each NAM line; blast hits were then filtered for query coverage (≥80%) and percentage identify (≥80%). The coordinates of the filtered blast hits were clustered using bedtools (version 2.27.1) (*107*) to identify the start and stop coordinates of the repeat clusters. IGV was then used to manually check and refine the boundaries of telomeric and subtelomeric repeats located on the ends of the short and long arm of each chromosome for each of the NAM lines.

Fractionation Analysis

For fractionation analyses, the exons from the outgroup Sorghum bicolor (Sbicolor_313_v3.1 from Phytozome) were aligned to the previously described repeatmasked NAM and B73 genomes; annotated maize genes were not used. Tandem arrays for primary Sorghum CDS transcripts were filtered out with the script s.paralog_clusters.pl by selecting

gene model paralogs (i.e., sharing the same gene tree) that were clustered with four or fewer non-paralogous intervening genes as determined by the file tree_id.sorghum_bicolor.txt generated by Gramene. Exons from this filtered Sorghum CDS set were extracted using the Sorghum gff file and the Sorghum genomic fasta file using bedtools getfasta (*107*) and were aligned to the repeatmasked maize genomes using BLAST (*76*), -task dc-megablast, no max target sequences (see project GitHub for scripts and detailed parameters). Sorghum and all the NAM founders plus B73v5 were also filtered for tandem arrays using Tandem Repeat Finder (*128*), parameters 2 7 7 80 10 50 2000 -l 1 -d –h. The coordinates of these filters were applied to the blast outputs and all blast hits that fell within these coordinates in either Sorghum or maize were removed using bedtools intersect with the parameter –v to select only blast hits with no tandem repeat overlap. All sorghum genes with a tandem repeat homeolog in any NAM/B73 were removed from consideration; this was found by running the same bedtools intersect command except with –wa –wb instead of –v for Sorghum hit coordinates that corresponded to any NAM/B73 tandem duplication. Only Sorghum genes that had clear and distinct homeolog associations were used; those that mapped to more than two syntenic regions were removed.

DagChainer (*129*) was run using parameters optimized for the large size and complexity of maize and its large distance between genes and between syntenic orthologs: -s -I -D 1000000 -g 40000 -A 15 (-A being much higher than the default value since exon collinearity was being determined, not whole-gene collinearity). Orthologs were scored in each NAM line based on alignment of at least one Sorghum exon to a single gene-space locus syntenic with the query Sorghum gene. Total Sorghum exon alignment counts per locus per maize genome post-DagChainer were deduced using bedtools groupBy (*107*). Fully retained orthologs were considered to be those that had all expected Sorghum exons aligned to the orthologous region in each maize genome. Partial deletions were those where fewer than the total number of exons of the Sorghum ortholog aligned. Cases where no Sorghum exons aligned at the expected orthologous region in each maize genome were scored as fully fractionated; an ortholog is considered not fully fractionated even if only one exon in one NAM line is present. Sorghum exon alignments were used instead of gene model alignments in order to capture partially deleted loci which may not be represented by a gene model annotation.

DagChainer results were then filtered for Sorghum exon alignments falling within the identified subgenome blocks of B73 version 4 associated with syntenic coordinates of Sorghum gene models from the file B73v4.subgenome_reconstruction.gff3 from Gramene (/iplant/home/yjiao/B73_RefGen_V4/Annotation). Since maize underwent a genome duplication event after diverging from Sorghum, there would be two expected sorghum orthologs in each

maize line; therefore, each Sorghum exon orthologous in maize would have been expected to have two syntenic copies unless fractionation had ensued. Only blast outputs in each NAM founder that share the same B73 subgenome chromosome as the sorghum orthologs were selected, such that if an exon is retained on both subgenomes, it would have two alignments to one Sorghum exon, differentiated in part by maize chromosome ID. Most inversions within the various maize lines were contained within subgenomic blocks, so they would not be excluded by this method. However, special consideration had to be made for Oh7B's translocation of distal chromosome 10 to chromosome 9; all alignments that fell within that translocated region were given the identity associated with the subgenome identity of distal chromosome 10 for the purposes of fractionation assignment. The fractionation pipeline was tested multiple times for accuracy using CoGe's GEvo visualization platform (*130*) and the pipeline was changed as needed to increase true positive alignments and reduce false fractionation calls, resulting in the finalized fractionation dataset (**Supplemental Dataset 1**). Segregating fractionation loci were manually checked in CoGe, and pipeline errors (i.e. false exon deletion calls) or missing exons associated with sequencing gaps as well as loci where flanking syntenic sequence could not be confirmed or exons were too fragmented to make a confident call were removed.

GO enrichment of both homeologs for unfractionated and segregating fractionating pairs was generated in AgriGOv2 (*131*) (http://systemsbiology.cau.edu.cn/agriGOv2/) using the B73 v4 Ensembl gene model dataset corresponding to the B73 NAM gene models (associations generated by CoGe SynFind, default parameters, using the B73 NAM gene model set as query), with parameters SEA, FDR 0.05, Bonferroni correction, and a minimum of 5 mapping entries.

Structural Variant Detection

Structural variants (SV) were characterized using data generated from 1) long reads of each NAM mapped to B73, 2) chromosomal genome assemblies of each NAM aligned to B73, and 3) *in silico* digested assemblies (to simulate a Bionano optical map) of each NAM line aligned to the B73 map.

For the long-read-based SV characterization, error corrected reads from each NAM line were mapped to B73 using NGMLR (v0.2.7) (*132*) with the "--presets" option set to "pacbio" and with "--bam-fix" enabled. The mapping step was trivially parallelized by splitting the input files (PacBio reads) and mapping them simultaneously to the reference genome, followed by merging the output bam files to a single bam file using samtools merge (v1.9). The merged BAM

file was then used with SNIFFLES (v1.0.11) (*132*) for calling structural variants in a two round process. The first round of SNIFFLES used stringent parameters (--max_num_splits 2, --min_support 20, --min_zmw 2, --min_seq_size 5000, --max_distance 5000, --cluster, and --cluster_support 2) with minimum SV size set to 100 (--min_length 100) and generated a VCF format output for each NAM line separately. The individual VCF files were then merged using SURVIVOR (v1.0.6) (*133*), with the max distance between breakpoints set to 1000, taking the SV type and strand into account, without using the estimating SV size option or taking the minimum size of SV into account. Since this merged SV set does not have genotype information, another round of SNIFFLES was run to force SV calls across all NAM lines. In the second round, the merged SVs were provided as input (--Ivcf) along with the BAM files (mapped reads). The final genotyped SVs were combined using SURVIVOR with the same options.

Whole genome sequence alignments of each NAM against the B73 reference were generated using minimap2 (v2.17-r941) (*68*). The PAF-formatted alignments were generated using default options along with -c, (output cigar string), -x asm5 (use of ~0.1% sequence divergence preset) and --cs (encode bases at mismatches and INDELs) options. The generated paf file was sorted using the core utilities sort command, followed by paftools (k8 paftools.js call) (*68*) to characterize variants. The output format was then converted to a bed file in order to visualize SV in IGV (*134*) using a simple awk command.

For characterizing large SVs, each NAM genome was subjected to *in silico* digestion with the fa2cmap_multi_color.pl script from the BioNano solve program, using CTTAAG as the enzyme motif. This generates a simulated, assembled BioNano map in cmap format. The cmap files were aligned against the B73 cmap file using RefAligner tool from runCharacterize.py and runSV.py script of BioNano solve. Default options were used for both steps, with the arguments supplied through an XML file (optArguments_nonhaplotype_noES_DLE1_saphyr.xml). The resulting smap file (with the list of structural variants detected between query maps and reference maps in tsv format), was then converted to VCF format using the smap_to_vcf_v2.py script. The final SV file in VCF format was filtered to only include SVs greater than 1 Mbp using an awk command. Due to lack of resolution near the breakpoints, the SVs were subjected to manual inspection using the paftools alignment in IGV and synteny dot-plots, to refine the start and stop of the SVs called using this method. Calls of Bionano SVs across all NAM lines were made by selecting common boundaries across the lines. The most 5' start position and the most 3' end position were used as the coordinates for the collapsed SV, and the genotypic calls for these overlapping SVs from the same individual were merged. The final curated SVs were

combined to generate a joint SV file using SURVIVOR, with similar options as explained before. The final SV set was generated by merging the SNIFFLES SVs with the curated BioNano SVs.

Analysis of Flowering-time Genes

As proof-of-concept that SVs affect important traits, we closely investigated 39 known flowering-time genes (*53*). We found the B73v5 coordinates for these 39 flowering-time genes and extracted the high confidence SVs of those gene coordinates (genic regions) plus 5 kb upstream (promoter regions) using bedtools (*107*). SVs for each genome relative to the B73v5 genome were further filtered to include only insertions or deletions. These data were formatted for the IGV browser (*134*). For each promoter and genic region of a flowering-time gene across all genomes, unique insertion or deletion events were catalogued manually. These candidate SVs were investigated for association with changes in gene expression using t-tests between lines with and without a unique indel.

Transcripts Per Million (TPM) was calculated for each candidate gene across six specific tissues: V11 leaf base, middle, and tip; V18 tassel; and R1 anthers and ears. The presence or absence of a candidate SV was used to predict the TPM of the candidate gene for a specific tissue (t-tests, accounting for (un)equal variances between groups). Out of a total of 62 unique indels and 372 tests while using the Benjamini-Hochberg procedure for multiple testing correction at alpha equal to 0.05 (*135*), we found 18 unique indels significant and 24 significant tests. Focus for intense study was on those significant indels that were present in at least 2 or more NAM lines and those genes which had multiple significant indels.

Additionally, we inspected the previous 39 candidates as well as an additional 134 known flowering time genes (Li et al 2016) for differences in gene expression between the temperate and tropical lines without tissue specificity, i.e. the TPM value was averaged across all tissues for a given line. Similar cut-off criteria were used as before. While no candidates surpassed the multiple testing cut-off, there were candidates with greater than +/- 2 log2 fold change between temperate and tropical lines. Candidates that met the log2 fold change cutoff were manually scanned for indels using the IGV browser as before (*134*). If an indel was found segregating between lines, an ANOVA determined if there were significant differences between indel haplotypes (Figure S17). Further confirmation was achieved using CoGe (*130*) to manually inspect these loci. TE annotations gave support to a TE origin for these candidate SVs.

Using a permutation test, the Li et al 2016 candidates were significantly enriched with GWAS SNPs for Days to Silking, Anthesis Silking Interval, and Days to Anthesis (exact p-value

ranged from 0 - 0.028). Neither the Li et al 2016 candidates or the Dong et al 2012 candidates were more variable (i.e. had greater coefficient of variation in expression) as random subsets of genes (p-value 0.677-0.995).

Glossy 15 analysis

Two insertions were identified as candidates, 337 bp and 881 bp in size, associated with changes in gene expression changes (short insertion: t = -3.932, p = 6.354×10^{-04}, long insertion: t = 3.151, p = 2.923×10^{-03}). The shorter insertion passed a log2 fold change cut off of (+/-) 2 at 2.06 while the longer one did not at -1.78. Those lines that contained only the shorter insertion had significantly higher expression in V11 middle (F = 24.51, p = 4.39×10^{-10}) and tip of the leaf (F = 24.51, p = 4.24×10^{-10}) tissue than any of the other haplotypes. Lines solely containing the shorter insertion were Oh43, Il14H, P39, M37W, and CML277. This insertion was confirmed with a local alignment in COGE where Oh43, Il14H, M37W, and CML277 all showed alignment with the P39 assembly while lines without the insertion were missing alignment.

ZCN10 analysis

ZCN10 had higher expression levels in tropical NAM lines compared to temperate NAM lines (est. difference = 8.49 TPM, t = -2.346, raw p = 0.0358, log2fc = 2.940). There is a single large insertion in CML247 and NC350, but this could not be verified by manual inspection with CoGe. The local alignment of CoGe did detect many deletions relative to NC350 in the upstream region of *ZCN10* in temperate lines with the exception of B73, Il14H, and Oh7b. Deletions were detected in the tropical lines CML333, CML52, and Ki11. Those with these deletions appear to have less expression than those without, but it is difficult to parse if these deletions are correlated with TPM and if so, which deletions are the most strongly correlated.

Dof21 analysis

Dof21 had higher expression in tropical NAM lines compared to temperate (est. difference = 32.123 TPM, t = -2.542, raw p = 0.01898, log2fc = 1.540). P39, B73, and Il14H were temperate outliers with higher expression while CML52, NC350, NC358, and CML247 were tropical outliers with lower expression. There were 2 insertions and 1 deletion with segregating haplotypes in the promoter window. Those lines with only one of the insertions had significantly lower expression than lines with both, neither, or the deletion (F = 8.658, p = 0.000317). Lines with only one of the insertions included most of the temperate lines (except

P39) and the tropical outliers. These insertions were confirmed by manual inspection with CoGe.

ZmCCT10 analysis

ZmCCT10 had higher expression in tropical NAM lines than in temperate lines (est. difference = 0.2459, t = -1.844, raw p = 0.0895, log2fc = 2.063). CML247 was an outlier for high expression. There was an insertion and deletion segregating between the NAM lines, but there were no significant differences in TPM between the different haplotypes (F = 1.252, p = 0.307). These deletions likely correspond to the *CACTA* insertion found in B73 (*52*). Because of the cyclical expression pattern of *ZmCCT10*, it is likely our method of calculating TPM across tissue with a single time sample limits our ability to connect these deletions to flowering time.

Analysis of Disease Resistance Genes

The NLRs were extracted from the genomic DNA sequences using NLR-Annotator (*136*) and from proteomes using hmmalign with reference HMM of the grass NB-ARC (*49*). Additionally, NLRs and NLR-IDs were characterized in the Brachypodium (*137*) and maize annotations using the plant_rgenes pipeline (https://github.com/krasileva-group/plant_rgenes) (*138*) (e-value cutoff 1×10^{-03}). The number of NB-ARC containing proteins was compared to those previously identified in Arabidopsis (*139*) and plotted using R package ggplot2 (*140*). The NB-ARC domain alignment was manually curated for the presence of NB-ARC domain functional motifs including Walker A, WALKER-B, RNBS-C, GLPL and RNBS-D. The NLR phylogeny was determined using RAxML MPI (v8.2.9,-f a, -x 12345, -p 12345, -# 100, -m PROTCATJTT) (*141*). The phylogeny was visualised and re-rooted on the longest internal branch in iTOL (*142*).

Population Genetic Analysis

GERP. Soft masked copies of 13 angiosperm genomes were aligned to the unmasked B73v5 reference genome using LAST (*143*–*148*). Repetitive elements in B73v5 were then masked in the aligned sequences. A tree with neutral evolutionary rates was estimated from four-fold degenerate sites in the alignment using rphast with default parameters (*149*). We then used the tools gerpcol and gerpelem from GERP++ (*150*) to estimate conservation scores at

aligned base pairs and identify conserved elements. For gerpcol we excluded the B73 genome from the alignment to avoid reference bias.

Enrichment analysis. To test whether structural variants were depleted in conserved elements, we measured the overlap between structural variants and conserved GERP elements and performed Fisher's exact tests. For tests involving combined deletions and insertions, we measured the overlap of base pairs in conserved elements with the presence of a structural variant in any of the NAM parental lines. We also tested for the depletion of deletions and insertions in conserved coding sequence, conserved noncoding sequence, and conserved non-genic sequence. In all three of these cases, the Fisher's exact test was testing depletion compared with non-conserved elements. For tests involving insertions, we measured the overlap of GERP elements with insertion start sites. As insertions may simply move conserved elements while maintaining their function, we speculated that insertion start sites may be more meaningful than base pairs of overlap with conserved elements. Insertions were also subdivided into quartiles based on size to test whether the size of insertions was associated with its depletion in GERP elements.

To test the relationship between genomic features and the presence of SVs, we used quasi-Poisson regression in 10kb windows to explain the number of overlapping SVs based on overlap with GERP elements, accessible chromatin (*5*), recombination rate (*151*), and the number of masked base pairs in B73 (see supplemental Transposable Element Annotation). The model takes the following form:

$$log(\lambda i) = \beta_0 + \beta_1 * \text{gerp element overlap} + \beta_2 * \text{recombination rate} + \beta_3 * \text{open chromatin} + \beta_4 * \text{masked base pairs}$$

Where λ_i is the number of occurrences of SVs within the i^{th} window. As this is a quasi-Poisson model, the expected value of λ_i, λ, is equal to the expected number of SVs in a window, and $\theta\lambda$ is equal to the variance of the number of SVs in a window, where θ is a dispersion parameter.

Simulations. We used SLiM (*152*) to generate simulations of a 20-Mbp region consisting of two genomic element types that represented coding and non-coding sequence. The size and number of the element types were based on the approximate median values of B73v5 genome annotations described in the main text. The simulated 20-Mbp region consisted of 300 genes, each separated by 30 Kbp of non-coding bases. Each gene consisted of four 200 bp exons, and three 300 bp introns. Three types of mutations were simulated to represent neutral, 0-fold non-synonymous, and structural variants. 4-fold and 0-fold mutation types were restricted to the

simulated exonic regions, where structural variants were allowed to occur anywhere along the 20 Mbp segment. The total mutation rate in exonic regions was modeled as the sum of the rate for single nucleotide mutations (μ) and structural variants (μ_{sv}). Each of the three types of exonic mutations occurred in proportion to the average number of 4-fold, 0-fold, and total number of exonic bases, which were 200 kbp, 57 kbp, and 240 kbp, respectively. The distribution of deleterious fitness effects for both non-neutral mutation types were modeled using a gamma distribution with parameters for the mean (s_0 and s_{sv}) and shape ($shape_0$ and $shape_{sv}$), and a dominance coefficient of 0.5.

We reduced the computation time by simulating 1000 individuals in the ancestral population. We maintained the population scaled mutation rate ($\theta = 4N_e\mu$) estimated from median pairwise diversity (π) in maize populations as ≈ 0.008 (*153*) by increasing the mutation rate from previous estimates of 3×10^{-8} (*154*) to 2×10^{-6}. Following recommendations in the SLiM manual (*155*), we rescaled recombination rate to match the change in mutation rate using $r_{scaled=}(1/2) * (1 - (1 - 2 * r)^n)$, where r is the original recombination rate and n is the rescaling factor determined by the ratio of the increased and original mutation rates. Previous estimates of median recombination in maize are 1.6×10^{-8}(*151*); following the equation above, our simulations used a constant recombination rate of 1.05×10^{-6}.

In addition to modeling the distribution of fitness effects, our simulations incorporated a simple demographic scenario based on previous studies of maize domestication (*156*, *157*). We assume a single panmictic ancestral population of constant size (N_a) that underwent an instantaneous bottleneck during domestication (N_b), which we assume occurred $B_T = 0.067N_a$ generations ago based on archaeological and genetic data (*156*, *158*). After the domestication bottleneck, we assume the population size grew exponentially to its present size N_0, where the growth rate was derived from the change in population size as $log(N_0/N_b)/B_T$.

Parameter Inference with ABC. We used Approximate Bayesian Computation (ABC) implemented in the R package *abc* (*159*) to jointly infer the distribution of fitness effects (DFE) and demographic parameters of our model. We used the folded site frequency spectra of variant sites from each mutation category generated from our simulations as input summary statistics to predict the joint posterior distribution of our model parameters. We normalized frequencies by their sum within each window and simulation. We accepted 0.5% of simulation draws with the smallest distance between simulated and observed mutation frequency bins. The posterior distribution was then inferred from the accepted draws using a neural network architecture with two hidden layers using the "neuralnet" method from the *abc* package in R. We conducted a total of 90,492 independent simulations by drawing parameters values from minimally

informative prior distributions reported in the table below. Our Snakemake (*160*) pipeline and SLiM code to reproduce the simulations are available here: https://github.com/HuffordLab/NAM-genomes/tree/master/abc.

***ABC model parameters and prior distributions**. U is short for Uniform. The prior distribution for s_0 and $s_s v$ is a mixture, where 90% of draws are from a uniform and the remaining 10% were fixed with a selection coefficient of zero.*

Parameter	Prior	Description
μ	2×10^{-6}	Neutral mutation rate per base pair.
μ_{sv}	$U(10^{-10}, 10^{-7})$	Structural variant mutation rate per base pair.
r	1.05×10^{-6}	Recombination rate (scaled to match mutation rate).
N_a	1×10^{3}	Ancestral effective population size.
N_b	$discrete\ U(0.01N_a, N_a)$	Instantaneous bottleneck effective population size.
N_0	$discrete\ log\ U(N_a, 20N_a)$	Modern effective population size.
B_T	$0.067N_a$	Bottleneck time (generations before present).
s_0	$0.9\ U(-0.1,0) + 0.1\ (s = 0)$	Mean selection coefficient of 0-fold non-synonymous mutations for the 0-fold Gamma DFE.
$shape_0$	$U(0,100)$	Shape parameter for 0-fold Gamma DFE.
s_{sv}	$0.9\ U(-0.1,0) + 0.1\ (s = 0)$	Mean selection coefficient of structural variant mutations for the 0-fold Gamma DFE.
$shape_{sv}$	$U(0,100)$	Shape parameter for structural variant Gamma DFE.

Model validation. We validated our approach by testing the accuracy of 100 randomly selected simulation runs. In each case, we held out the results of one simulation and predicted its parameters using the remaining simulated data. We evaluated the accuracy and reliability of the model across all 100 runs by calculating: 1. proportion of posterior draws greater than true value (prop_gt), 2. proportion times true values fell within the 95% credible interval (w.in_cred),

3. proportion of times the mean posterior values fell within the prior (w.in_prior), and 4. The natural log of the ratio of standard deviations of the prior and and posterior distributions (log(var_sc)).

Analysis of empirical data. To fit our model to empirical data, we constructed 103 20-Mbp windows along the B73v5 genome. We excluded the remainder of bases at the end of each chromosome, which varied from approximately 1 Mbp to 18 Mbp. We developed a script to categorize sites as 0-fold and 4-fold Using the B73v5 reference genome and gff annotation file (https://github.com/silastittes/cds_fold). We also developed a script to calculate the folded allele frequency spectrum of each of the three mutations types in each window (https://github.com/HuffordLab/NAM-genomes/blob/master/abc/predict/src/get_nam_sfs.py). We followed the same ABC approach that was used in our model validation methods above to infer the DFE and demography parameters from the empirical data, fitting each of the 103 windows independently. To summarize across 20-Mbp windows, we used the average value of each parameter from each of the 103 posteriors.

To assess the degree of similarity between SFS data generated by the model and the empirical data, we ran simulations using 20 random draws from the posterior distributions of each genomic window. Before sampling, we excluded posterior draws that fell outside of parameter domains, and rounded demographic parameters to the nearest whole integer. From these 20 draws per window, we calculated the proportion of mutation counts in each frequency bin of the simulated SFS that were greater than observed counts, where 50% of the simulated draws should be greater than the observed under an adequate model of the data.

Mean and standard deviation of average posterior predictions across the 103 genomic windows. *Population size and mutation rate estimates are reported on the original scale, 100 times that of the simulated values.*

parameter	mean	sd
N_0	2.58×10^5	1.87×10^5
N_b	2.95×10^4	1.58×10^4
μ_{sv}	2.45×10^{-10}	1.88×10^{-10}
s_0	0.0197	0.0210
s_{sv}	0.0274	0.0204
$shape_0$	29.8557	24.870
$shape_{sv}$	50.148	7.965

Genome-wide Association Study and Variance Component Analysis

We collected NAM phenotype datasets from eight publications (*13*, *161–167*). Seven of the datasets are available at https://www.panzea.org/data. The phenotypic data include 36 traits, covering agronomic, developmental, domestication-related, and metabolic characteristics. Traits had already been processed by fitting a model of best linear unbiased predictions (BLUPs) on the multi-environment trial for each trait within each study. A total of 4,027 NAM RILs were used for genome-wide association study and variance component analysis. Genotype projection from NAM parents onto RILs was carried out as follows:

1. Parental SV and Marker Identification. Markers were identified in the parental genotypes using the PacBio and Illumina sequence data described above. During the merge step of the SNIFFLES SV calling pipeline some SVs with non-perfect overlapping boundaries were not merged. If the genotypic calls for overlapping SVs were the same across all of the parents that had genotypic calls, the genotypic information was subsequently collapsed. The boundaries were retained for the SV with the least amount of missing data or the largest one (if they had the same amount of missing data). If there was a disagreement between genotypic calls across all parents, both SVs were retained.

2. Dataset for SV and SNP projections. All SNIFFLES SV markers were reduced to a binary state (SV is the reference state (A) or SV is the alternate state (T)) and converted to hapmap format for projection to the RIL progeny using the middle position of the SV as the variant point position. The identified SNPs were filtered on a per family (RIL population) basis and all families were combined after per-family projections were completed. The per family filters included 1) remove parental SNPs within the boundaries of deletions using vcftools v0.1.17 (*168*) and 2) remove monomorphic SNPs.

3. *GATK SNP calling for NAM founders.* Short reads (PE150 libraries sequenced on the Illumina NextSeq 500 for polishing NAM genomes) were used for calling SNPs by mapping to the B73 genome as reference. The Genome Analysis Toolkit (GATK v4.1.3.0) HaplotypeCaller (*64*, *169*), and best practices published by the Broad institute (*170*), were used along with numerous utilities in the Picard Toolkit (v2.23.3) for SNP discovery and final variant filtering (http://broadinstitute.github.io/picard/). For each read pair in fastq format, Picard was used to convert to SAM format through the FastqToSam utility. MarkIlluminaAdapters was run on SAM

files to mark the Illumina adapters and generate metrics files. The SAM formatted files were converted back to interleaved fastq files using the Picard SamToFastq utility and these were mapped to the BWA-MEM-indexed B73 genome using recommended options (-M) (*171*). The obtained SAM file was converted to BAM using samtools and aligned reads were merged with unaligned reads using Picard's MergeBamAlignment utility, marking duplicates with the MarkDuplicates utility. In the last step of processing BAM files, AddOrReplaceReadGroups was used to add the correct read-group identifier before calling variants with HaplotypeCaller. HaplotypeCaller was trivially parallelized by running simultaneously on 1-Mbp intervals of the genome (2,813 chunks, including scaffolds), and the VCF files were gathered to generate a merged, coordinate-sorted, unfiltered set of variants (SNPs and INDELS). Stringent filtering was performed on the raw set of SNPs using the expression (QD < 2.0 || FS > 60.0 || MQ < 45.0 || MQRankSum < -12.5 || ReadPosRankSum < -8.0 || DP > 5916), where DP was estimated from the DP values of the SNPs (standard deviation times 5 + mean). This filtered set of SNPs was used as "known-sites" with Picard's BaseRecalibrator and ApplyBQSR for recalibrating the processed BAM files from the previous round. The second round of GATK HaplotypeCaller was run using the same method as before and the variants were separated (SNPs and INDELS), quality filtered, and finalized for downstream analyses.

4. *GBS SNP calling for RILs using stacks*. We followed methods, along with commands and parameters for GBS SNP calling using Stacks, from the online workbook (https://bioinformaticsworkbook.org/dataAnalysis/VariantCalling/gbs-data-snp-calling-using-stacks.html). Briefly, metadata obtained from the CyVerse Data Commons and data downloaded from NCBI-SRA (BioProject ID: SRP009896) were processed using the Stacks (v2.53) (*172*) recommended pipeline. Barcodes were formatted and used with the "process_radtags" function to demultiplex the data. The demultiplexed reads were then aligned to the B73 genome using BWA-MEM under default parameters. Output SAM files were converted to BAM, sorted, and indexed after adding the correct Read-Group for each sample with the Picard Toolkit (v2.23.3). The Stacks program command "gstacks" was run using all bam files together, followed by the "populations" command (default options except --vcf, for VCF-formatted output) to generate the final GBS SNPs file. Redundant positions were collapsed to a single line in this file.

5. RIL Genotyping-by-Sequencing Anchor Markers. SNPs identified from GBS data were used to define haplotype blocks for projection of our dense SV and SNP parental markers to the 4,950 NAM RILs. The GBS SNPs were filtered prior to conducting the projections. These filters and subsequent projections were applied on a per family (RIL population) basis and then all

families were combined after the per-family projections were complete. The per family filters included: 1) remove SNPs that were contained within a parental deletion of 100 kbp or less (95% of all deletions) using vcftools v0.1.17 (*168*), 2) remove monomorphic SNPs, and 3) remove SNPs with greater than 70% missing data. Finally, a sliding window approach was applied to correct for possible errors during genotyping as described by (*173*). For this, a 15-bp window, with 1-bp step size, and minimum of five markers per window was used. Only SNPs with allele frequency between 0.4 and 0.6 were retained. After these filtering steps, approximately 13,000-52,000 SNPs were retained per family and used to define haplotype blocks for the parental SV and SNP projections.

6. Parental Marker Projection to RILs. The FILLIN plugin from TASSEL v 5.2.56 (*174*) was used to project SVs in a two-step process. First, haplotypes were created based on SNP and SV information in the parents using FILLINFindHaplotypesPlugin (-hapSize 3000 -minTaxa 1). Then, the parental haplotypes were projected onto missing genotypes in the RILs with FILLINImputationPlugin (-hapSize 3000 -hybNN false). The projections were done for each NAM family independently. Projections of the polymorphic SNPs were completed using the same methods except the haplotype size was set to a larger size (-hapSize 70000). A sliding window was again applied to the projected genotypes to correct possible errors in the projection using a 45-bp window slide, 1bp step size, and a minimum of 15 markers per window. Finally, all monomorphic SNPs were filled back into each family and all SV and SNP markers across the families were combined into a single file.

7. *Additional marker filtering for GWAS*. A genome-wide association study (GWAS) was performed by using the mixed linear model implemented in GCTA-MLMA (*175*). A total of 71,196 SVs with missing rate < 20% were included to estimate the genomic relationship matrix used for SV-based GWAS and a total of 20,470,711 SNPs with missing rate < 20% were included in the SNP-based GWAS. While the first three principal components (PCs) were calculated to correct for the population structure, we excluded the fixed terms of PCs from the GWAS models for all the traits, due to the equal to or slightly lower genetic variances compared to those in the original models.

The GCTA-GREML (Genome-wide Complex Trait Analysis-REstricted Maximum Likelihood) method (*175*) was used to estimate the ratio of genetic variance to phenotypic variance. Differing from trait heritability, this method is to estimate the variance explained by genome-wide markers. We estimated three ratios from this analysis: phenotypic variance explained by all the SVs (SV-based heritability), all the SNPs (SNP-based heritability), and both SVs and SNPs (Combined-genetic heritability). The last estimation uses a method to estimate

SVs-based and SNP-based heritability simultaneously in one model that was implemented with the function “mgrm”.

Supplementary Figures

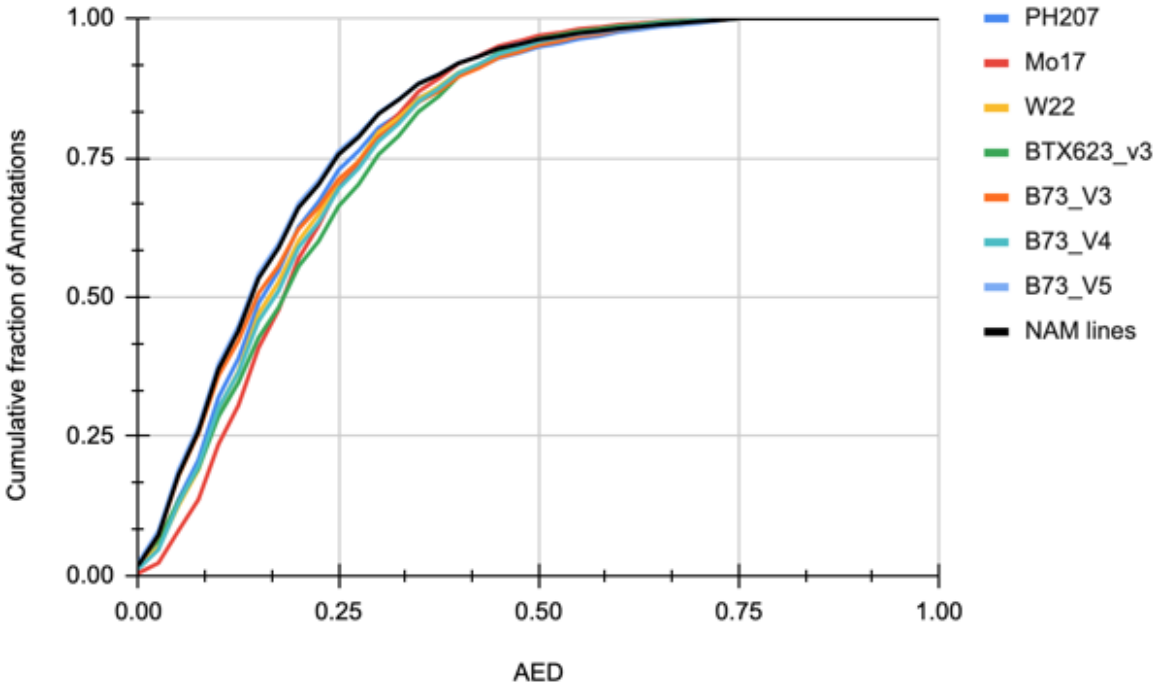

Figure S1. Cumulative Annotation Edit Distance (AED) scores in multiple recent genome assemblies. An AED score closer to zero indicates that more evidence supports the gene models. 83% of B73_V5 (blue) and NAM (black) gene models showed better AED values than other maize or sorghum reference annotations (*2*, *6*, *10*, *20*–*22*). BTx623 is the sorghum reference genome. All others are maize assemblies.

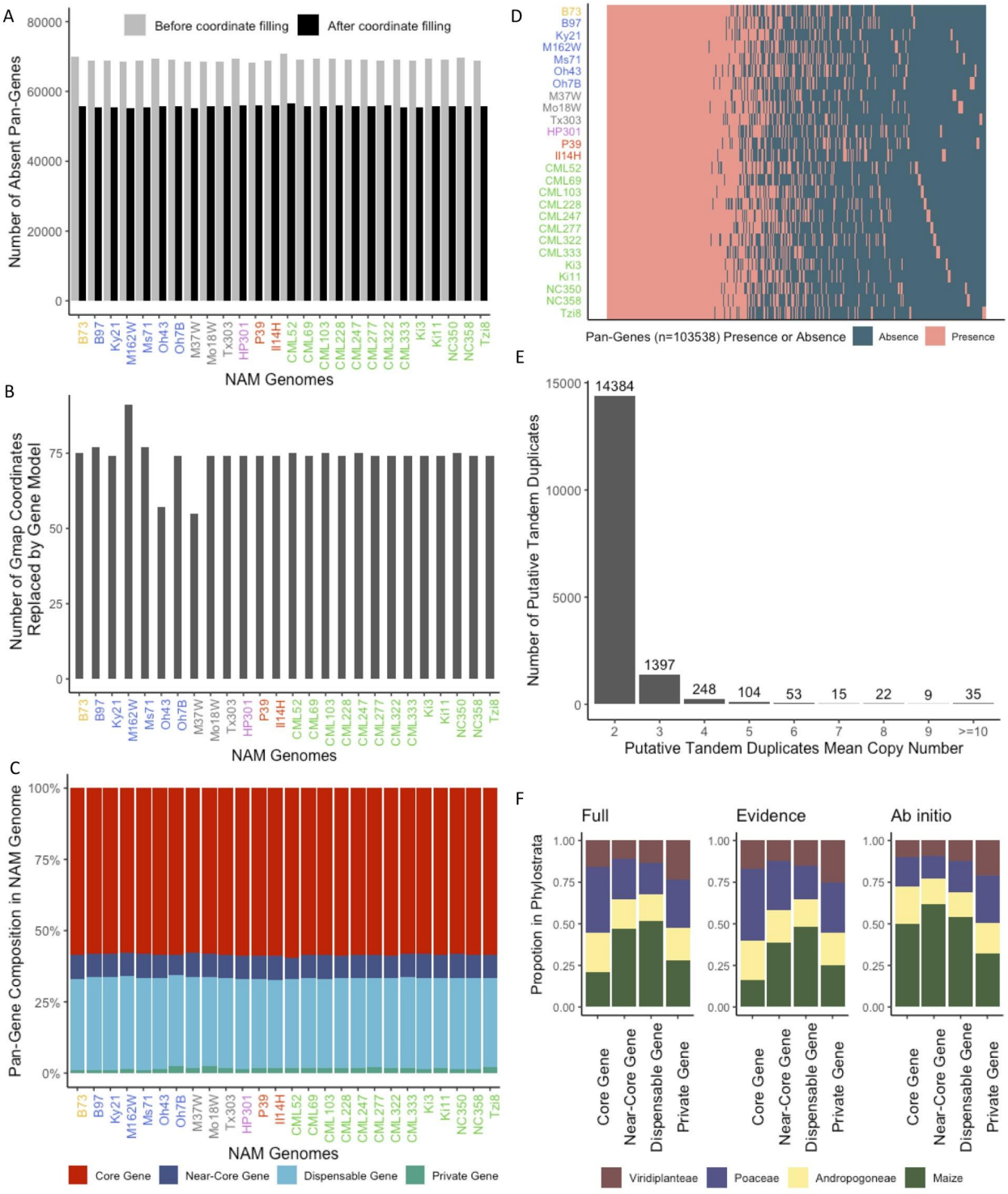

Figure S2. Pan-genome analysis of the gene space. **A**) Number of absent pan-genes in each genotype before and after coordinate filling. **B**) Number of GMAP coordinate fills that

overlapped an annotated gene model at greater than 90% coverage. The coordinate fill was then replaced with the annotated gene model in the final pan-genome matrix. **C**) Proportion of the genes in each genome that are part of the core, near-core, dispensable, and private fractions of the pan-genome. **D**) Presence/absence (PAV) variation of each pan-gene in each genotype with pan-gene order sorted by core, near-core, dispensable, and private. In C and D, tandem duplicates were counted as a single pan-gene and coordinates were filled in when a gene was not annotated but an alignment with greater than 90% coverage and 90% identity was present within the correct homologous block. **E**) Distribution of mean copy number across genotypes that had ≥ 2 tandem copies for the 16,267 pan-genes that had a tandem duplicate in at least one genotype. Values over bars indicate the number in each copy number class. **F**) Proportion of annotated genes in each phylostrata level broken down by pan-gene frequency categories (i.e. core, near-core, dispensable, and private genes). Full is the full set of annotated gene models, Evidence is the set of gene models that were generated based on RNAseq expression evidence from 10 unique tissues, and *Ab initio* are the augmented set of *ab initio* annotated gene models.

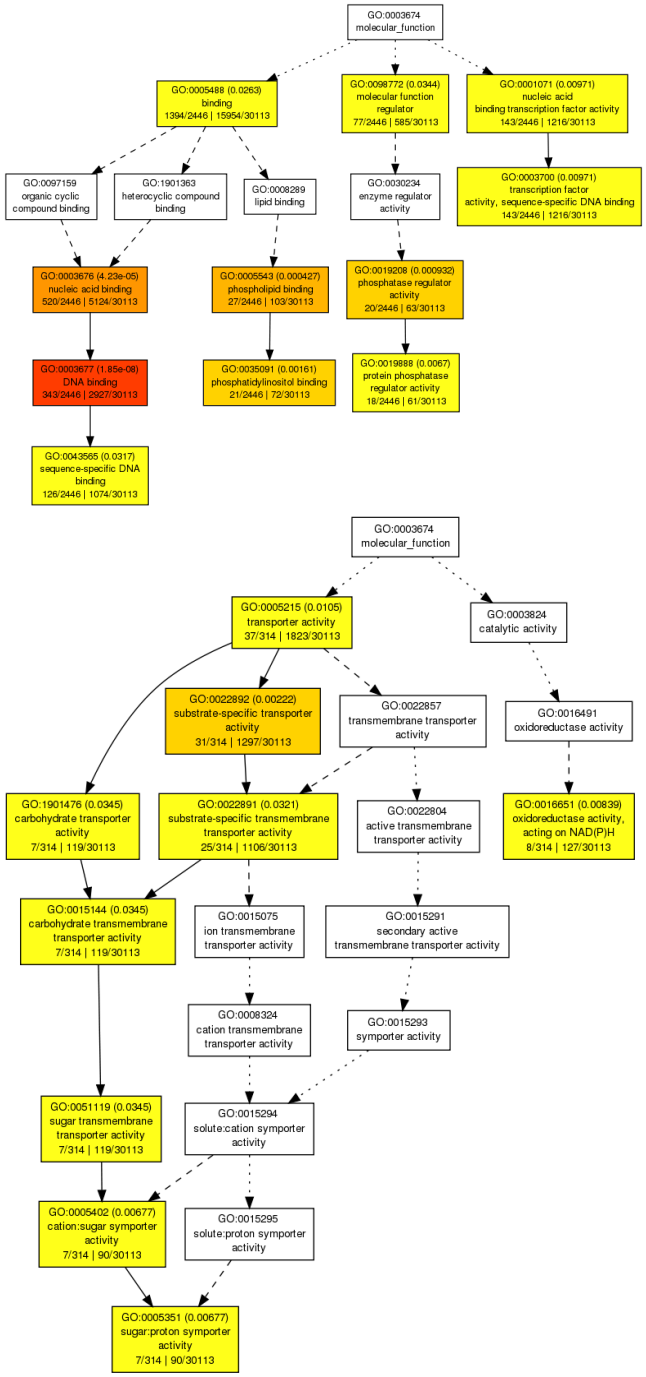

Figure S3: Bonferroni-corrected molecular function GO term enrichment (FDR 0.05) for loci in fully retained homeologs (top) vs loci in fractionating homeologs (bottom). Red shows strongest enrichment; yellow shows weaker (though still statistically significant) enrichment.

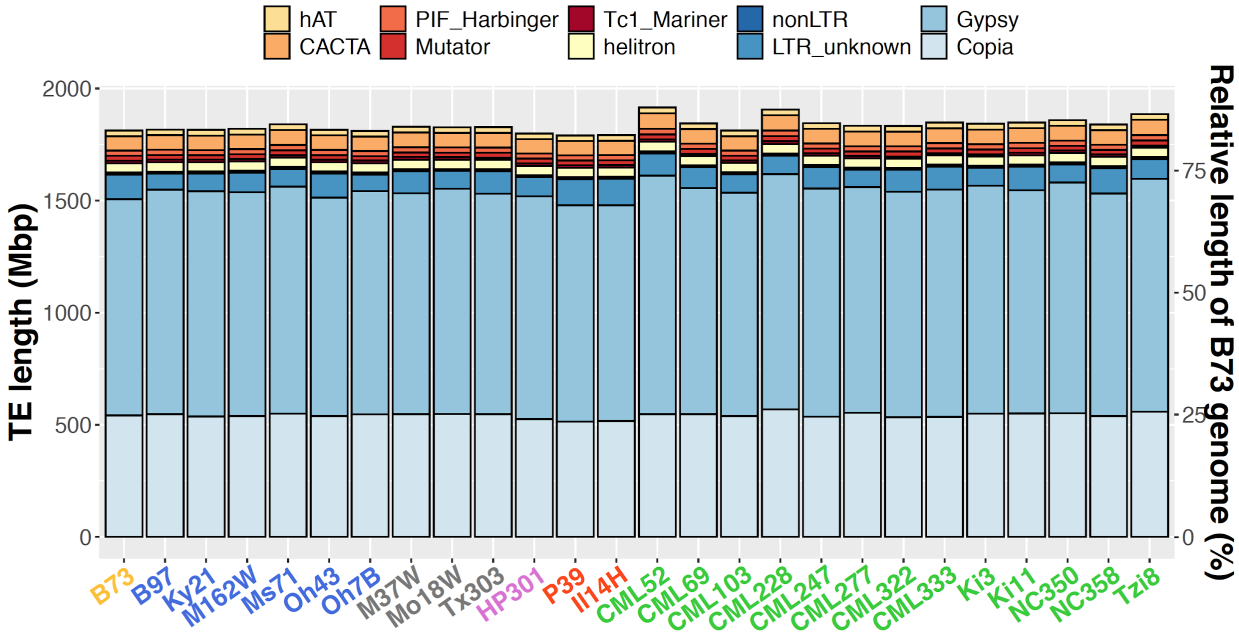

Figure S4. The cumulative length of repetitive sequences in NAM genomes. The right y-axis indicates the size relative to the B73v5 assembly (listed first). Genes and low-copy intergenic regions make up the rest of the assembly.

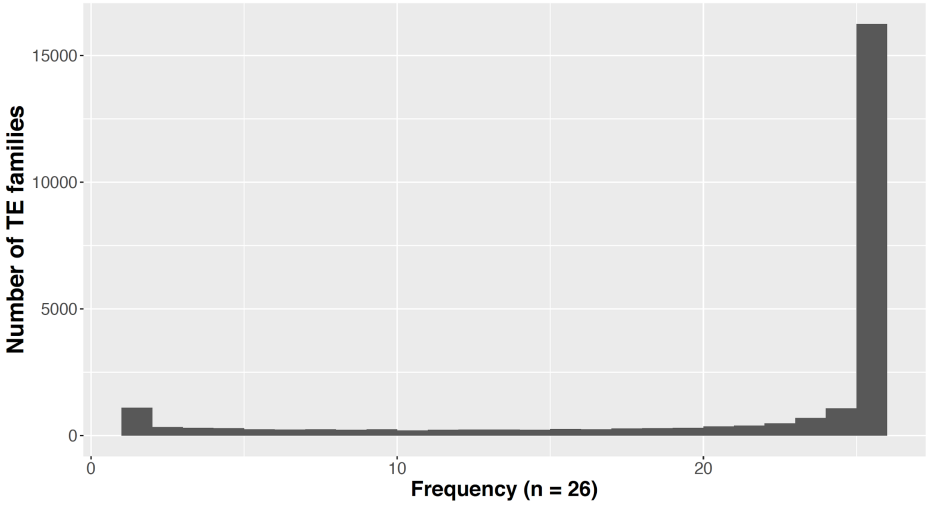

Figure S5. Distribution of TE families in the 26 genomes. The X axis shows the number of genomes, where 1 indicates the number of TE families found in only one genome, 2 indicates the number of TE families found in two genomes, etc.

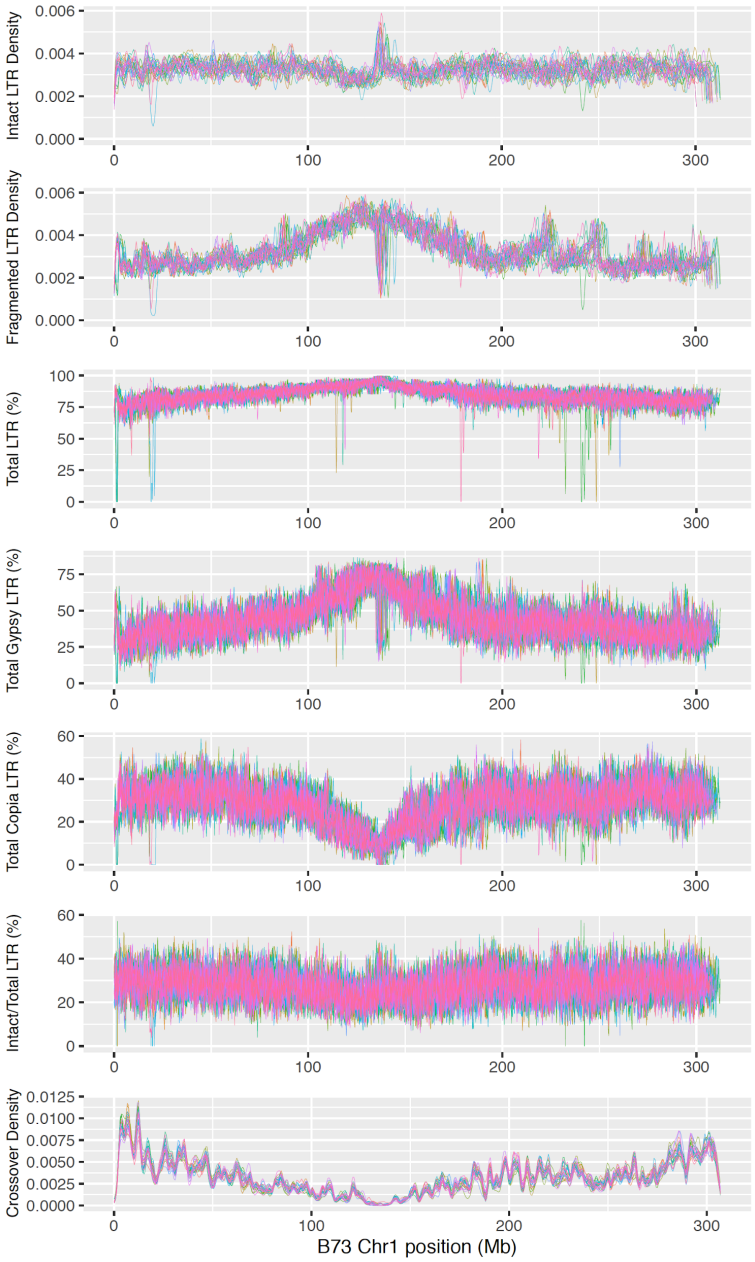

Figure S6. Distribution of LTR retrotransposons on chromosome 1. Each genome is represented by one color. Densities are non-parametric probability densities of the target variable (e.g., the number of intact LTR-RTs). The area under a density line sums to 1. Total LTR (including *Copia*, *Gypsy*, and unknown LTR), Total *Copia*, and Total *Gypsy* percentages are the proportion of respective LTR sequences (including both intact LTR retrotransposons and associated fragmented sequences) of the total assembled sequence length calculated in 500-kbp windows and 100-kbp steps. Intact/Total LTR percent is calculated with Intact LTR percentage (in 500-kbp windows and 100-kbp steps) divided by Total LTR percentage. The LTR makeup is very similar among lines at the Mbp scale. Crossover density (with B73) for each NAM line was calculated using data from (*13*).

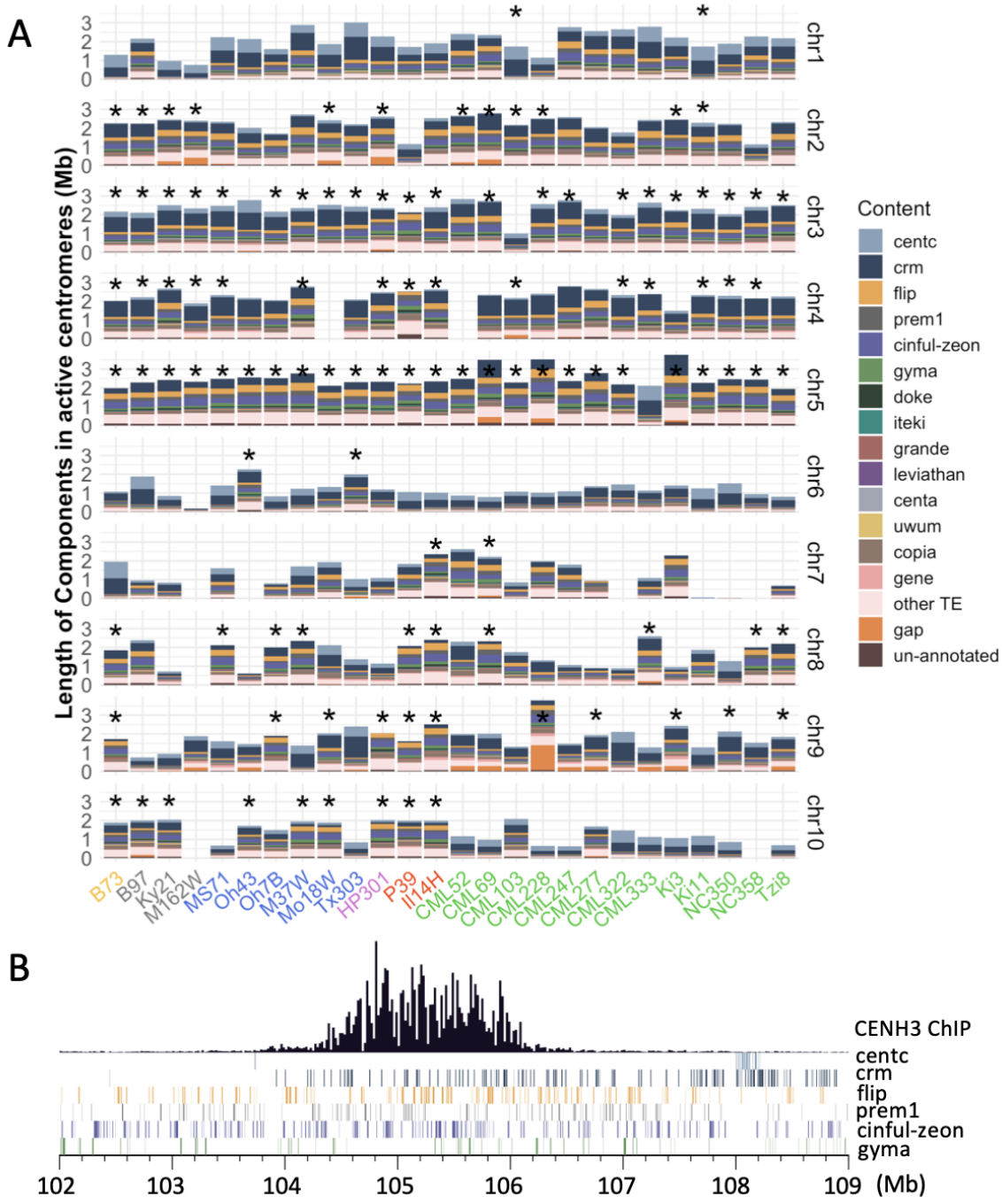

Figure S7. Assembly and components of functional centromeres. **A**) Distribution of transposable elements and repeats in 260 active centromeres among NAM lines. Asterisks depict fully assembled centromeres. Gap only includes gaps of known sizes. **B**) Active centromere on chromosome 5 in B73. CentC and the five most abundant transposable element families are shown as tracks in the lower panel.

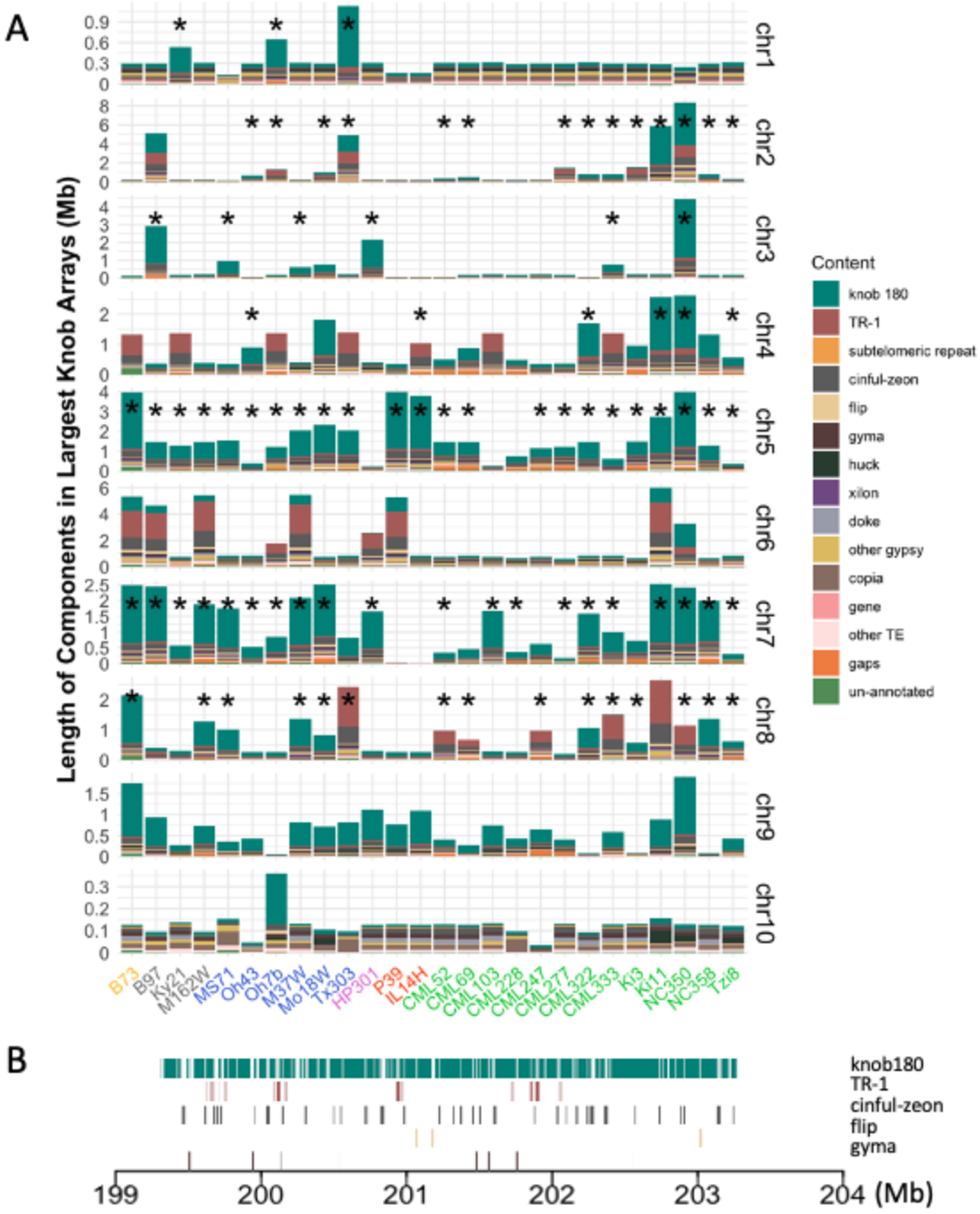

Figure S8. Assembly and components of repeats and transposons in the single largest knob array on each chromosome. **A**) Distribution of transposable elements and repeats in the single largest knob array on each chromosome. Lengths are based on assemblies and only include gaps of known sizes. Asterisks depict fully assembled knobs. Unknown is unannotated. **B**) Largest knob on chromosome 5 in B73. Knob repeats and the three most abundant TE families are shown as tracks.

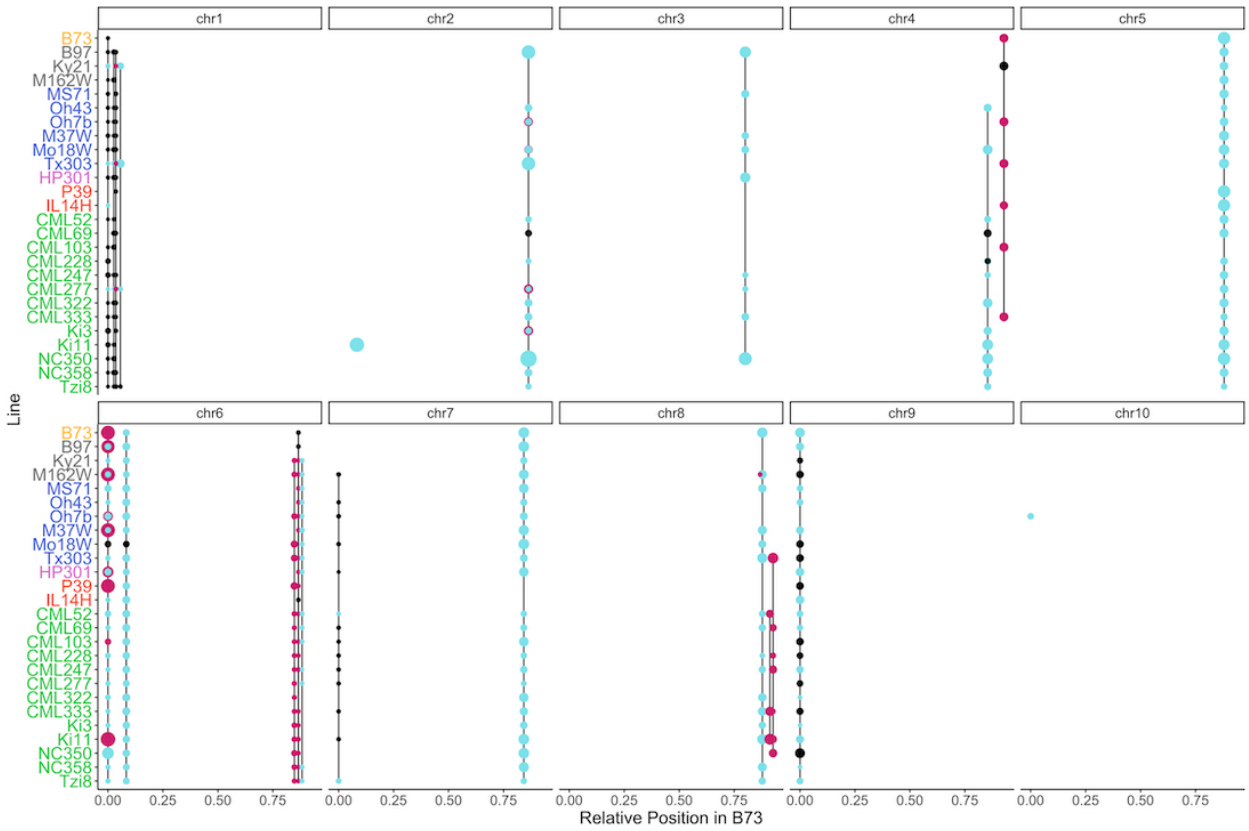

Figure S9. Synteny of classical knobs. Knob arrays corresponding to classical knob180 knobs (blue) and TR-1 knobs (red) are shown. Dot size corresponds to assembled array size. Syntenic arrays that are not cytologically visible are represented in black. The absence of a dot indicates there is no knob array present at the syntenic location.

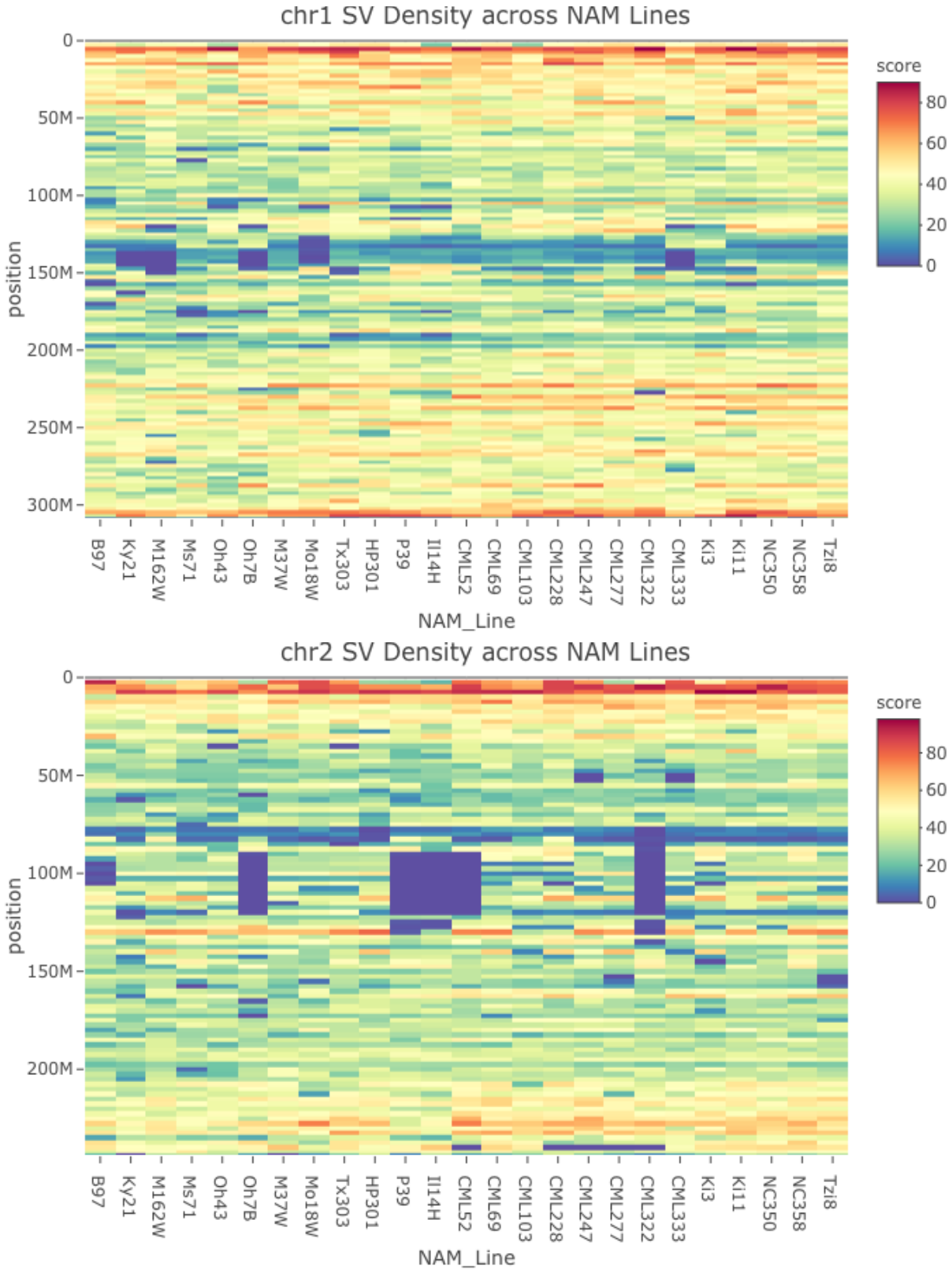

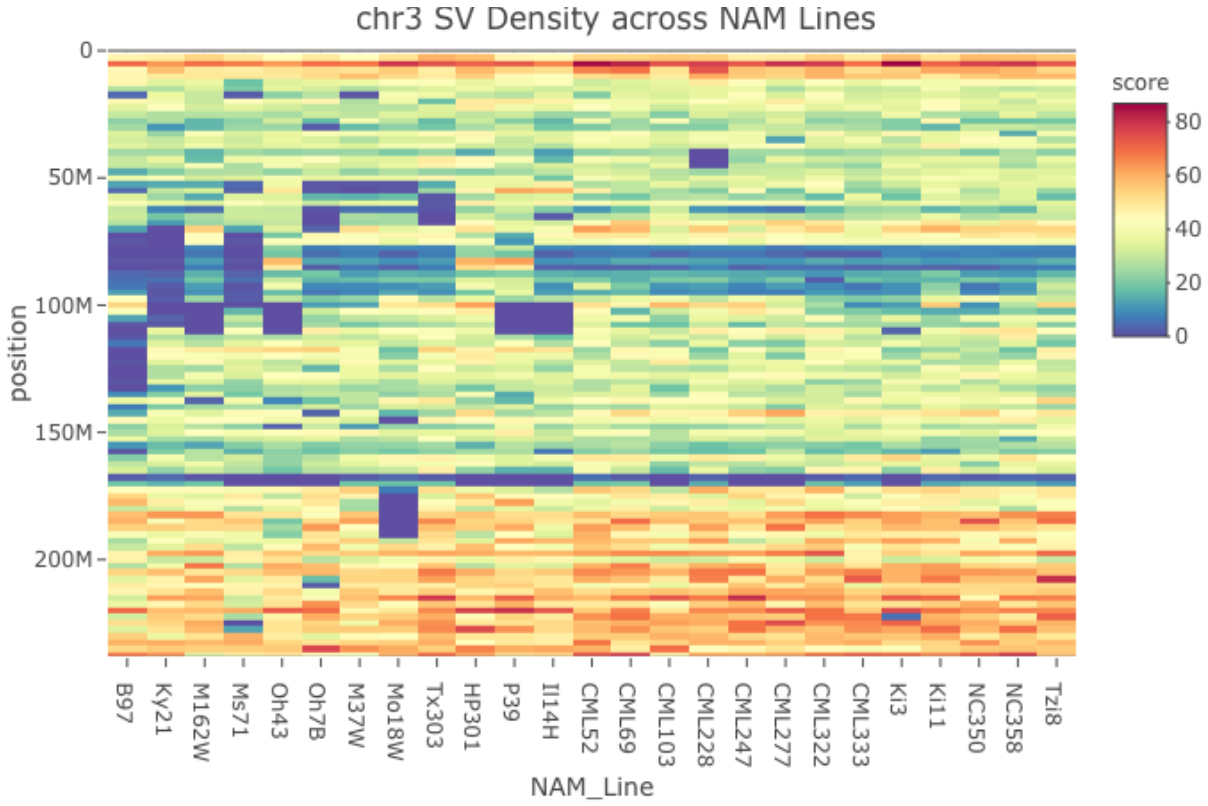

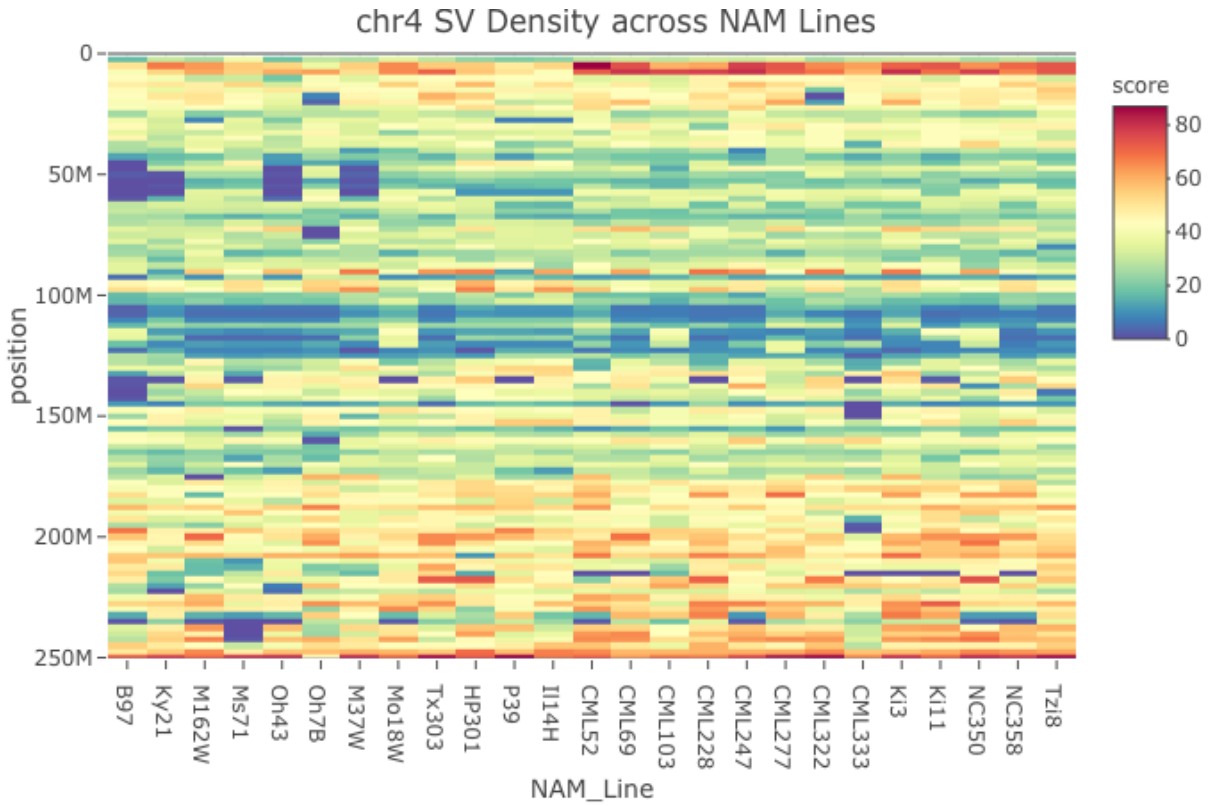

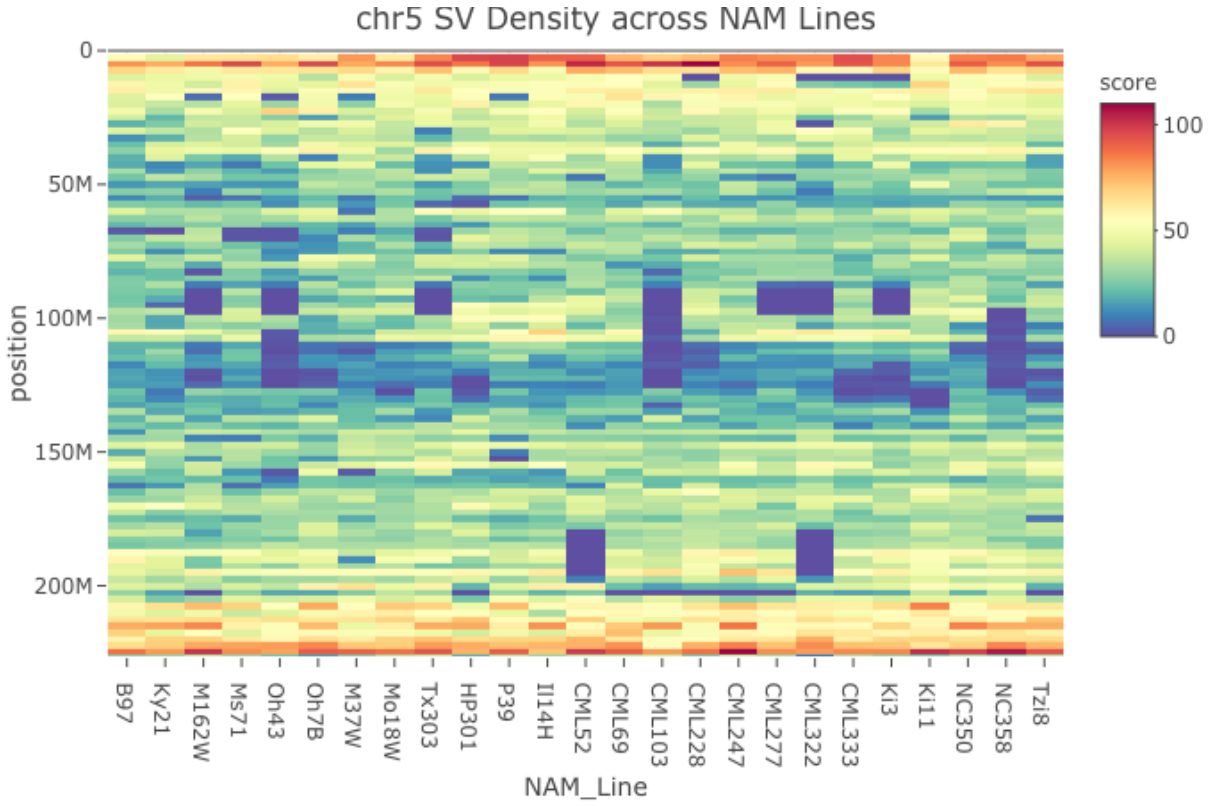

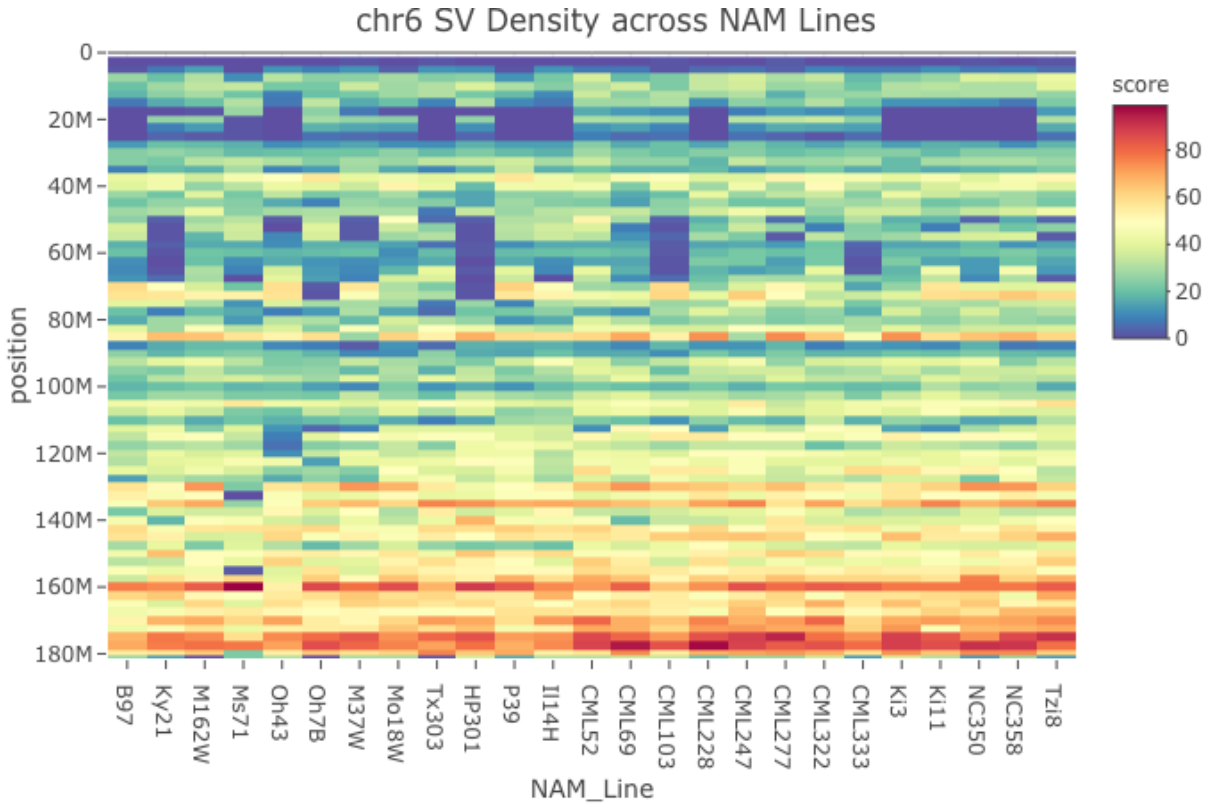

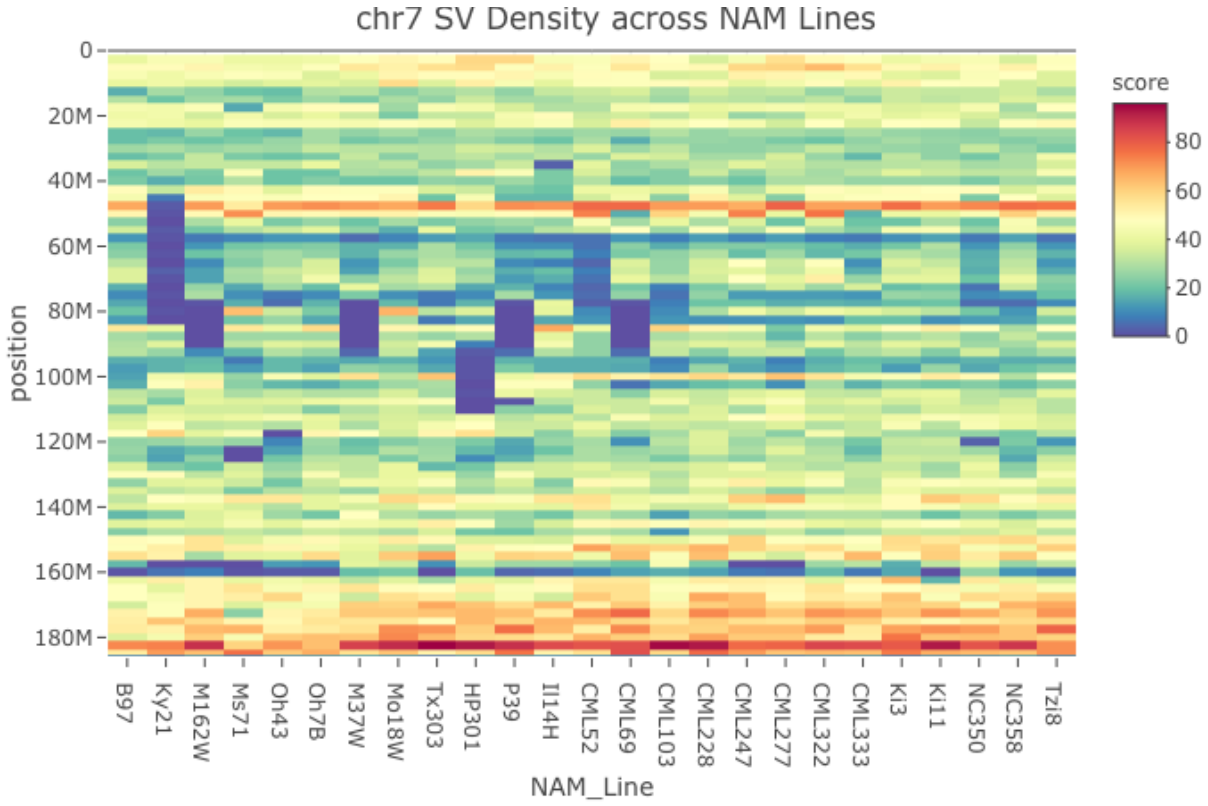

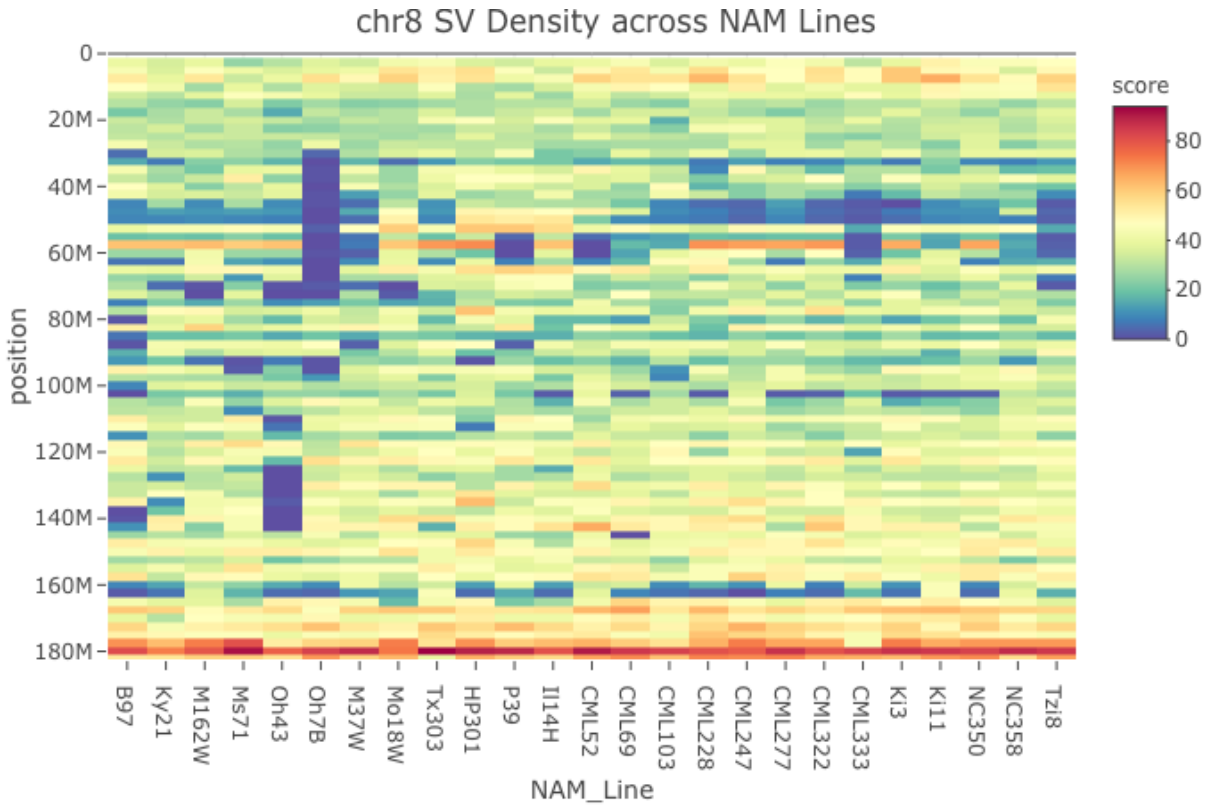

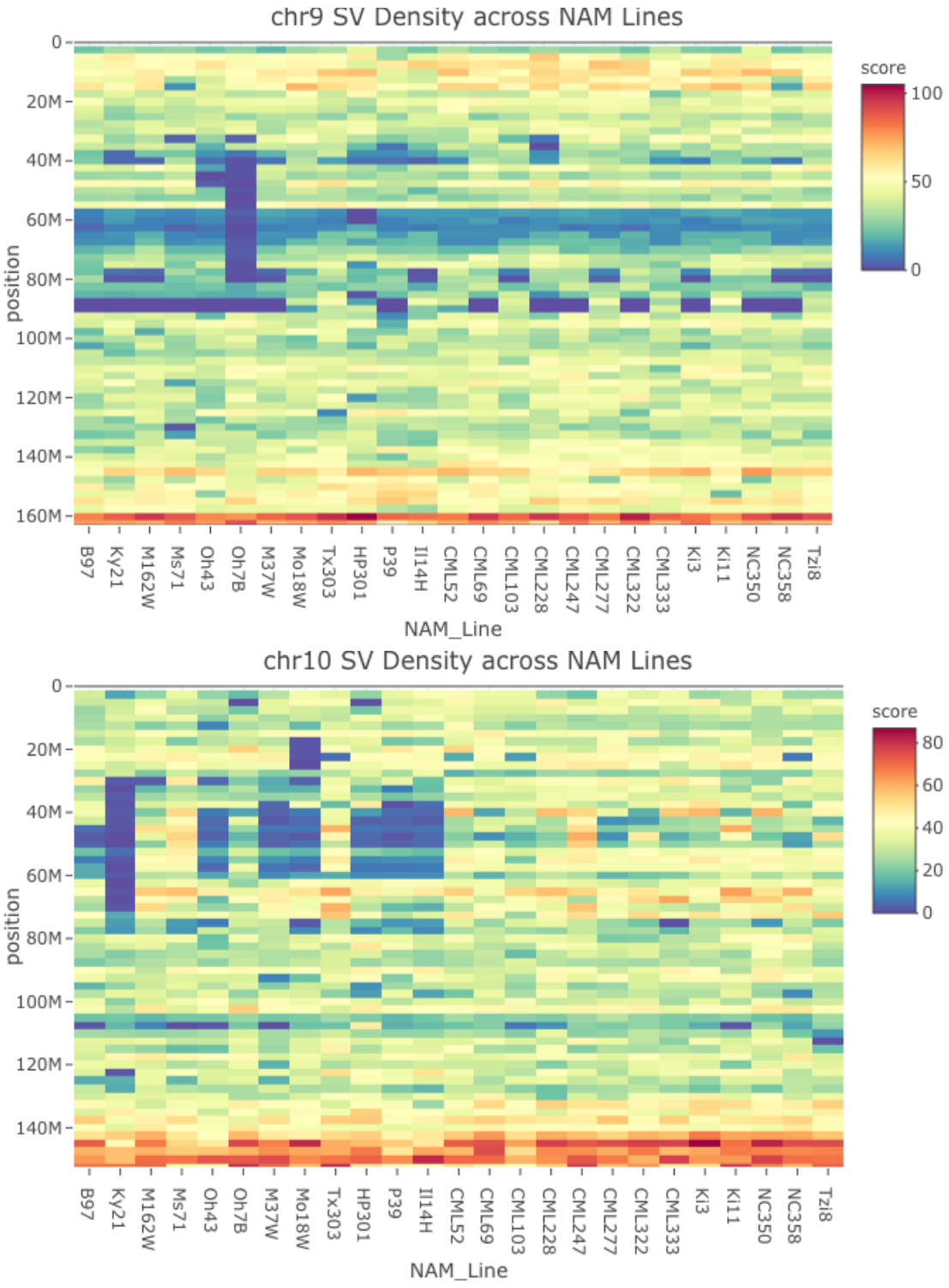

Figure S10. Density of structural variation across the NAM genome assemblies relative to the B73 genome. The scores represent the number of SVs per 2500kb. The minimum size of SVs in this analysis is 100bp or larger. Warmer color indicates higher density of SVs and cooler colors indicates lower density of SVs.

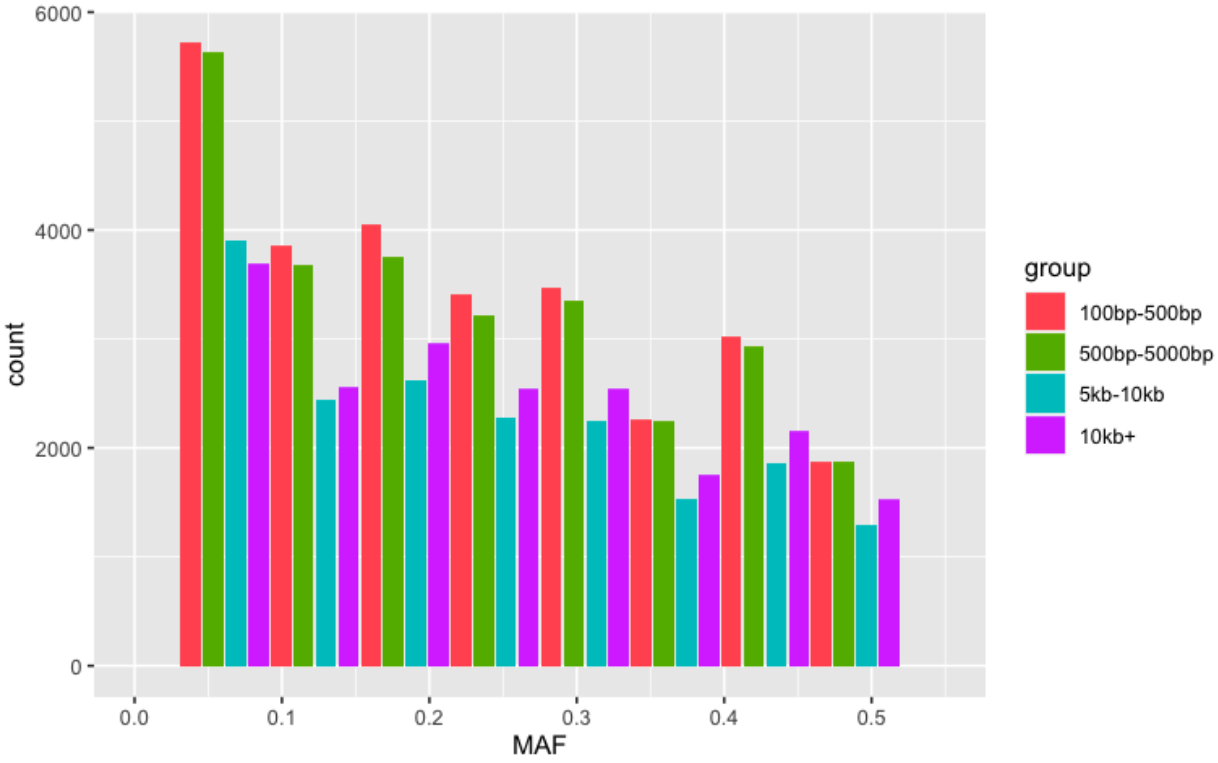

Figure S11. Distribution of structural variation across minor allele frequency (MAF) bins for various classes of size.

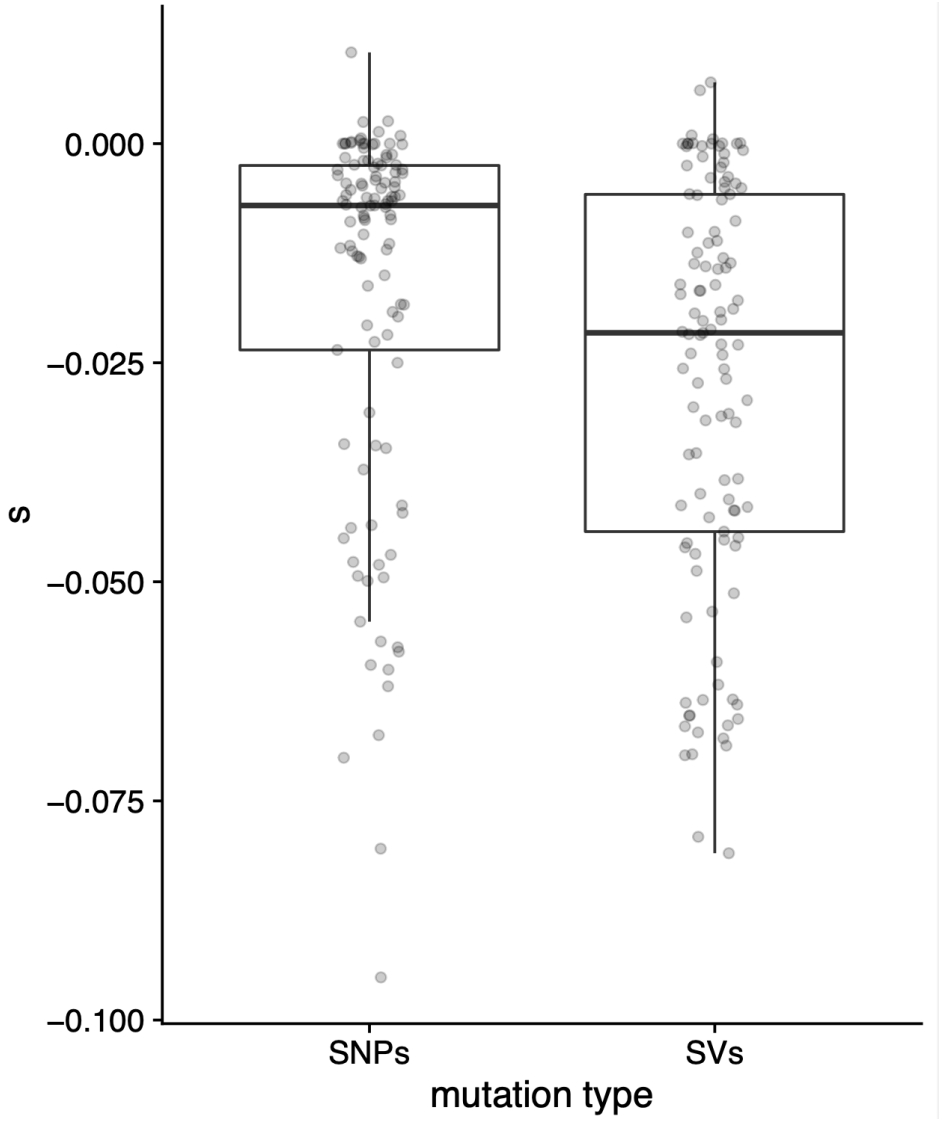

Figure S12. Distribution of mean selection coefficients (s) from 20-Mbp windows.

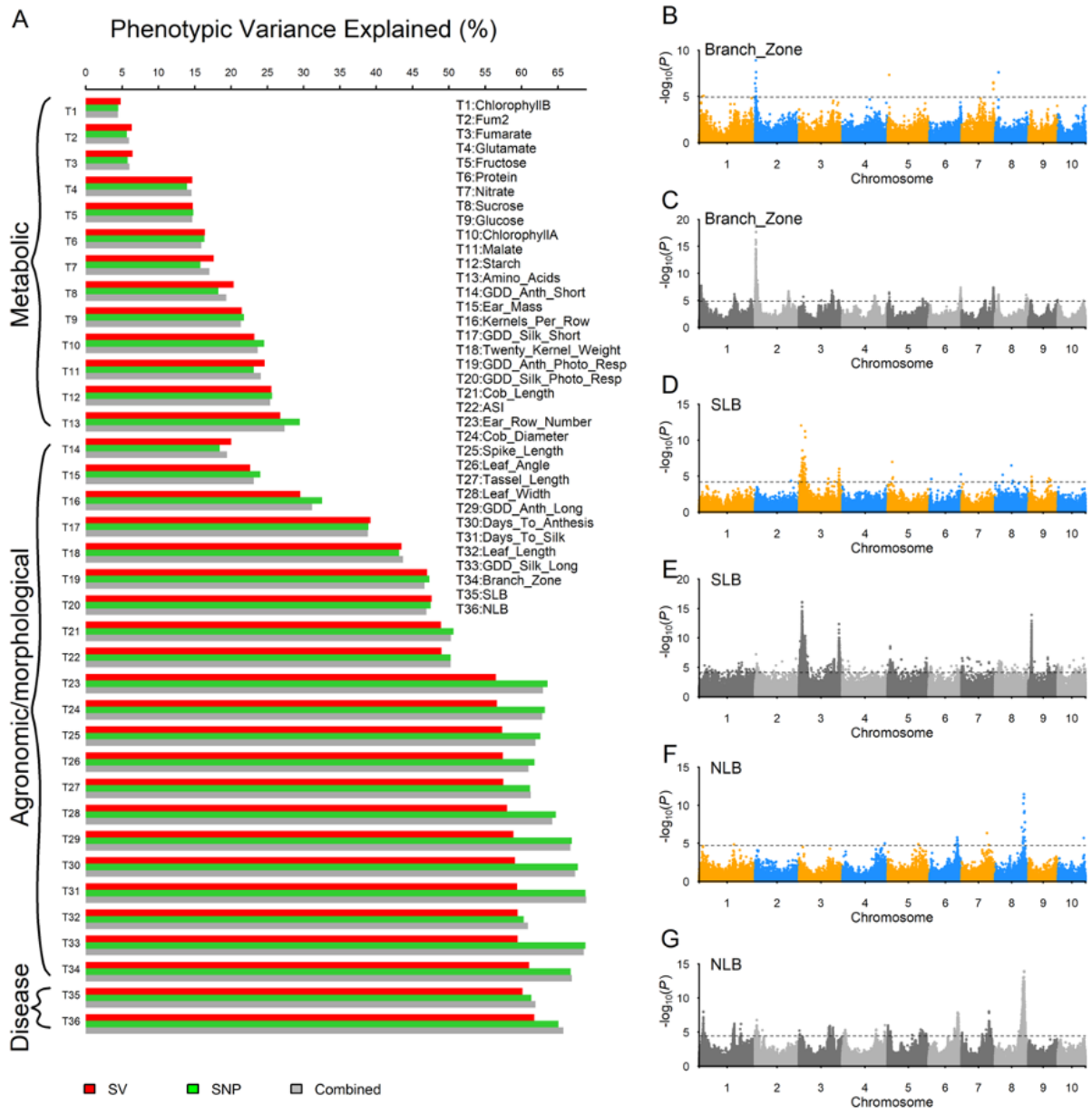

Figure S13. Genetic contributions from SVs and SNPs to complex traits in the population of NAM RILs. **A**) Phenotypic variance explained (PVE) by genome-wide SVs, SNPs, and combined. The 36 traits are organized into three groups: metabolic, agronomic/morphological, and disease-related traits. **B-G**) Manhattan plots of genome-wide association analyses (GWAS) of three traits with the highest PVEs by SVs. The GWAS with SVs (B, D, and F) detected significant QTLs, most of them overlapping with QTLs detected with SNPs (C, E, and G), but one on chromosome 10 for NLB was unique to SVs. The statistical significance thresholds on the Manhattan plots were obtained by controlling FDR on p-value 0.05. NLB and SLB are northern leaf blight and southern leaf blight, respectively.

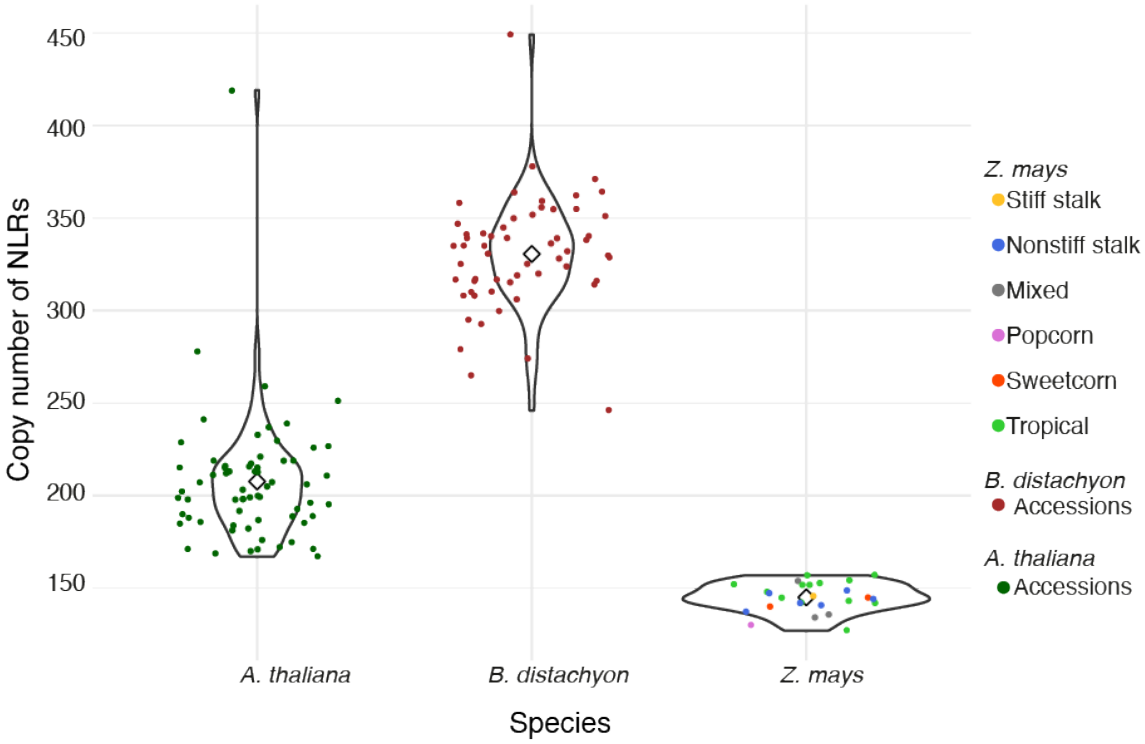

Figure S14. Violin plot of NLR variation in the pan-genomes of a eudicot (*A. thaliana*) and two monocot species (*B. distachyon and Z. mays*).

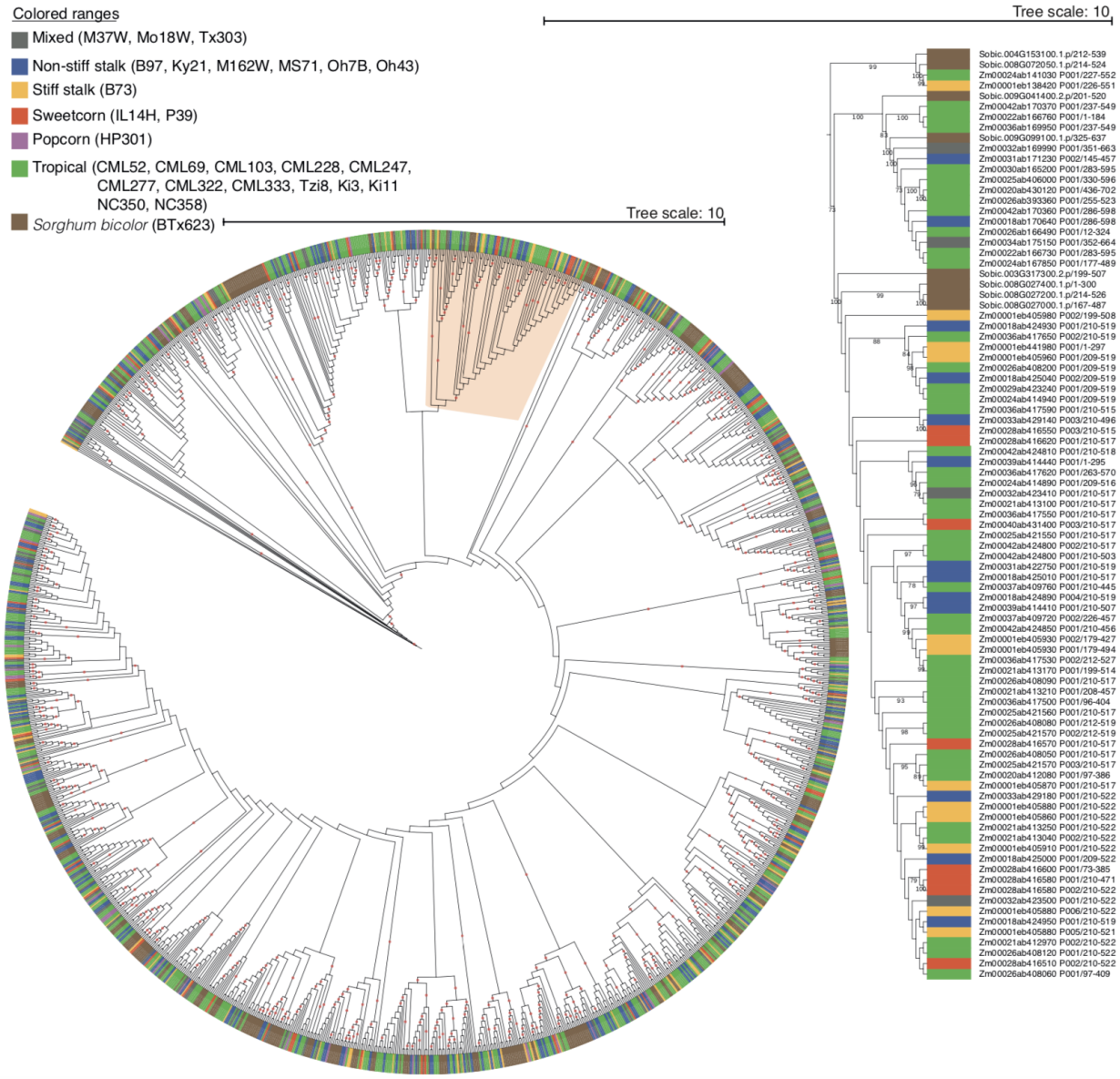

Figure S15. Maximum likelihood phylogeny of all NLR containing transcripts from NAM maize lines and *S. bicolor.* Dots indicate bootstrap values >80. The circle phylogeny shows all NAM NLRs. The linear phylogeny to the right is a zoom of the rose colored region illustrating the general trend that the NLR clades are broadly distributed across the maize NAM founder groups.

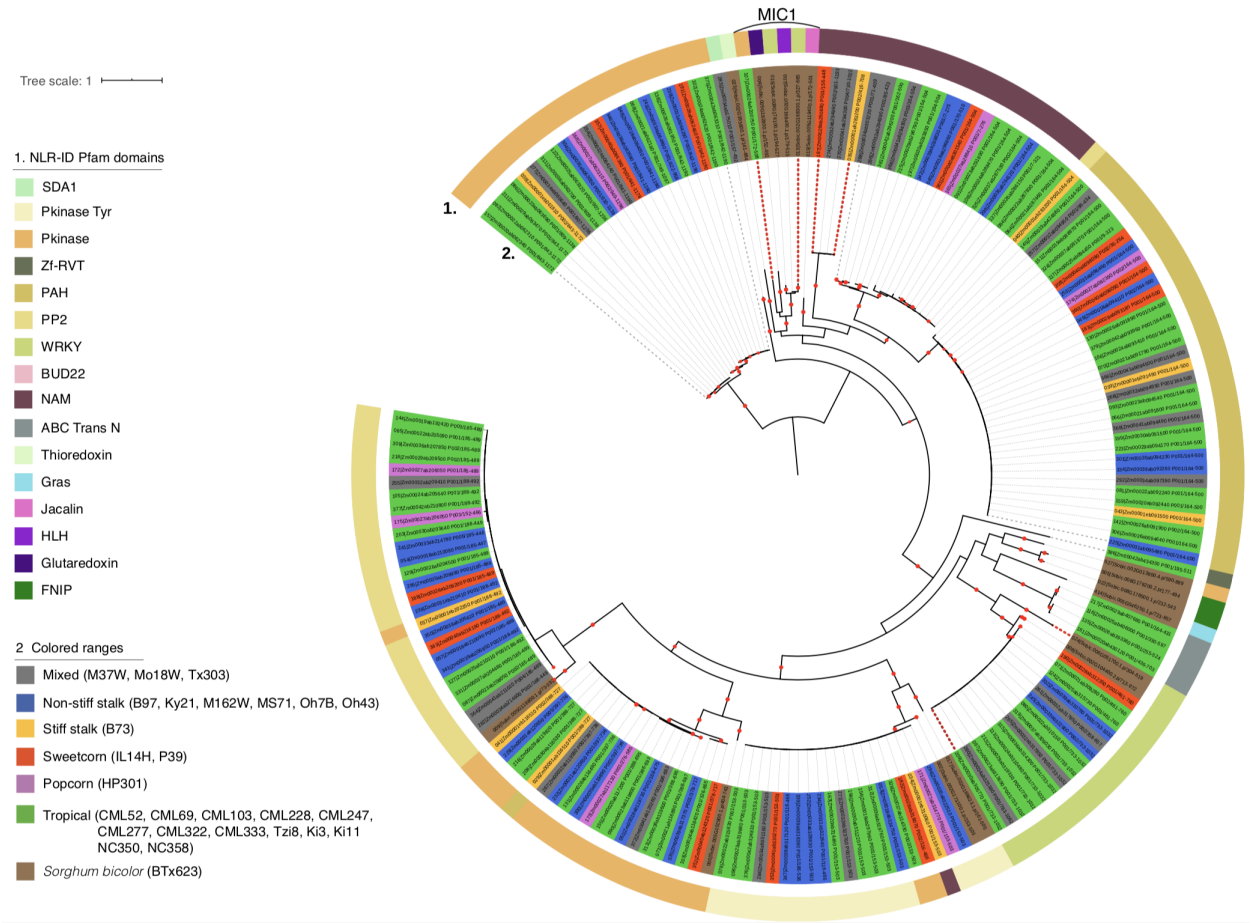

Figure S16. Maximum likelihood phylogeny of NLRs from NAM maize lines and *S. bicolor.* Single red dots on branches indicate bootstrap values >80. Ring one shows NLR-ID Pfam domains. Ring two shows the genes that have the corresponding Pfam domains. The colors represent the NAM founder groups (or Sorghum). Clades delimited by red dotted lines are segregating and not present in all NAM founders within a group.The MIC1 NLR clade (highlighted at top) is particularly fast-evolving in Poaceae (*49*).

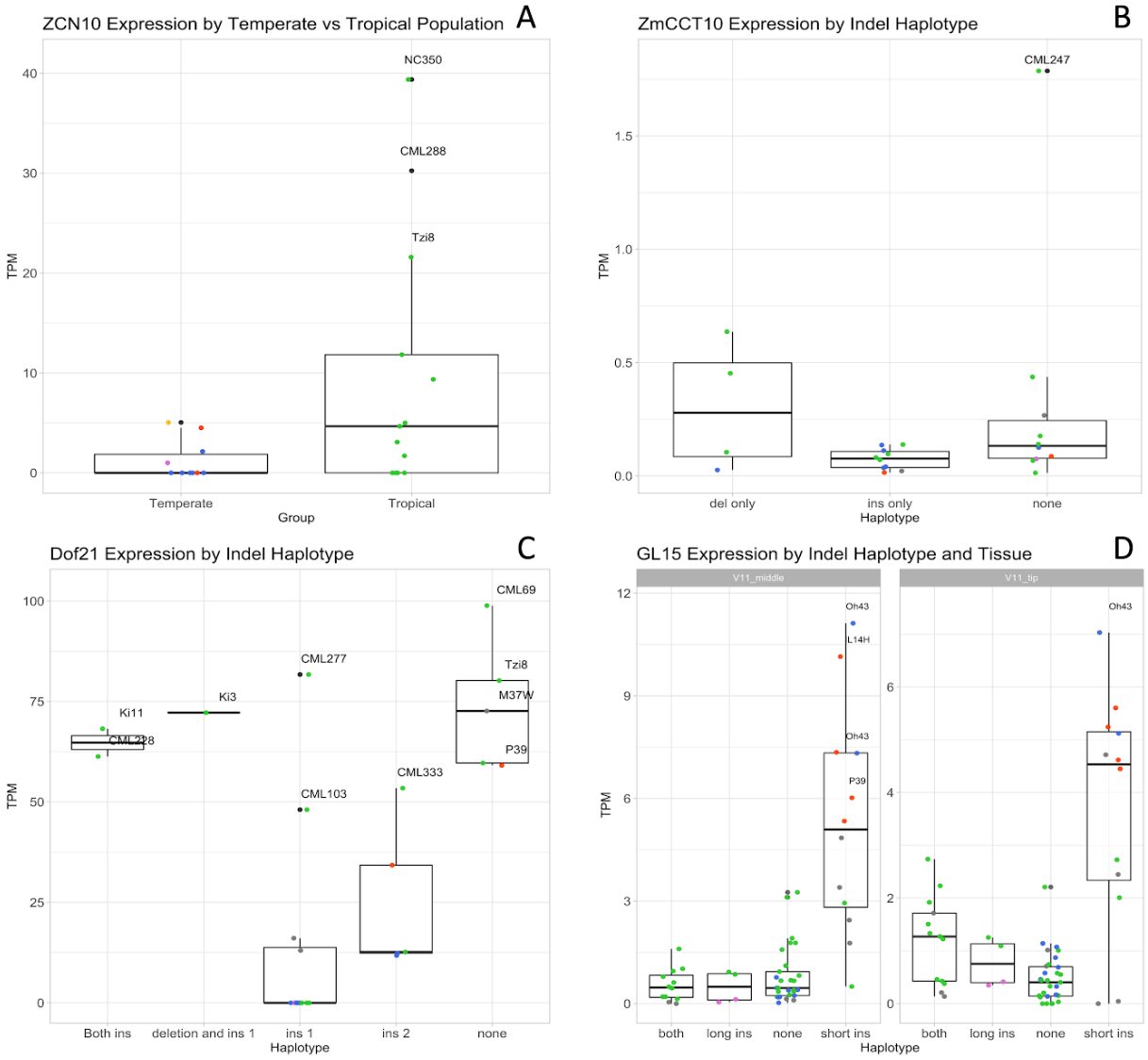

Figure S17. Candidate flowering time gene expression (Transcripts Per Million, TPM) by indel haplotypes. Point colors represent the population (green = tropical, orange = sweet corn, pink = popcorn, blue = non-stiff stalk, yellow = stiff stalk, and grey = mixed). For A-C, each point represents the average TPM across tissues and replicates. **A**) *ZCN10* expression in temperate and tropical groups (indel haplotype in the promoter region is unresolved). **B**) *ZmCCT10* expression in promoter haplotypes containing a deletion, an insertion, or neither indel. **C**) *Dof21* expression in promoter haplotypes containing two insertions and a deletion. **D**) *GL15* expression in promoter haplotypes with insertions. *GL15* showed significant expression differences in V11 middle (left) and tip leaf tissue (right), which was not detected when all tissues were averaged together. Since *GL15* is active for a short window of development in early vegetative stages, this fits with established knowledge of this gene. Expression is plotted based on the haplotypes created by presence/absence of a short and long insertion.

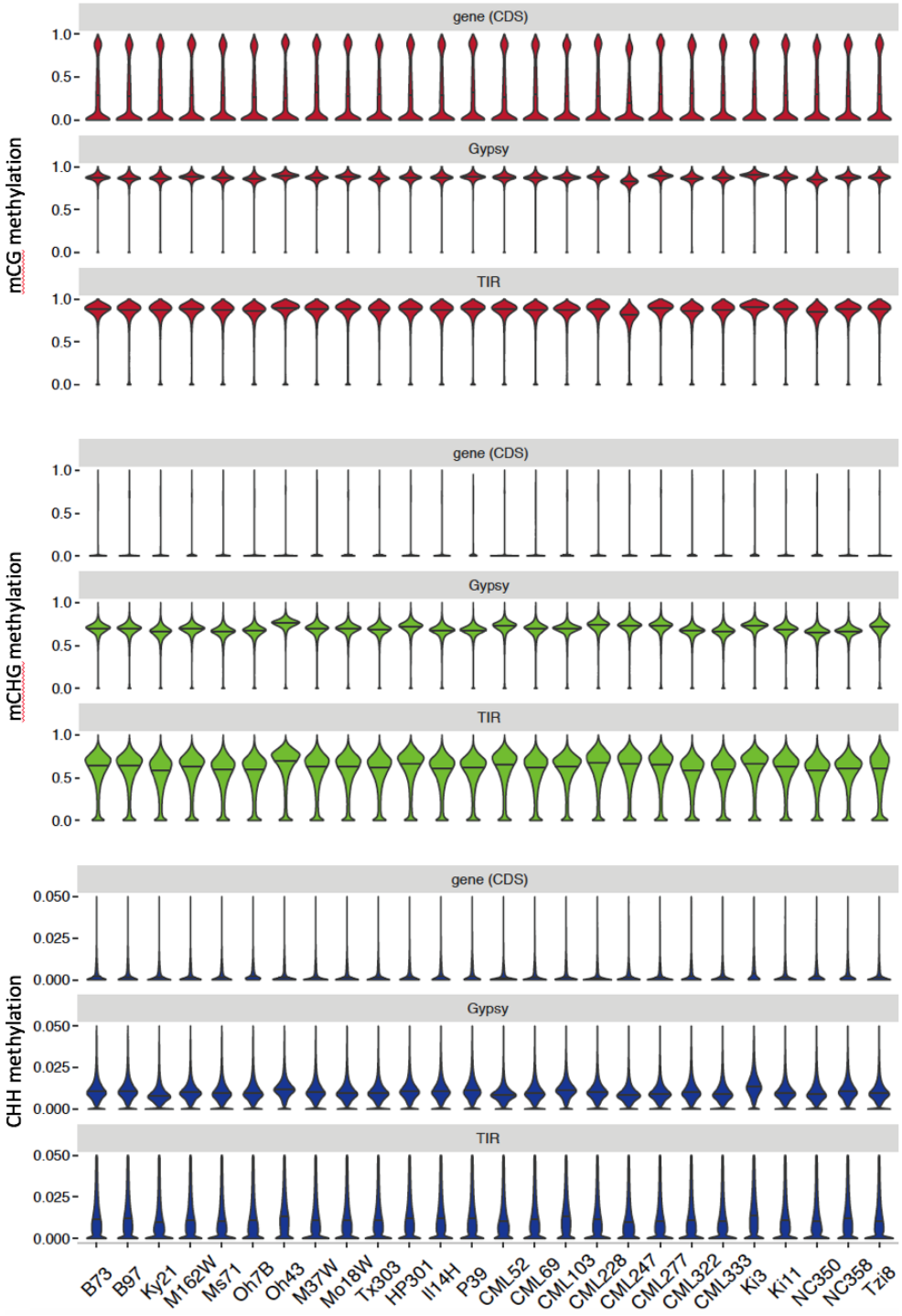

Figure S18. Spread of methylation levels for three representative genetic elements, genes (coding DNA only), *Gypsy* LTR retrotransposons, and TIR DNA transposons (*Tc1*/*Mariner*, *hAT*, *Harbinger*, and *Mutator*). Methylation is mC/total C for each sequence context. Horizontal lines indicate medians. To be included in this analysis, loci had to have a minimum of 10 cytosines in the specified context (CG, CHG, or CHH) that were covered by EM-seq reads. EM-seq reads from each methylome were mapped to their own genomes.

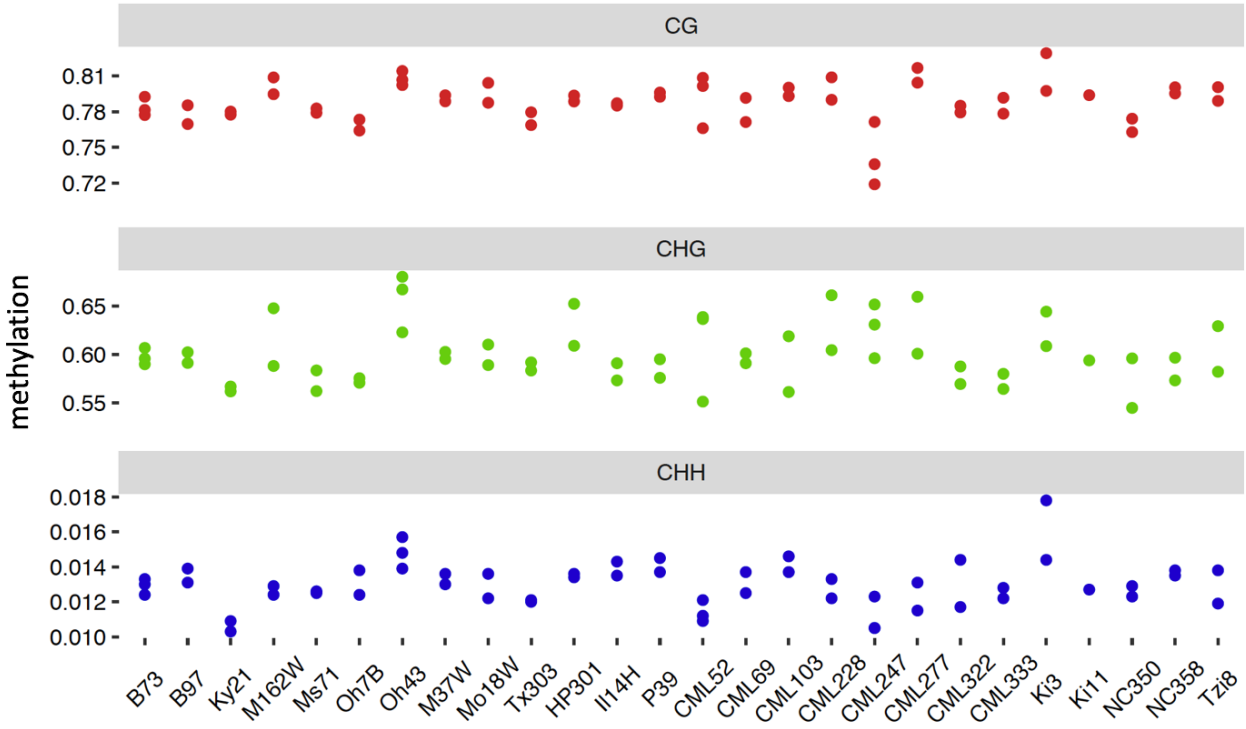

Figure S19: Whole-genome methylation levels for individual biological replicates. Methylation is mC/total C for each sequence context. EM-seq reads from each methylome were mapped to their own genomes.

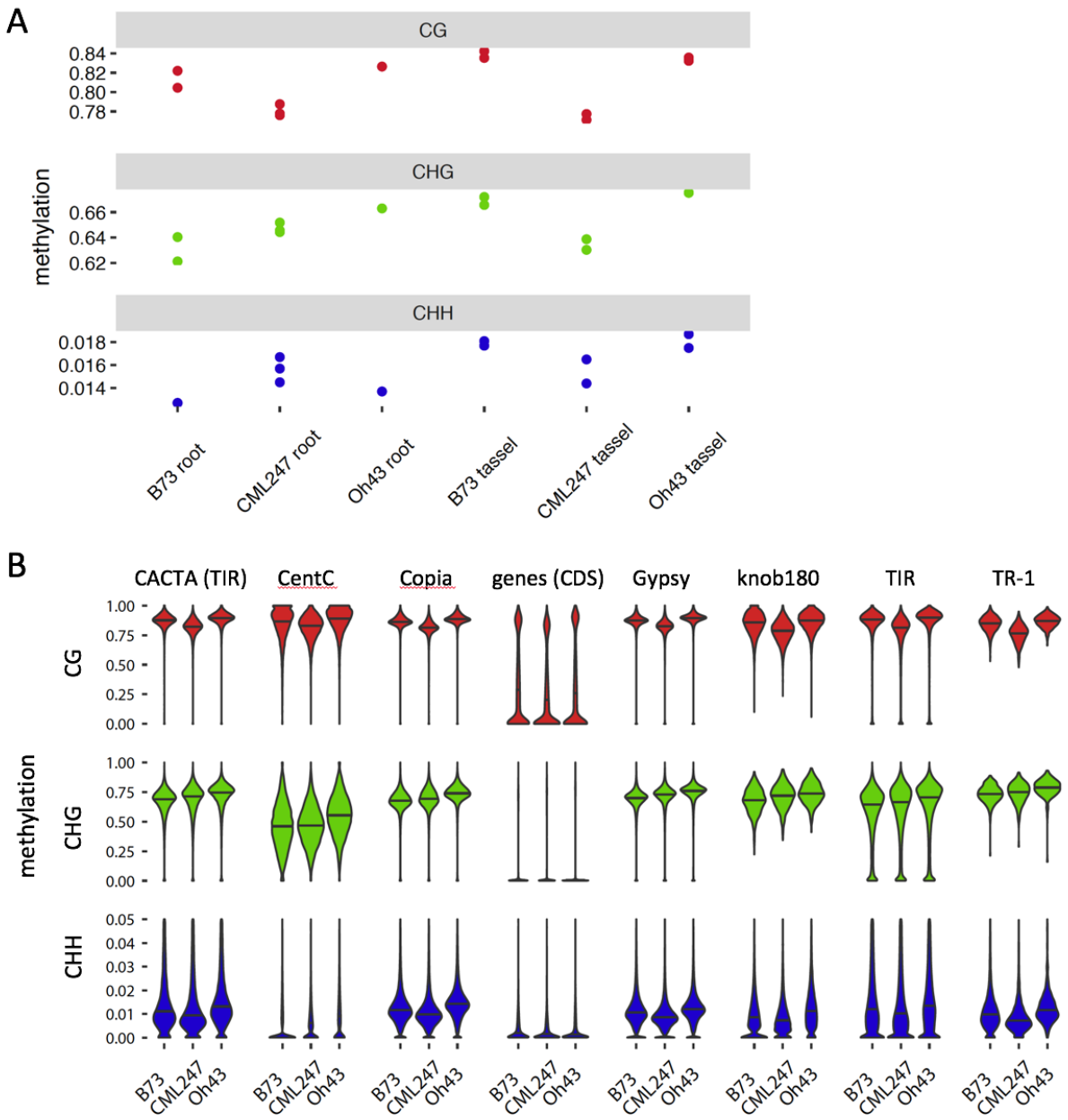

Figure S20. Additional comparisons of B73, CML247, and Oh43 methylation. **A**) Whole-genome methylation levels for individual biological replicates of primary root six days after planting and V18 growth stage meiotic tassel. Methylation is mC/total C for each sequence context. EM-seq reads from each methylome were mapped to their own genomes. **B**) Spread of methylation levels for representative genetic elements in developing second leaves. The same data are shown as in Fig. S18 but with the addition of five more genetic elements. Methylation is mC/total C for each sequence context. Horizontal lines indicate medians. All loci except CentC had to have a minimum of 10 cytosines in the specified context (CG, CHG, or CHH) that were covered by EM-seq reads. CentC was required to have 3 CGs or 5 CHGs. EM-seq reads from each methylome were mapped to their own genomes.

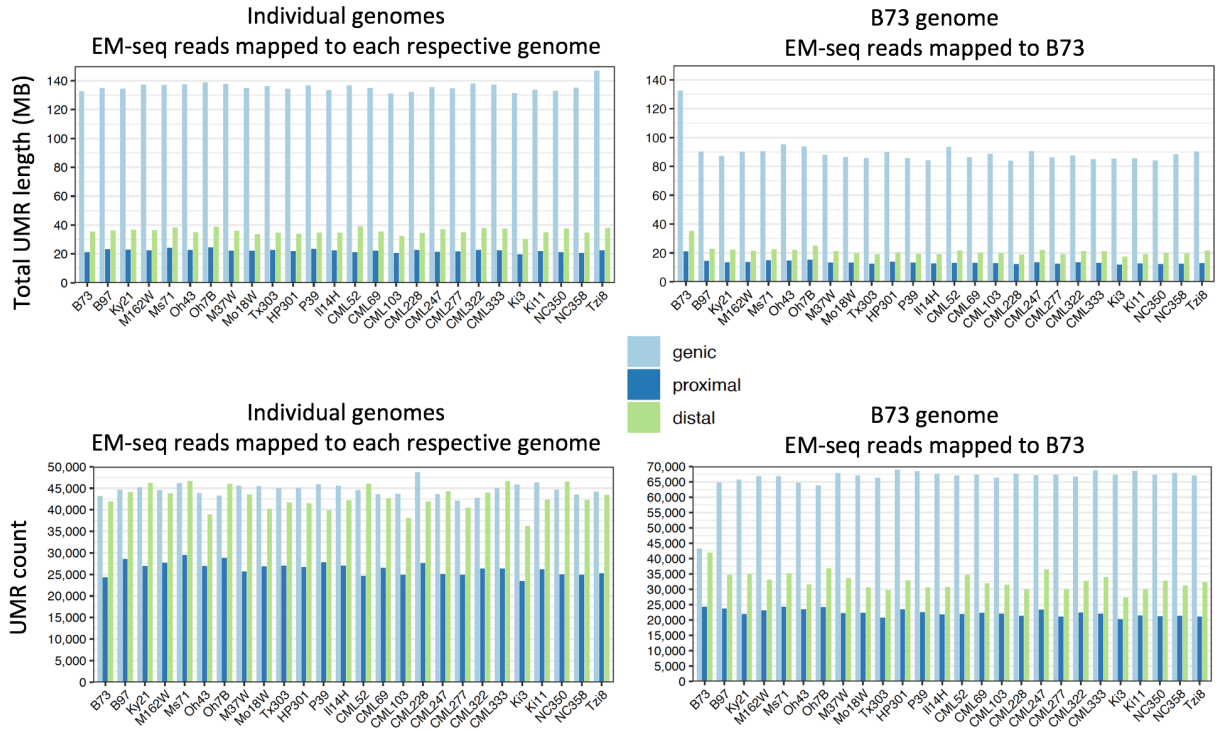

Figure S21. Total length and counts of UMRs. UMRs were defined relative to individual genomes by mapping each set of EM-seq reads to its own genome and defined relative to the B73 genome by mapping to B73. Position categories are as follows: UMRs with any overlap with genes are genic; of the remaining set, those with any overlap with the 5-KB flanks of genes are proximal; and the rest are distal.

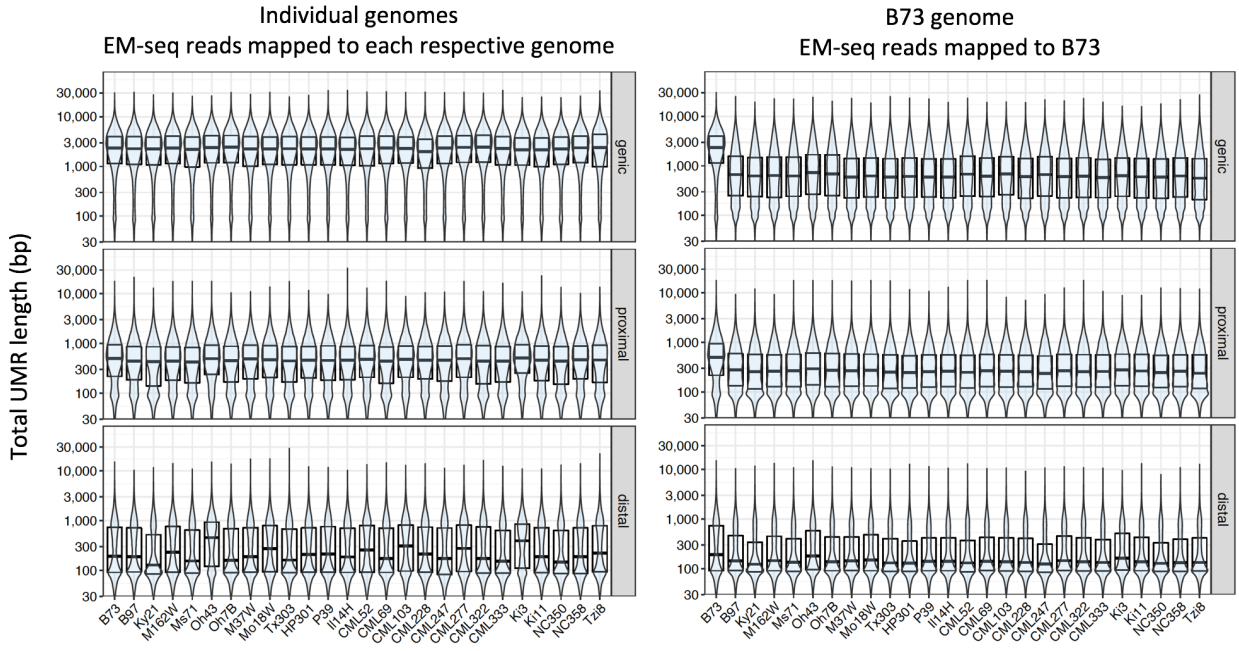

Figure S22. Spread of UMR lengths. UMRs were defined relative to individual genomes by mapping each set of EM-seq reads to its own genome and defined relative to the B73 genome by mapping to B73. Position categories are as follows: UMRs with any overlap with genes are genic; of the remaining set, those with any overlap with the 5-KB flanks of genes are proximal; and the rest are distal. This analysis includes UMRs that are less than 150 bp in length (which were excluded from all other analyses). Y-axes are on a log10 scale. Boxplots denote medians and quartiles.

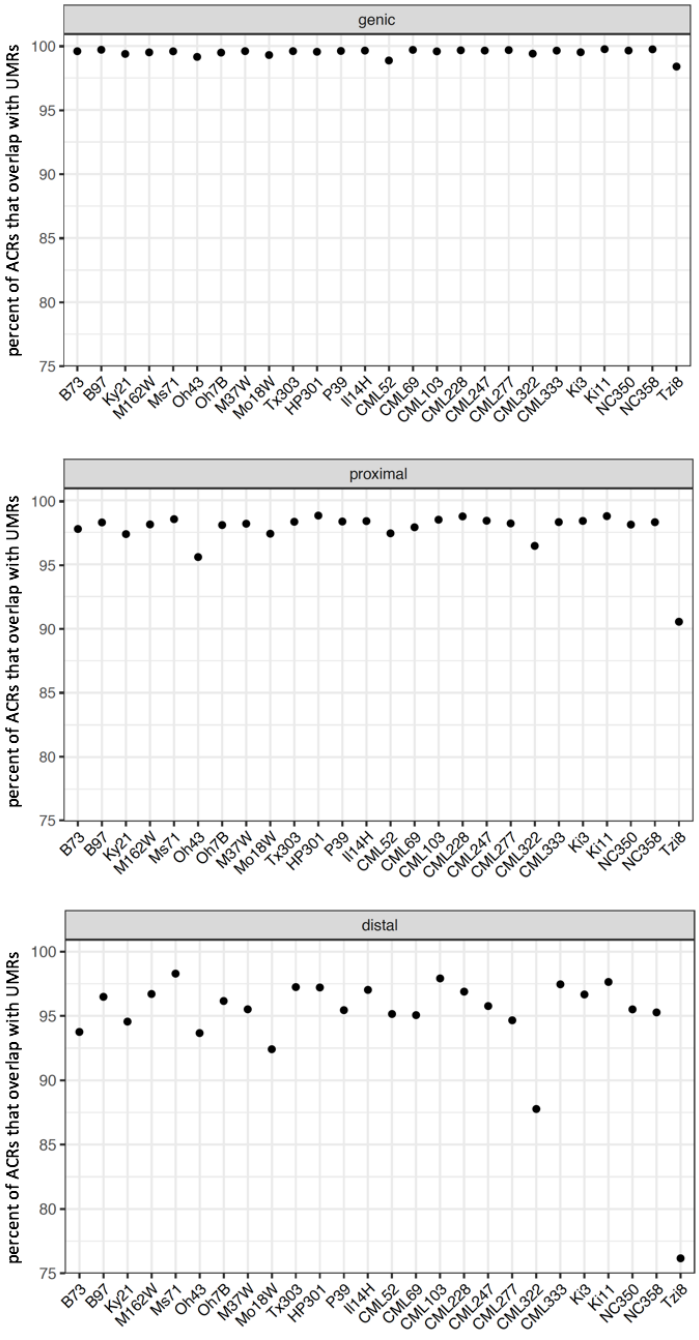

Figure S23. Overlaps of accessible chromatin regions (ACRs) by UMRs. Overlaps are >= 1 bp. UMRs and ACRs were defined relative to individual genomes by mapping each set of EM-seq and ATAC-seq reads to its own genome. Position categories are as follows: ACRs with any overlap with genes are genic; of the remaining set, those with any overlap with the 5-KB flanks of genes are proximal; and the rest are distal.

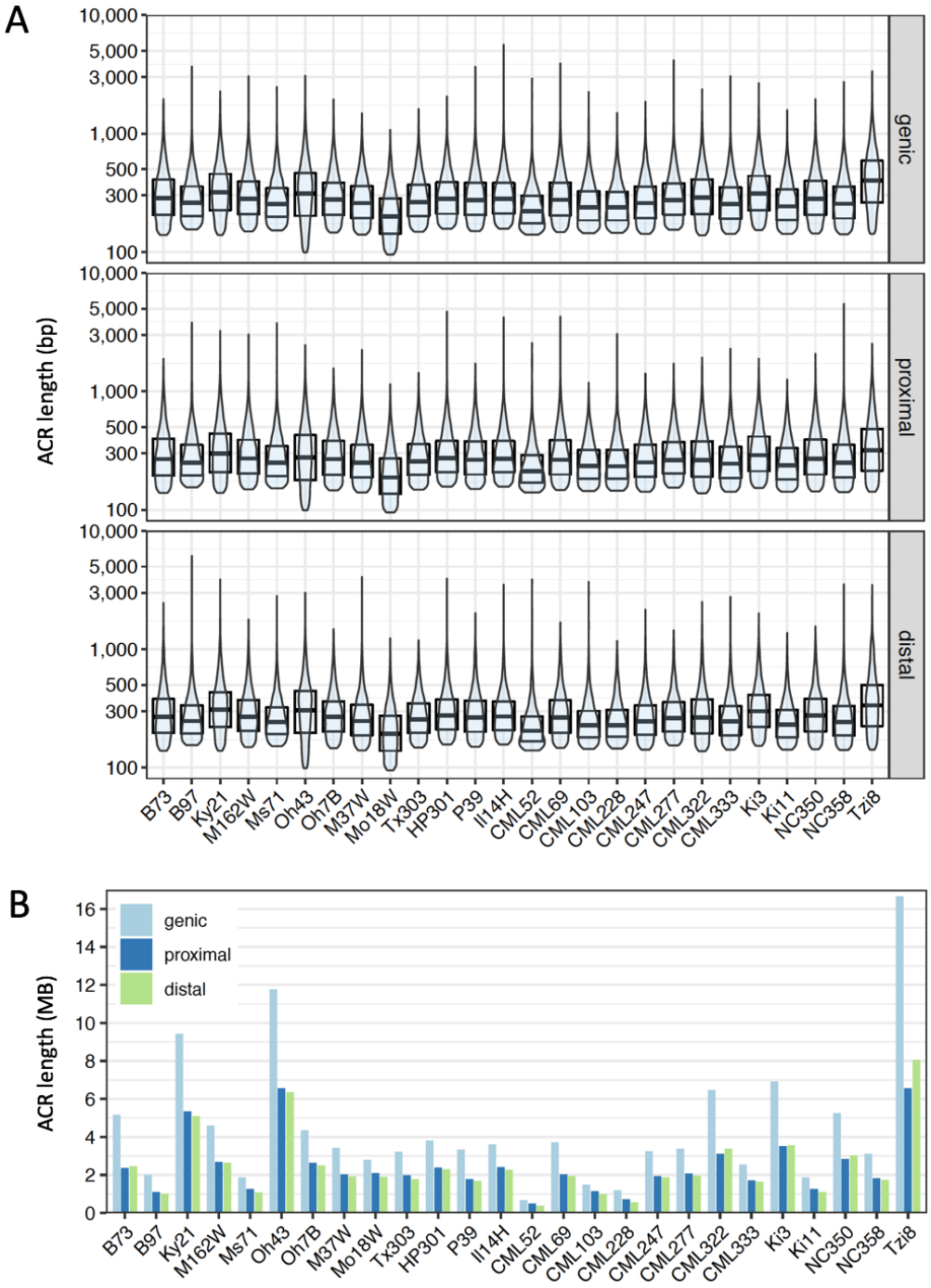

Figure S24. Lengths of Accessible Chromatin Regions (ACRs). **A**) Distributions of lengths of ACRs in each genome. Y-axes are on log10 scale. Position categories are as follows: ACRs/UMRs with any overlap with genes are genic; of the remaining set, those with any overlap with the 5-KB flanks of genes are proximal; and the rest are distal. Horizontal lines indicate medians. **B**) Cumulative length of ACRs in each genome.

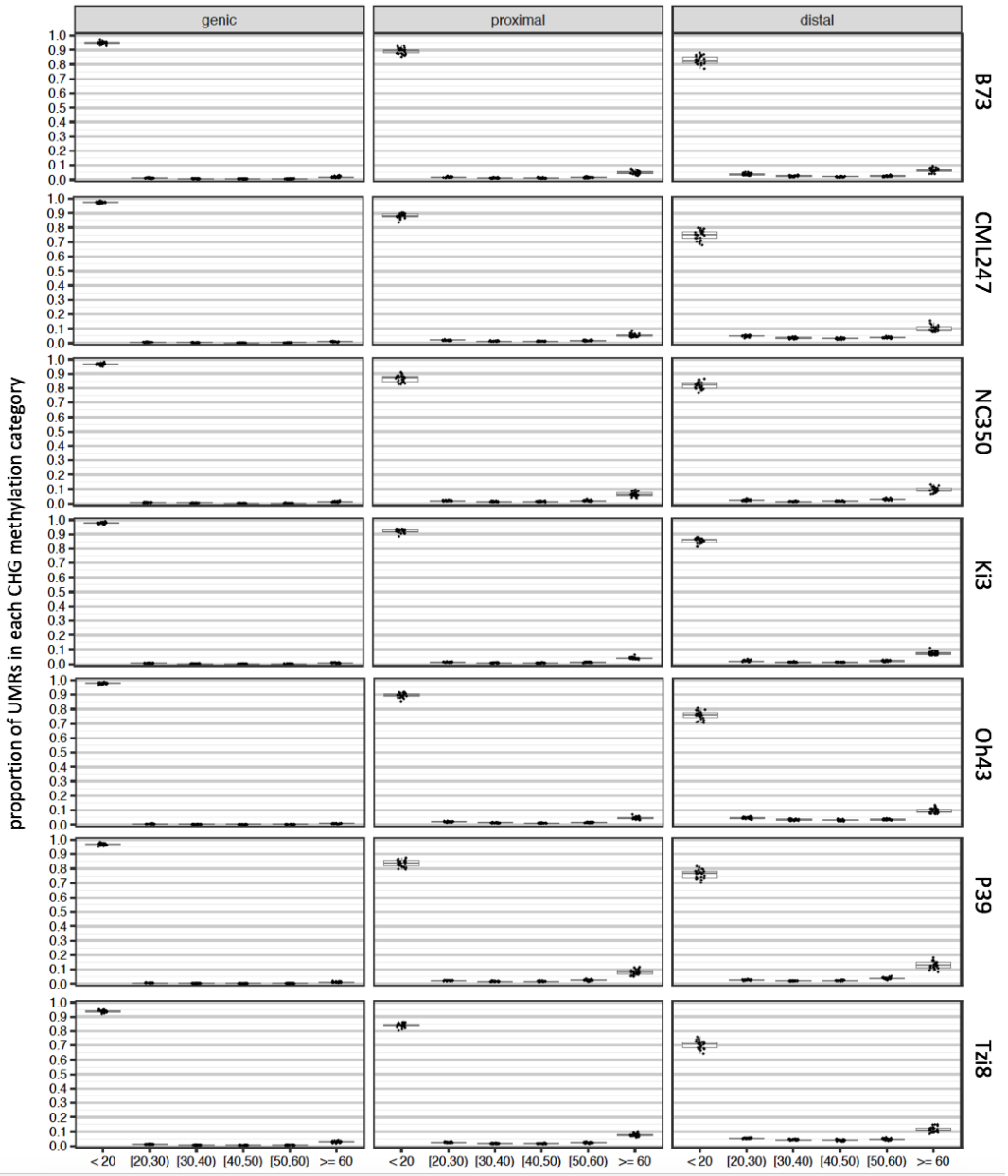

Figure S25. Conserved low CHG methylation in UMRs. UMRs were defined by mapping EM-seq reads from seven inbreds indicated at right. For each of the seven, UMRs were then categorized into one of six methylation bins (percent mCHG relative to total CHG) based on mapping EM-seq reads from the other 25 inbreds. Dots represent the proportion of the UMRs in each category. The "<20" category is what was used to define UMRs. The data are further categorized based on position relative to genes: UMRs with any overlap with genes are genic; of the remaining set, UMRs with any overlap with the 5-kbp flanks of genes are proximal; and the rest are distal. Boxplots denote medians and quartiles. For these analyses, all EM-seq reads were mapped to the B73 genome.

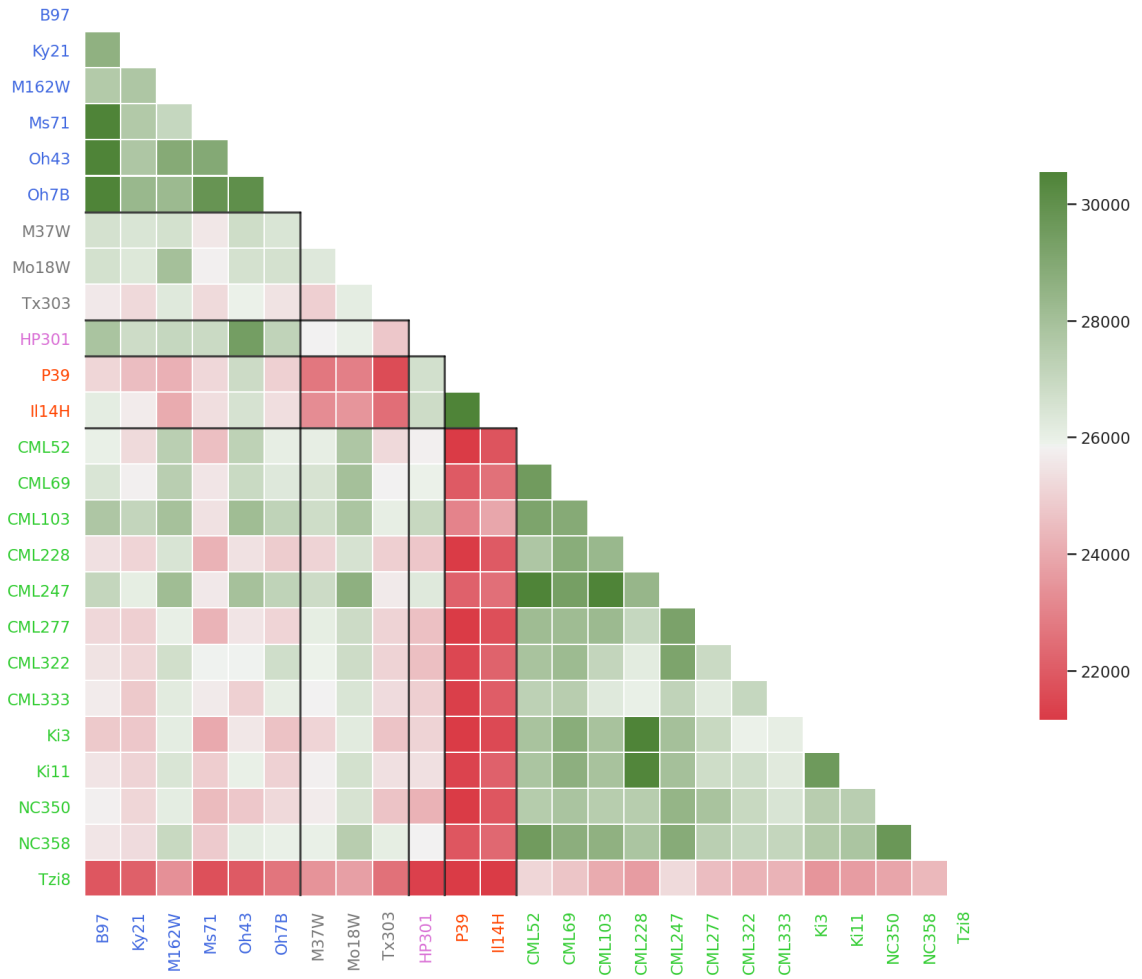

Figure S26. Heat map of the number of shared UMR regions across all pairwise comparisons of NAM lines. Boxed areas represent group by group comparisons.

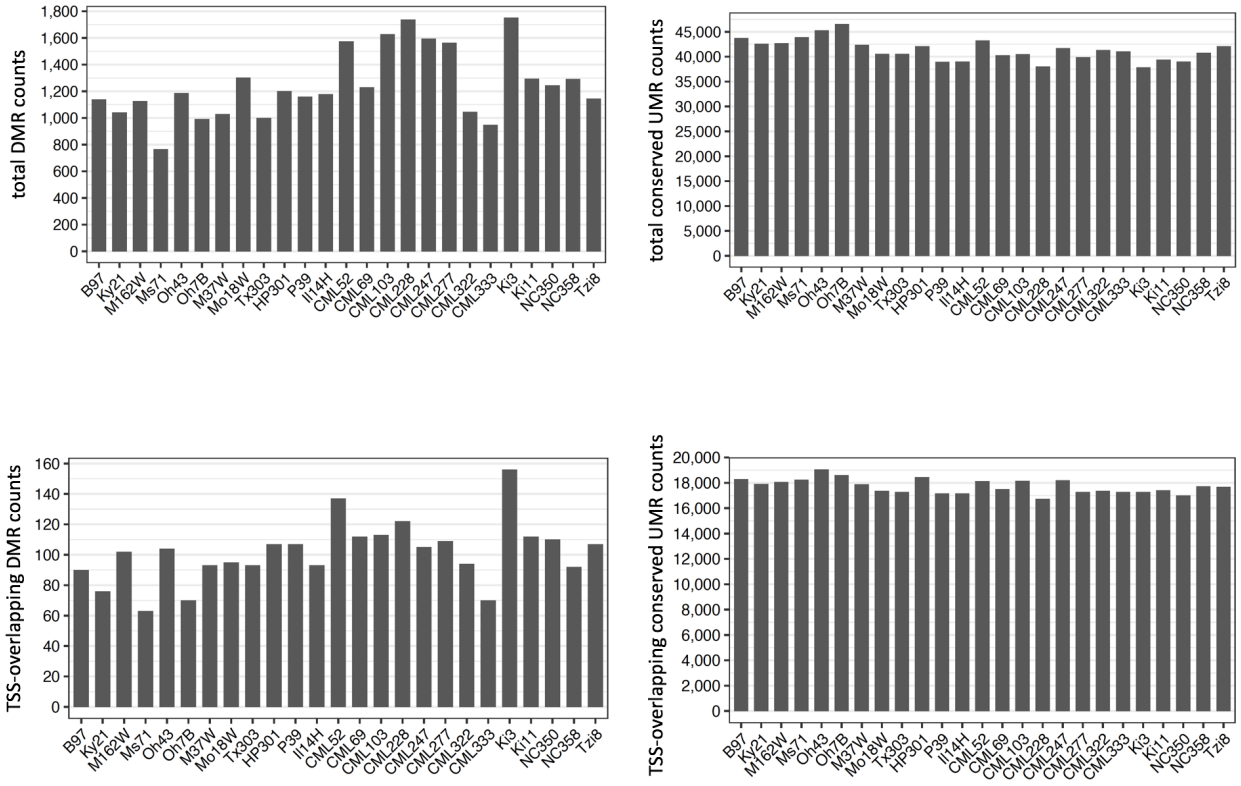

Figure S27. Numbers of differentially methylated regions (DMRs) in each NAM founder methylome. B73 UMRs that had greater than or equal to 60% CHG methylation in another methylome were categorized as DMRs, while B73 UMRs with less than 20% methylation in another methylome were categorized as conserved UMRs. Methylation was measured using the EM-seq reads from each methylome mapped to the B73 genome and was defined as percent mCHG relative to total CHG. A subset of TSS-overlapping pan-genes were selected as those where a region from -10 to +400 bp of the transcription start site was at least 98% overlapped by a DMR or conserved UMR.

Supplementary Tables

Table S1: Accession and DNA isolation information for NAM lines

Inbred Line	Original Accession	Sequenced Individual Accession	DNA Isolation Method
B73	PI 550473	PI 692136	CTAB
B97	PI 564682	PI 692135	nuclei
Ky21	Ames 27130	PI 692149	CTAB
M162W	Ames 27134	PI 692151	nuclei
Ms71	PI 587137	PI 692153	nuclei
Oh43	Ames 19288	PI 692157	CTAB
Oh7B	Ames 19323	PI 692156	CTAB
M37W	Ames 27133	PI 692150	nuclei
Mo18W	PI 550441	PI 692152	nuclei
Tx303	Ames 19327	PI 692159	CTAB
HP301	PI 587131	PI 692145	CTAB
P39	Ames 28186	PI 692158	CTAB
Il14H	Ames 27118	PI 692146	nuclei
CML52	PI 595561	PI 692137	CTAB
CML69	Ames 28184	PI 692138	CTAB
CML103	Ames 27081	PI 692139	nuclei
CML228	Ames 27088	PI 692140	CTAB
CML247	PI 595541	PI 692141	CTAB
CML277	PI 595550	PI 692142	CTAB
CML322	Ames 27096	PI 692143	CTAB
CML333	Ames 27101	PI 692144	nuclei
Ki3	Ames 27123	PI 692147	CTAB
Ki11	Ames 27124	PI 692148	CTAB
NC350	Ames 27171	PI 692154	CTAB
NC358	Ames 27175	PI 692155	CTAB
Tzi8	PI 506246	PI 692160	CTAB

Table S2: Quality metrics for the NAM genome assemblies.

	Assembly Size (Mb)	Placed Scaffolds Size (Mb)	Total Number of Scaffolds	Placed Scaffolds Number	Largest Scaffold (Mb)	Smallest Scaffold (Mb)	All Contigs N50 (Mb)	All Contigs L50	All Scaffolds N50 (Mb)	All Scaffolds L50	Placed Scaffolds N50 (Mb)	Placed Scaffolds L50	Pseudomolecule %N	Placed Scaffolds %N	Placed Scaffolds BUSCO %	LAI
B73	2182.08	2132.8	695	20	242.93	0.0308	52.3551	13	160.85	6	162.82	5	0.17	0.13	95.76	27.84
B97	2193.12	2135.16	817	27	236.26	0.0303	49.7671	12	137.68	6	137.68	6	0.15	0.16	95.69	28.06
Ky21	2171.65	2121.14	664	27	238.07	0.03	19.0707	31	115.38	7	115.38	7	0.3	0.31	96.04	28.08
M162W	2184.33	2129.28	813	27	237.44	0.03	27.8072	22	111.38	6	111.38	6	0.17	0.18	96.04	28.09
Ms71	2214.05	2128.11	1034	32	202.96	0.03	34.1022	19	98.45	9	101.56	8	0.22	0.21	95.97	27.91
Oh43	2176.4	2116.4	777	30	198.84	0.03	28.631	26	105.60	8	105.60	8	0.12	0.12	95.76	27.89
Oh7B	2164.7	2124	634	29	239.51	0.0302	13.62	41	140.10	6	140.10	6	0.4	0.41	95.80	28.04
M37W	2192.4	2144.22	758	29	234.27	0.0301	39.6241	17	105.37	7	105.37	7	0.08	0.09	95.97	28.09
Mo18W	2223.23	2132.06	1097	31	201.21	0.0302	24.9769	26	111.10	7	111.10	7	0.33	0.33	96.60	27.81
Tx303	2215.81	2124.95	1067	32	240.2	0.0302	27.971	24	99.16	8	99.16	8	0.31	0.26	95.83	27.71
HP301	2140.95	2114.55	408	23	233.97	0.0304	35.6	21	135.87	6	135.87	6	0.19	0.2	95.63	28.05
P39	2138.71	2104.38	424	21	249.96	0.0305	35.7844	21	147.88	6	147.88	6	0.11	0.12	95.76	27.61
Il14H	2124.54	2102.61	297	25	238.22	0.03	19.6425	31	135.80	6	135.80	6	0.15	0.16	95.63	27.83
CML52	2307.69	2149.15	1708	36	200.09	0.03	11.2031	58	92.05	9	94.80	8	0.93	0.96	95.76	27.92
CML69	2224.9	2133.04	1352	31	239.36	0.0301	21.3376	31	107.57	7	107.57	7	0.29	0.31	95.90	28.34
CML103	2162.44	2117.65	648	26	234.9	0.0301	11.3391	59	129.92	6	129.92	6	0.24	0.25	95.56	28.3
CML228	2300.77	2145.83	1555	32	240.54	0.03	9.55255	57	108.07	7	140.27	6	1.2	1.08	96.25	27.93
CML247	2214.75	2142.86	1091	32	200.43	0.0301	11.4266	60	101.10	9	101.77	8	0.45	0.47	96.32	28.44
CML277	2190.8	2133.12	928	32	194.76	0.0301	6.2549	100	98.85	9	98.85	9	0.42	0.44	96.18	27.95
CML322	2219.25	2120.08	1290	32	240.12	0.0301	30.4894	24	102.20	8	104.77	7	0.14	0.14	95.42	28.44
CML333	2231.26	2141.31	1116	34	236.82	0.03	28.8179	20	99.84	8	99.84	8	0.14	0.11	96.32	28.33
Ki3	2215.86	2139.35	1184	29	244.14	0.0301	16.1777	43	107.93	7	107.93	7	0.39	0.41	96.67	28.27
Ki11	2273.84	2151.7	1417	29	240.57	0.0301	31.4035	23	110.07	6	200.72	5	0.12	0.13	95.83	27.64
NC350	2290.5	2163.61	1399	30	200.52	0.0303	49.0042	13	100.66	8	102.34	7	0.07	0.07	96.18	27.96
NC358	2227.42	2126.56	1335	32	237.4	0.03	25.9366	27	98.95	8	99.55	7	0.17	0.16	96.18	28.22
Tzi8	2271.03	2134.06	1570	32	239.1	0.03	11.6145	54	100.58	8	101.61	7	0.56	0.53	96.11	27.9

Table S3: Categorization of pan-genes for the NAM genomes. Numbers in parentheses are identified based on coordinate filling.

Genome	Core Gene	Near-Core Gene	Dispensable Gene	Private Gene
B73	27910 (3974)	4015 (1752)	15426 (8439)	414
B97	27910 (3622)	4030 (1687)	15603 (8048)	533
Ky21	27910 (3605)	3979 (1652)	15607 (7919)	564
M162W	27910 (3600)	3932 (1631)	15838 (7918)	606
Ms71	27910 (3607)	4000 (1631)	15477 (7943)	558
Oh43	27910 (3654)	3959 (1665)	15356 (8182)	620
Oh7B	27910 (3677)	3546 (1624)	15191 (7919)	1204
M37W	27910 (3626)	3993 (1671)	15507 (7894)	846
Mo18W	27910 (3590)	3849 (1612)	14918 (7558)	1244
Tx303	27910 (3617)	4009 (1642)	15071 (7583)	797
HP301	27910 (3671)	3987 (1649)	14947 (7994)	708
P39	27910 (3580)	3858 (1566)	14881 (6963)	872
Il14H	27910 (3626)	3948 (1642)	14758 (7480)	810
CML52	27910 (3863)	3600 (1649)	14634 (8537)	807
CML69	27910 (3666)	4000 (1671)	15016 (8121)	903
CML103	27910 (3726)	3980 (1668)	15008 (7972)	802
CML228	27910 (3670)	3796 (1624)	15045 (8056)	781
CML247	27910 (3641)	4002 (1694)	15038 (8011)	908
CML277	27910 (3635)	3977 (1659)	14957 (8062)	966
CML322	27910 (3601)	3803 (1592)	15014 (7495)	785
CML333	27910 (3701)	4015 (1675)	15250 (8067)	865
Ki3	27910 (3610)	4035 (1684)	15346 (7931)	708
Ki11	27910 (3696)	3966 (1676)	15110 (8274)	776
NC350	27910 (3635)	4028 (1673)	15280 (8217)	691
NC358	27910 (3672)	4019 (1698)	15179 (8350)	684
Tzi8	27910 (3618)	3904 (1618)	15116 (7812)	938

Table S4: Percentage of repetitive sequences in NAM parent genomes.

Genome	LTR/Copia	LTR/Gypsy	LTR/unknown	TIR/CACTA	TIR/Mutator	TIR/PIF_Harbinger	TIR/Tc1_Mariner	TIR/hAT	DNA/Helitron	LINE/L1	LINE/RTE	LINE/unknown	centromeric_repeat	knob (knob180 & TR-1)	rDNA_spacer	subtelomere	low_complexity	Total TIR elements	Total DNA TE	Total non-LTR RT	Total LTR RT	Total TE	Total non-TE repeat	Total Repeat
B73	24.92%	44.25%	5.02%	2.96%	0.99%	1.06%	0.55%	1.15%	1.89%	0.26%	0.09%	0.06%	0.22%	1.67%	0.09%	0.05%	0.04%	6.71%	8.60%	0.41%	74.19%	83.20%	2.07%	85.27%
B97	25.01%	45.69%	3.27%	2.97%	0.91%	1.07%	0.56%	1.15%	1.92%	0.26%	0.09%	0.06%	0.27%	2.11%	0.09%	0.06%	0.01%	6.66%	8.58%	0.41%	73.97%	82.96%	2.54%	85.50%
Ky21	24.83%	46.38%	3.65%	2.96%	0.91%	1.06%	0.56%	1.19%	1.91%	0.26%	0.09%	0.06%	0.25%	1.22%	0.05%	0.04%	0.01%	6.68%	8.59%	0.41%	74.86%	83.86%	1.57%	85.43%
M162W	24.73%	45.79%	3.98%	2.99%	0.95%	1.06%	0.51%	1.16%	1.89%	0.26%	0.09%	0.07%	0.38%	1.37%	0.15%	0.04%	0.01%	6.67%	8.56%	0.42%	74.50%	83.48%	1.95%	85.43%
Ms71	24.88%	45.82%	3.58%	3.02%	0.96%	1.07%	0.51%	1.15%	1.90%	0.26%	0.09%	0.06%	0.32%	1.88%	0.03%	0.04%	0.01%	6.71%	8.61%	0.41%	74.28%	83.30%	2.28%	85.58%
Oh43	24.79%	44.80%	4.93%	2.99%	0.94%	1.07%	0.51%	1.16%	1.91%	0.27%	0.09%	0.07%	0.29%	1.46%	0.02%	0.04%	0.01%	6.67%	8.58%	0.43%	74.52%	83.53%	1.82%	85.35%
Oh7B	25.37%	46.20%	3.39%	2.99%	0.91%	1.07%	0.57%	1.16%	1.91%	0.26%	0.09%	0.06%	0.24%	1.00%	0.05%	0.04%	0.01%	6.70%	8.61%	0.41%	74.96%	83.98%	1.34%	85.32%
M37W	24.97%	44.97%	4.54%	3.03%	0.90%	1.07%	0.56%	1.15%	1.90%	0.26%	0.09%	0.06%	0.24%	1.61%	0.08%	0.04%	0.01%	6.71%	8.61%	0.41%	74.48%	83.50%	1.98%	85.48%
Mo18W	24.74%	45.34%	3.58%	2.93%	0.91%	1.05%	0.50%	1.13%	1.87%	0.25%	0.08%	0.06%	0.34%	2.58%	0.13%	0.05%	0.01%	6.52%	8.39%	0.39%	73.66%	82.44%	3.11%	85.55%
Tx303	24.77%	44.52%	4.53%	2.96%	1.02%	1.06%	0.43%	1.16%	1.89%	0.25%	0.09%	0.06%	0.32%	2.44%	0.03%	0.03%	0.02%	6.63%	8.52%	0.40%	73.82%	82.74%	2.84%	85.58%
HP301	24.58%	46.51%	4.02%	2.99%	0.97%	1.08%	0.53%	1.17%	1.93%	0.26%	0.09%	0.06%	0.25%	0.80%	0.05%	0.04%	0.01%	6.74%	8.67%	0.41%	75.11%	84.19%	1.15%	85.34%
P39	24.09%	45.15%	5.42%	3.00%	0.99%	1.08%	0.53%	1.17%	1.96%	0.27%	0.09%	0.06%	0.31%	1.01%	0.04%	0.03%	0.01%	6.77%	8.73%	0.42%	74.66%	83.81%	1.40%	85.21%
Il14H	24.37%	45.36%	5.55%	3.01%	1.00%	1.09%	0.53%	1.18%	1.95%	0.27%	0.09%	0.06%	0.27%	0.52%	0.03%	0.04%	0.01%	6.81%	8.76%	0.42%	75.28%	84.46%	0.87%	85.33%
CML52	23.96%	46.52%	4.32%	3.01%	1.02%	1.07%	0.43%	1.18%	1.89%	0.25%	0.09%	0.06%	0.28%	1.46%	0.05%	0.04%	0.01%	6.71%	8.60%	0.40%	74.80%	83.80%	1.84%	85.64%
CML69	24.68%	45.45%	4.19%	2.93%	0.99%	1.07%	0.42%	1.16%	1.84%	0.25%	0.09%	0.07%	0.21%	2.15%	0.06%	0.04%	0.01%	6.57%	8.41%	0.41%	74.32%	83.14%	2.47%	85.61%
CML103	25.00%	46.16%	3.85%	2.98%	0.95%	1.07%	0.52%	1.17%	1.89%	0.26%	0.09%	0.07%	0.27%	1.03%	0.05%	0.04%	0.01%	6.69%	8.58%	0.42%	75.01%	84.01%	1.40%	85.41%
CML228	25.01%	46.17%	3.63%	3.00%	1.01%	1.07%	0.56%	1.13%	1.88%	0.26%	0.08%	0.06%	0.24%	1.40%	0.06%	0.03%	0.01%	6.77%	8.65%	0.40%	74.81%	83.86%	1.74%	85.60%
CML247	24.34%	46.12%	4.33%	2.96%	0.94%	1.05%	0.51%	1.14%	1.88%	0.26%	0.09%	0.07%	0.27%	1.52%	0.05%	0.04%	0.00%	6.60%	8.48%	0.42%	74.79%	83.69%	1.88%	85.57%
CML277	25.36%	46.16%	3.56%	3.01%	0.94%	1.06%	0.51%	1.16%	1.89%	0.25%	0.08%	0.06%	0.24%	1.11%	0.05%	0.04%	0.01%	6.68%	8.57%	0.39%	75.08%	84.04%	1.45%	85.49%
CML322	24.11%	45.34%	4.43%	2.92%	1.02%	1.06%	0.43%	1.15%	1.84%	0.26%	0.09%	0.06%	0.34%	2.60%	0.05%	0.04%	0.01%	6.58%	8.42%	0.41%	73.88%	82.71%	3.04%	85.75%
CML333	24.02%	45.53%	4.53%	2.95%	0.99%	1.06%	0.42%	1.15%	1.88%	0.25%	0.09%	0.06%	0.31%	2.43%	0.05%	0.05%	0.01%	6.57%	8.45%	0.40%	74.08%	82.93%	2.85%	85.78%
Ki3	24.93%	46.03%	3.61%	2.96%	1.02%	1.06%	0.43%	1.15%	1.86%	0.25%	0.09%	0.06%	0.34%	1.72%	0.07%	0.04%	0.01%	6.62%	8.48%	0.40%	74.57%	83.45%	2.18%	85.63%
Ki11	24.24%	43.81%	4.64%	2.90%	0.92%	1.02%	0.51%	1.10%	1.83%	0.25%	0.09%	0.06%	0.30%	3.83%	0.05%	0.05%	0.03%	6.45%	8.28%	0.40%	72.69%	81.37%	4.26%	85.63%
NC350	24.10%	44.95%	3.55%	2.88%	0.89%	1.02%	0.49%	1.11%	1.82%	0.25%	0.08%	0.06%	0.35%	4.06%	0.09%	0.03%	0.03%	6.39%	8.21%	0.39%	72.60%	81.20%	4.56%	85.76%
NC358	24.25%	44.63%	5.06%	2.93%	0.91%	1.05%	0.49%	1.13%	1.86%	0.25%	0.09%	0.07%	0.35%	2.44%	0.06%	0.05%	0.01%	6.51%	8.37%	0.41%	73.94%	82.72%	2.91%	85.63%
Tzi8	24.72%	46.00%	3.87%	3.02%	1.00%	1.06%	0.42%	1.15%	1.87%	0.26%	0.08%	0.06%	0.20%	1.80%	0.05%	0.04%	0.01%	6.65%	8.52%	0.40%	74.59%	83.51%	2.10%	85.61%

Table S5: Characterization of assembly content of chromosome ends. Numbers are shown in bp.

Inbred	Repeat	1S	1L	2S	2L	3S	3L	4S	4L	5S	5L	6S	6L	7S	7L	8S	8L	9S	9L	10S	10L
B73	telomere	0	1872	0	2169	2520	1820	1758	1796	0	1405	1967	2412	2669	1989	1868	1540	0	2910	2106	2687
	subtelomere	0	1382	0	0	0	0	231616	64907	282947	8291	87701	0	0	0	0	52576	0	0	0	6930
	TR-1	0	0	0	0	0	0	0	0	0	0	5309688	0	0	0	0	0	0	0	0	0
	knob180	16625	0	0	183855	117201	0	0	0	0	83695	0	628802	0	0	263042	0	1744659	80845	0	128022
B97	telomere	0	972	0	3279	625	2631	2993	1515	0	3521	1304	0	3560	2415	0	255	0	600	2675	2075
	subtelomere	0	0	0	0	0	0	253333	76960	37492	8289	74748	4648	0	0	78691	133091	0	0	0	14566
	TR-1	0	0	0	0	0	0	0	0	0	0	4652167	0	0	0	0	0	0	0	0	0
	knob180	23920	0	0	55622	0	0	0	0	0	0	0	821406	0	0	406150	0	933214	59582	0	0
Ky21	telomere	0	1882	169	1304	0	5951	0	2886	0	1946	0	1740	806	5373	0	574	0	3180	582	1210
	subtelomere	0	0	54369	0	0	0	65537	70502	24316	0	0	0	0	0	0	112338	0	0	0	0
	TR-1	0	0	0	0	0	0	0	0	0	0	0	0	0	0	0	0	0	0	0	0
	knob180	72322	0	0	180286	205371	0	0	0	0	73300	68525	637709	0	0	303302	0	276793	51248	0	138114
M162W	telomere	0	1246	0	1249	2999	4523	1608	269	0	0	1386	2177	907	6636	576	526	0	3257	1938	1865
	subtelomere	0	0	0	0	0	0	238664	64939	22079	0	0	0	0	0	0	128515	0	0	0	0
	TR-1	0	0	0	0	0	0	0	0	0	0	5439392	0	0	0	0	0	0	0	0	0
	knob180	10187	0	0	174149	214753	0	0	0	0	28663	0	642355	49068	0	255749	0	733871	51342	0	0
Ms71	telomere	0	9838	0	2081	6098	3575	0	0	0	4135	0	5367	10537	8683	5137	4014	0	2606	3358	4976
	subtelomere	0	0	0	0	0	0	24227	0	35423	0	0	0	0	0	0	91024	0	0	0	6792
	TR-1	0	0	0	0	0	0	0	0	0	0	0	0	0	0	0	0	0	0	0	0
	knob180	26027	0	0	124867	202501	0	0	0	0	75472	566943	82065	0	0	266305	0	353293	49249	15554	130313
Oh43	telomere	0	4515	0	398	9530	4469	945	5693	0	2563	0	1991	5470	6515	337	574	0	519	428	0
	subtelomere	0	0	0	0	0	0	238296	76984	30830	8321	0	0	0	0	0	89358	0	0	0	0
	TR-1	0	0	0	0	0	0	0	0	0	0	0	0	0	0	0	0	0	0	0	0
	knob180	22783	0	0	146257	0	0	0	0	0	71482	75588	673981	26404	0	255157	0	424845	48039	0	46637
Oh7B	telomere	0	215	0	4391	468	2372	0	3892	0	1533	2234	0	968	6665	2228	3202	1123	2389	0	951
	subtelomere	0	1565	0	1570	0	0	0	64943	29676	5191	0	0	0	0	0	91852	0	0	0	0
	TR-1	0	0	0	0	0	0	0	0	0	0	1801070	0	0	0	0	0	0	0	0	0
	knob180	13020	0	0	190821	205105	0	252203	0	0	69862	0	520782	49126	0	263067	0	13787	51378	360273	0
M37W	telomere	0	630	0	5477	1359	316	920	4354	0	0	173	863	923	5832	1270	720	0	1984	2352	1421
	subtelomere	0	0	54369	0	0	0	157106	83442	52488	32504	0	0	0	0	0	92274	0	0	0	0
	TR-1	0	0	0	0	0	0	0	0	0	0	5460139	0	0	0	0	0	0	0	0	0
	knob180	41910	0	0	180277	202674	33881	0	0	0	11562	0	648807	0	0	262124	0	807328	46137	14542	131920
Mo18W	telomere	0	0	0	0	0	765	0	0	0	315	0	983	0	0	156	157	0	0	0	0
	subtelomere	0	0	0	1570	0	0	101944	93270	16610	5174	0	0	0	0	0	91775	0	0	0	0
	TR-1	0	0	0	0	0	0	0	0	0	0	0	0	0	0	0	0	0	0	0	0
	knob180	20479	0	0	180284	214753	0	0	0	0	64546	203592	717268	37558	0	265595	0	719550	35903	22284	0
Tx303	telomere	0	5824	0	5584	3634	6821	6474	6750	5012	8732	0	4341	5044	3820	5760	9005	0	7821	5955	6146
	subtelomere	0	0	0	0	0	0	202462	0	202693	5168	0	0	0	0	0	90612	0	0	0	0
	TR-1	0	0	0	0	0	0	0	0	0	0	0	0	0	0	0	0	0	0	0	0
	knob180	25992	0	0	193347	212403	0	0	0	0	0	147257	719938	0	0	309155	0	811431	76566	18402	0
HP301	telomere	0	3628	0	0	454	4211	1306	1417	0	1178	204	0	0	5495	0	2024	534	1966	599	467
	subtelomere	0	0	18536	0	0	0	160262	52523	8818	198723	0	0	0	0	3591	117525	0	0	0	6965
	TR-1	0	0	0	0	0	0	0	0	0	0	2589643	0	0	0	0	0	0	0	0	0
	knob180	21938	0	0	173089	0	34203	0	0	0	11562	0	605418	17668	0	306780	0	477680	35908	0	125803
P39	telomere	0	2108	1608	4008	4441	3031	3312	0	2634	5621	0	4906	0	3408	1729	0	0	1704	5293	3613
	subtelomere	0	0	49654	0	0	0	274084	77004	57281	5187	0	0	0	0	0	121994	0	0	0	6930
	TR-1	0	0	0	0	0	0	0	0	0	0	5298128	0	0	0	0	0	0	0	0	0
	knob180	0	0	0	186491	0	0	0	0	0	66929	0	643617	0	0	262879	0	769659	60681	0	128952
Il14H	telomere	0	5879	0	6257	182	5238	0	0	0	783	0	216	1836	4683	937	301	0	1741	0	388
	subtelomere	0	0	0	0	0	0	0	75935	77026	0	0	0	0	0	259406	122506	0	0	0	6924
	TR-1	0	0	0	0	0	0	0	0	0	0	0	0	0	0	0	0	0	0	0	0
	knob180	17653	0	0	191458	0	35247	0	0	0	67251	91524	716090	0	0	262010	0	1100389	60347	0	125725
CML52	telomere	0	3447	0	2751	159	159	0	2728	0	5865	0	0	776	2693	700	0	0	0	979	2759
	subtelomere	0	0	0	0	0	0	37453	69741	16601	0	0	46600	0	0	0	44750	0	0	0	6933
	TR-1	0	0	0	0	0	0	0	0	0	0	0	0	0	0	0	0	0	0	0	0
	knob180	10491	0	0	180254	0	35463	0	0	0	67210	67634	567446	29952	0	264776	0	192608	43105	0	128720
CML69	telomere	0	885	0	4805	2999	1521	0	2689	0	0	0	475	667	3372	991	91	0	1887	209	933
	subtelomere	0	0	0	142458	0	0	40705	70499	93427	0	0	54159	0	0	0	71712	0	0	0	0
	TR-1	0	0	0	0	0	0	0	0	0	0	0	59433	0	0	0	0	0	0	0	0
	knob180	0	0	0	198669	208393	42780	0	0	0	28660	88909	452215	29809	0	268164	0	276388	49960	0	126899
CML103	telomere	0	448	0	258	1362	571	0	3382	0	2887	0	75	0	354	2277	161	0	3491	0	1505
	subtelomere	0	1382	0	0	0	0	67564	254868	20527	5141	0	5398	0	0	21716	91778	0	0	0	6929
	TR-1	0	0	0	0	0	0	0	0	0	0	345923	0	0	0	0	0	0	0	0	0
	knob180	14602	0	0	178072	212402	36115	0	0	0	65873	0	671900	24929	0	282078	0	738875	74020	0	134670
CML228	telomere	0	974	0	1014	3014	250	0	409	0	126	0	702	481	4806	430	2840	0	2386	2219	565
	subtelomere	0	0	0	112149	0	0	194338	62822	8120	263212	0	610475	0	0	259635	91222	0	7915	0	0
	TR-1	0	0	0	0	0	0	0	0	0	0	0	0	0	0	0	0	0	0	0	0
	knob180	11997	15038	0	148828	205456	56244	0	0	0	11562	204086	636781	29842	0	270894	0	426860	78464	14416	46648
CML247	telomere	0	3944	0	0	310	2079	1218	0	0	0	0	1367	189	196	0	2973	0	0	648	775
	subtelomere	0	0	0	0	0	0	229468	57410	18166	5167	0	524985	0	0	0	102275	0	0	0	17691
	TR-1	0	0	0	0	0	0	0	0	0	0	0	0	0	0	0	0	0	0	0	0
	knob180	156565	14828	0	174717	203301	58056	0	0	0	62456	62150	556036	29562	0	200471	0	150215	35744	13332	0
CML277	telomere	0	2832	0	0	216	1505	0	4464	0	1782	0	0	1608	8784	0	0	0	2611	0	147
	subtelomere	0	0	0	0	0	0	0	64695	77404	5195	0	0	0	0	0	23925	0	0	0	6926
	TR-1	0	0	0	0	0	0	0	0	0	0	0	0	0	0	0	0	0	0	0	0
	knob180	15911	0	0	189286	11489	57514	0	0	0	72309	69451	570369	30785	0	212293	0	162657	88286	22276	133283
CML322	telomere	0	0	0	6492	828	1700	3879	1124	0	1856	0	574	1208	8172	0	2096	0	4068	1943	1212
	subtelomere	0	0	0	0	0	0	214038	75517	16654	207581	0	0	0	0	0	84328	0	0	0	0
	TR-1	0	0	0	0	0	0	0	0	0	0	0	0	0	0	0	0	0	0	0	0
	knob180	12144	0	0	182822	0	57708	0	0	0	11565	114425	665666	0	0	245563	0	37154	68899	14145	90491
CML333	telomere	0	0	0	3878	823	4813	0	0	0	2204	0	4182	458	1501	717	887	0	667	1031	3035
	subtelomere	0	0	0	142416	0	0	70414	78959	27400	14894	0	655955	0	0	21755	252584	0	7914	0	6930
	TR-1	0	0	0	0	0	0	0	0	0	0	0	0	0	0	0	0	0	0	0	0
	knob180	22450	0	0	197699	0	0	0	0	0	72164	68082	685710	29634	0	261854	0	576635	48036	0	128366
Ki3	telomere	0	3000	0	1655	802	352	1786	2888	372	2591	0	0	2796	5081	1999	1688	0	2162	0	223
	subtelomere	0	0	0	0	0	0	204288	26364	53664	0	0	0	0	0	0	70126	0	0	0	6971
	TR-1	0	0	0	0	0	0	0	0	0	0	0	0	0	0	0	0	0	0	0	0
	knob180	211656	0	0	177272	214245	56346	0	0	0	114821	64737	579799	0	0	272906	0	31076	35923	0	133348
Ki11	telomere	0	3042	0	1336	2999	1897	1761	2395	0	738	2270	212	1827	7266	3011	1839	0	3365	1820	0
	subtelomere	0	0	0	0	0	0	204313	76319	37920	368749	0	0	0	0	0	86477	0	0	0	0
	TR-1	0	0	0	0	0	0	0	0	0	0	5988847	0	0	0	0	0	0	0	0	0
	knob180	29687	0	0	179712	217673	36936	0	0	0	11565	0	655432	33205	0	347420	0	884538	71958	14016	0
NC350	telomere	0	6751	0	4747	5562	5559	5972	4675	0	4163	0	6854	5242	9225	3862	5181	4350	5872	5073	6582
	subtelomere	0	0	0	0	0	0	235643	60064	192258	0	0	0	0	0	0	87596	0	0	0	6928
	TR-1	0	0	0	0	0	0	0	0	0	0	0	0	0	0	0	0	0	0	0	0
	knob180	23837	0	0	183109	0	0	0	0	0	62065	3245561	761843	0	0	272025	0	1903033	64439	0	0
NC358	telomere	0	4432	0	2350	3749	3037	2919	3034	0	2178	0	1272	1761	7803	238	3187	0	2425	970	1244
	subtelomere	0	0	0	0	0	0	206675	60044	18125	119933	0	0	0	0	0	84333	0	0	0	6926
	TR-1	0	0	0	0	0	0	0	0	0	0	0	0	0	0	0	0	0	0	0	0
	knob180	12367	0	0	180719	193728	0	0	0	0	0	101392	655320	27813	0	283525	0	33821	70630	0	127053
Tzi8	telomere	0	1172	0	374	2156	2395	812	325	0	0	0	1661	0	412	183	757	0	1459	824	1867
	subtelomere	0	0	0	0	0	0	205963	75293	22836	0	0	0	0	0	0	77357	0	0	0	0
	TR-1	0	0	0	0	0	0	0	0	0	0	0	0	0	0	0	0	0	0	0	0
	knob180	10480	0	0	178077	205093	0	0	0	0	81085	92693	700411	164155	0	270196	0	432572	72508	0	0

Table S6: Extent of structural variation relative to B73 across the NAM assemblies including deletions (DEL), insertions (INS), inversions (INV), duplications (DUP), and translocations (TRA).

nam_line	type	count	size(Mbp)	nam_line	type	count	size(Mbp)	nam_line	type	count	size(Mbp)	nam_line	type	count	size(Mbp)	nam_line	type	count
B97	DEL	23533	267.27	B97	INS	4249	1.69	B97	INV	84	0.61	B97	DUP	10	0.0061	B97	TRA	950
Ky21	DEL	22851	256.46	Ky21	INS	4117	1.71	Ky21	INV	69	0.97	Ky21	DUP	4	0.0015	Ky21	TRA	904
M162W	DEL	25060	278.52	M162W	INS	4635	1.85	M162W	INV	73	0.73	M162W	DUP	8	0.0030	M162W	TRA	1029
Ms71	DEL	23974	270.59	Ms71	INS	4329	1.74	Ms71	INV	74	0.52	Ms71	DUP	6	0.0025	Ms71	TRA	992
Oh43	DEL	22755	253.28	Oh43	INS	3988	1.57	Oh43	INV	82	1.09	Oh43	DUP	6	0.0033	Oh43	TRA	881
Oh7B	DEL	22243	241.38	Oh7B	INS	5923	5.72	Oh7B	INV	71	0.56	Oh7B	DUP	8	0.0025	Oh7B	TRA	909
M37W	DEL	24652	271.33	M37W	INS	4497	1.76	M37W	INV	74	0.60	M37W	DUP	6	0.0032	M37W	TRA	968
Mo18W	DEL	25811	286.33	Mo18W	INS	4577	1.78	Mo18W	INV	85	1.27	Mo18W	DUP	9	0.0033	Mo18W	TRA	1034
Tx303	DEL	25311	277.33	Tx303	INS	6612	6.87	Tx303	INV	87	0.83	Tx303	DUP	10	0.0033	Tx303	TRA	999
HP301	DEL	25033	273.35	HP301	INS	6612	6.87	HP301	INV	82	1.07	HP301	DUP	8	0.0053	HP301	TRA	946
P39	DEL	25207	284.57	P39	INS	4486	1.72	P39	INV	86	1.08	P39	DUP	7	0.0024	P39	TRA	957
Il14H	DEL	25141	286.65	Il14H	INS	4238	1.69	Il14H	INV	88	0.75	Il14H	DUP	4	0.0021	Il14H	TRA	970
CML52	DEL	25534	276.54	CML52	INS	6717	6.65	CML52	INV	73	0.73	CML52	DUP	5	0.0022	CML52	TRA	1017
CML69	DEL	25754	283.95	CML69	INS	6637	6.52	CML69	INV	68	0.32	CML69	DUP	6	0.0021	CML69	TRA	919
CML103	DEL	25482	283.17	CML103	INS	4468	1.73	CML103	INV	87	0.82	CML103	DUP	4	0.0014	CML103	TRA	1024
CML228	DEL	25969	281.35	CML228	INS	6674	6.59	CML228	INV	77	0.56	CML228	DUP	5	0.0016	CML228	TRA	991
CML247	DEL	26361	288.40	CML247	INS	6838	6.65	CML247	INV	70	0.60	CML247	DUP	13	0.0045	CML247	TRA	941
CML277	DEL	25663	280.11	CML277	INS	6440	6.14	CML277	INV	73	0.83	CML277	DUP	9	0.0027	CML277	TRA	968
CML322	DEL	24665	267.92	CML322	INS	6362	6.15	CML322	INV	67	0.68	CML322	DUP	11	0.0043	CML322	TRA	974
CML333	DEL	25061	275.46	CML333	INS	4478	2.04	CML333	INV	78	0.93	CML333	DUP	13	0.0052	CML333	TRA	943
Ki3	DEL	25536	274.63	Ki3	INS	6495	6.53	Ki3	INV	86	0.76	Ki3	DUP	8	0.0025	Ki3	TRA	953
Ki11	DEL	26223	287.32	Ki11	INS	6816	7.17	Ki11	INV	83	0.85	Ki11	DUP	7	0.0029	Ki11	TRA	994
NC350	DEL	25807	284.24	NC350	INS	6941	7.40	NC350	INV	75	0.46	NC350	DUP	13	0.0047	NC350	TRA	1066
NC358	DEL	25434	278.31	NC358	INS	6613	6.71	NC358	INV	77	0.90	NC358	DUP	11	0.0041	NC358	TRA	965
Tzi8	DEL	25456	278.79	Tzi8	INS	6461	6.23	Tzi8	INV	73	0.41	Tzi8	DUP	11	0.0036	Tzi8	TRA	944

Table S7: Extent of structural variation across the major groups of NAM lines relative to B73. Mean/Median total sizes are shown in Mbp and mean/median sizes are shown in bp.

Group	sv_type	mean_total_size(Mbp)	median_total_size(Mbp)	mean_total_count	median_total_count	mean_size	median_size
non-stiff-stalk	del	261.25	261.86	23,402.67	23,192.00	11,163.25	11,291.11
flints	del	281.52	284.57	25,127.00	25,141.00	11,204.05	11,318.84
tropical	del	280.01	280.11	25,611.15	25,536.00	10,933.29	10,969.03
mixed	del	278.33	277.33	25,258.00	25,311.00	11,019.47	10,957.02
non-stiff-stalk	ins	2.38	1.72	4,540.17	4,289.00	523.97	402.10
flints	ins	3.43	1.72	5,112.00	4,486.00	670.21	384.17
tropical	ins	5.89	6.53	6,303.08	6,613.00	933.84	988.04
mixed	ins	3.47	1.78	5,228.67	4,577.00	663.80	389.32
non-stiff-stalk	inv	0.75	0.67	75.50	73.50	9,883.52	9,102.57
flints	inv	0.97	1.07	85.33	86.00	11,317.03	12,411.92
tropical	inv	0.68	0.73	75.92	75.00	8,967.27	9,768.79
mixed	inv	0.90	0.83	82.00	85.00	11,010.98	9,764.09
non-stiff-stalk	dup	0.0031	0.0027	7.00	7.00	446.86	390.93
flints	dup	0.0033	0.0024	6.33	7.00	515.32	344.14
tropical	dup	0.0032	0.0029	8.92	9.00	359.06	319.11
mixed	dup	0.0032	0.0033	8.33	9.00	389.52	361.22
non-stiff-stalk	tra	.	.	944.17	929.50	.	.
flints	tra	.	.	957.67	957.00	.	.
tropical	tra	.	.	976.85	968.00	.	.
mixed	tra	.	.	1,000.33	999.00	.	.

Table S8: Coordinates and copy number of the *rp1* tandem array on chromosome 10S. Coordinates are referenced to each of the individual genome assemblies.

genome	rp1 alignment locus start	rp1 alignment locus stop	size	copy number	# gaps in rp1 locus
B73	2823128	3532004	708876	14	10
B97	3454017	3917737	463720	14	0
Ky21	4184592	4460903	276311	10	0
M162W	3214938	3531971	317033	11	1
Ms71	3007141	3073115	65974	8	0
Oh43	3847294	4311005	463711	12	0
Oh7B	3485246	3551229	65983	5	5
M37W	3089289	4252158	1162869	30	29
Mo18W	2870789	3095369	224580	7	0
Tx303	2607068	3056758	449690	13	0
HP301	3172164	3238132	65968	7	0
P39	2746503	2880037	133534	4	0
Il14H	3585827	4088413	502586	15	0
CML52	2596259	2756085	159826	5	0
CML69	3439600	3736711	297111	8	0
CML103	3211757	4325999	1114242	23	36
CML228	3114513	4067585	953072	20	20
CML247	2762984	2858688	95704	7	0
CML277	2707651	3004761	297110	7	0
CML322	2950611	3216435	265824	10	0
CML333	2819939	3359941	540002	20	0
Ki3	2861923	3119062	257139	7	0
Ki11	3192016	3738606	546590	17	2
NC350	3699401	4027572	328171	15	0
NC358	3225450	3761930	536480	19	0
Tzi8	3730377	4252564	522187	17	4

Table S9: Number of significant GWAS SNPs ($p \leq 0.05$ after FDR correction) for each trait within and outside of UMR intervals.

Traits	Trait ID	Non-Genic UMRs	Genic UMRs	Non-Genic, Not in UMRs
Days_To_Silk	T2	158,365	129,278	585,696
ASI	T3	161,772	129,806	536,267
Leaf_Length	T4	160,487	125,367	592,425
Leaf_Width	T5	165,028	128,798	548,964
Leaf_Angle	T7	167,842	131,599	548,246
NLB_Index	T8	163,889	128,753	581,637
Ear_Mass	T10	161,378	123,497	617,330
Kernels_Per_Row	T12	158,128	127,793	590,508
Twenty_Kernel_Weight	T15	164,603	128,236	556,810
Tassel_Length	T16	164,883	130,534	580,184
Spike_Length	T17	164,876	135,222	545,094
Branch_Zone	T19	157,589	133,458	493,808
Cob_Length	T20	155,803	126,585	527,054
Cob_Diameter	T21	162,893	131,872	546,333
Ear_Row_Number	T22	167,956	132,579	554,642
GDD_Anth_Long	T23	150,234	130,778	591,526
GDD_Anth_Short	T24	164,127	122,255	640,282
GDD_Anth_Photo_Resp	T25	159,969	120,768	691,542
GDD_Silk_Long	T26	163,678	130,114	580,472
GDD_Silk_Short	T27	162,665	130,710	624,963
GDD_Silk_Photo_Resp	T28	154,231	115,941	673,853
SLB	T29	164,783	129,207	610,486
Days_To_Anthesis	T30	159,054	130,507	577,097
ChlorophyllA	T31	156,771	130,643	541,779
ChlorophyllB	T32	172,509	119,504	701,721
Malate	T33	164,180	133,006	540,370
Fumarate	T34	165,037	126,789	651,454
Fum2	T35	173,892	124,777	657,173
Glutamate	T36	157,213	138,957	580,812
Amino_Acids	T37	167,341	132,337	572,995
Protein	T38	162,263	128,924	687,760
Nitrate	T39	158,667	140,264	629,072
Starch	T40	160,254	133,203	613,835
Sucrose	T41	158,926	129,010	609,554
Glucose	T42	164,502	124,720	615,003
Fructose	T43	162,445	125,856	637,147

Supplementary Dataset

Dataset S1. Spreadsheet with data used for fractionation analysis. Data show the exon count matrix, genomic coordinates of regions syntenic with sorghum, and loci used for the GO analysis.